UNIVERSITÀ DEGLI STUDI DI MILANO

***Scuola di Dottorato in Scienze Biologiche e Molecolari***

Dipartimento di Bioscienze

XXXVIII CICLO

# Integrated characterization of Dual Specificity Phosphatase 12 (DUSP12): from putative regulation of eIF6 to mediation of cellular adaptation to stress

PhD candidate: Giorgia Deroma
Matricola: R14004
ORCID**:** 0009-0004-6342-9928

Scientific tutor: Prof. Stefano Biffo
Co-tutor: Annarita Miluzio
PhD course coordinator: Stefano Ricagno

A.A. 2024-2025

# Table of contents

*1. Introduction* *1*

**1.1. Translational control: the role of phosphorylation in translation and ribosome biogenesis 1**
1.1.1. Translation intiation and eukaryotic initiation factors regulated by phosphorylation 1
1.1.2. Phosphorylation as a mechanism to control ribosome biogenesis 9
1.1.3. Phosphorylation-dependent signaling networks in eukaryotic protein synthesis and ribosome biogenesis 12

**1.2. Experimental strategies to study protein phosphorylation and phospho-site mapping 17**
1.2.1 MS-based phosphoproteomics 18
1.2.2. Complementary approaches for validation 22

**1.3. The Eukaryotic Initiation Factor 6 (eIF6): A translation factor at the crossroads of ribosomal biogenesis and protein synthesis 23**
1.3.1 eIF6 properties, structure and functions 23
1.3.2. Models for eIF6 release 26
1.3.3. eIF6 in physiological and pathological contexts 28

**1.4. Phosphatases: understudied regulators of translational control 30**
1.4.1. Classification of protein phosphatases 31
1.4.2. Phosphatases in translational control 31

**1.5. DUSP12: A pleiotropic and understudied Dual-Specificity Phosphatase 34**
1.5.1. DUSP12 structural domains and enzymatic activity 34
1.5.2. Early characterization in yeast and evolutionary conservation 35
1.5.3. Open questions in Yvh1/DUSP12-mediated ribosome assembly 38
1.5.4. DUSP12 functions in human cells 39
1.5.5. DUSP12 involvement in disease contexts 40
1.5.6. From eIF6 to DUSP12: A hypothesis-driven shift in focus 41

**1.6.Aim of thesis 43**

*2. Materials and Methods* *44*

**2.1 Molecular cloning and plasmid generation 44**
2.1.1. Generation of eIF6 expression constructs 44
2.1.2. Site-Directed mutagenesis for eIF6 constructs 44
2.1.3 Generation of ΔZBD DUSP12 mutant constructs 45

**2.2. Cell culture and transient transfection 46**
2.2.1. Cell culture 46
2.2.2. Cellular transient transfection 46

**2.3. Purification and testing of recombiant eIF6 protein 47**
2.3.1. Bacterial colture 47
2.3.2. Bacterial lysis 47
2.3.3. His-Trap affinity purification and quality control 47
2.3.4. Ribosome purification 48
2.3.5. 60S Binding Assay 48

**2.4 Functional Translation Assays 49**
2.4.1. Rabbit Reticulocyte Lysate (RRL) Assay 49
2.4.2. Preparation of translationally active lysates and *in vitro* translation 49

**2.5. Molecular and biochemical techniques 49**
2.5.1. Protein extraction and quantification 49
2.5.2. Western Blotting 50
2.5.3. Nucleus-Cytoplasm fractionation 50
2.5.4. Polysome profiling 51
2.5.5. RNA extraction and quality assessment 51
2.5.6. ELISA assay 52

**2.6. Metabolic assays 52**
2.6.1. ATP quantification 52
2.6.2. Pyruvate quantification 52

**2.7. Immunofluorescence (IF) and Confocal Microscopy** **53**
2.7.1. Cell preparation and staining 53
2.7.2. Confocal micrscopy and image analysis 53

**2.8. Quantitative omics** **54**
2.8.1. Quantitative proteomics and phosphoproteomics 54
2.8.2. High-Resolution Mass Spectrometry and Data Analysis 54

**2.9. Bioinformatics for integrated omics analysis** **54**
2.9.1. Phosphoproteomic data analysis 55
2.9.2. RNA-Seq and Proteomics Integration 55
2.9.3. Functional enrichment and network analysis 55
2.9.4. Kinase Substrate Enrichment Analysis (KSEA) 55

***3. Results*** ***57***

**3.1. *In vitro* characterization of eIF6 activity and Ser235 mutation** **57**
3.1.1. Expression, purification and biochemical characterization of the S235A mutation 57
3.1.2. Functional validation of S235A in a cell-free translation system 58

**3.2. Cellular overexpression reveals functional impact of Ser235 phosphorylation on translation dynamics** **59**
3.2.1. Generation and validation of tagged eIF6 constructs for cellular studies 59
3.2.2. The S235A mutation does not alter the spatial distribution of eIF6 60
3.2.3. Quantitative analysis confirms that eIF6 S235A retains WT-like nuclear–cytoplasmic distribution 62
3.2.4. Ser235A mutation causes accumulation of free 60S and reduces translation initiation efficiency 63
3.2.5. Phosphomimetic eIF6 S235E restores normal ribosome assembly by promoting 60S release 64

**3.3. eIF6 interactome characterization: from technical challenges to *in silico* and structure-based evidence** **65**
3.3.1. Affinity purification approaches reveal limitated sensitivity for detecting eIF6 interactors 65
3.3.2. Identification of DUSP12 as a potential eIF6 interactor through proximity labeling and network analysis 67
3.3.3 Structural evidence places the yeast DUSP12 homolog Yvh1 in spatial proximity to eIF6 to eIF6 on a late pre-60S particle 68

**3.4. DUSP12 as a putative modulator of eIF6 activity** **69**
3.4.1. Overexpressed DUSP12 shows preferential cytoplasmic colocalization with phosphorylated eIF6 69
3.4.2. DUSP12 overexpression decreases the organization of active ribosomal complexes without recapitulating eIF6 dephosphorylation 71
3.4.3. DUSP12 overexpression does not globally reduce eIF6 Ser235 phosphorylation 73

**3.5. Dissecting the molecular functions of DUSP12 through integrated omics** **75**
3.5.1. Quantitative phosphoproteomics show that DUSP12 targets nuclear components and RNA splicing machinery 75
3.5.2. DUSP12 activity associates with suppression of CK/CDK-driven phosphorylation events 77
3.5.3. The C-terminal Zinc-Binding Domain of DUSP12 contributes to selective phosphoregulation 79
3.5.4. DUSP12 overexpression is associated with a mitochondrial-enriched proteomic profile that is lost upon ZBD deletion 80
3.5.5. Metabolic remodeling induced by DUSP12 overexpression occurs without detectable changes in mitochondrial abundance 81
3.5.6. Transcriptomic profiling reveals modest and selective transcriptional changes and limited RNA–protein correspondence following DUSP12 overexpression 83

***4. Discussion*** ***86***

**Conclusions and Future Perspective** **91**

***Supplementary information*** ***92***

***References*** ***94***

# Abstract

Precise regulation of protein synthesis and ribosome biogenesis is fundamental for cellular homeostasis, growth, and adaptation. These energy-intensive processes are tightly controlled by signaling networks in which reversible phosphorylation plays a central role. A key node is eukaryotic initiation factor 6 (eIF6), a conserved anti-association factor that binds the 60S ribosomal subunit to prevent premature joining with the 40S subunit. Its release, required for 80S ribosome formation, is regulated by post-translational modifications, with phosphorylation of Ser235 emerging as a critical switch.

Using non-phosphorylatable (S235A) and phosphomimetic (S235E) mutants, we showed that Ser235 phosphorylation is required for efficient eIF6 release and optimal translational output *in vivo*. However, unbiased biochemical approaches failed to identify stable upstream regulators of this modification, suggesting that eIF6 phosphorylation is controlled by transient or context-dependent interactions. Guided by proximity-labeling datasets, we focused on the atypical dual-specificity phosphatase DUSP12, a high-confidence proximity interactor of eIF6 previously implicated in ribosome biogenesis.

Functional analyses revealed that DUSP12 overexpression enhances global protein synthesis, as measured by puromycin incorporation, without inducing major alterations in polysome profiles. Quantitative phosphoproteomics identified a broad set of DUSP12-dependent phosphorylation changes affecting nuclear proteins, ribosome biogenesis factors, and components of protein quality control, including the ER chaperone Calnexin and the nucleolar protein NOLC1. Comparative analyses further demonstrated that the C-terminal Zinc-Binding Domain (ZBD) of DUSP12 plays a critical role in shaping the downstream phosphoproteomic and proteomic landscape,

Beyond its impact on translation-related pathways, DUSP12 overexpression was associated with a ZBD-dependent remodeling of the mitochondrial proteome, characterized by increased abundance of proteins involved in oxidative metabolism. This proteomic signature occurred in the absence of detectable changes in mitochondrial mass and was accompanied by functional metabolic alterations, including increased ATP levels and reduced lactate production. Integration with transcriptomic data revealed that these mitochondrial changes are largely uncoupled from corresponding transcriptional regulation, indicating a dominant contribution of post-transcriptional mechanisms. RNA sequencing instead revealed a limited and selective transcriptional response centered on stress-adaptive and signaling-related genes.

Overall, this work indicates that DUSP12 influences cellular physiology through multilayered regulatory mechanisms operating predominantly downstream of transcription. Rather than functioning as a global transcriptional regulator, DUSP12 is positioned at the intersection of translational output, proteostasis, and mitochondrial metabolism in a domain-dependent manner, thereby contributing to cellular adaptation to biosynthetic and metabolic demands. These findings place DUSP12 as a regulatory node linking ribosome-associated processes to metabolic and stress-response pathways, with broader implications for understanding cellular adaptation in both physiological and pathological contexts.

# *1. Introduction*

## 1.1. Translational control: the role of phosphorylation in translation and ribosome biogenesis

The expression of genes can be regulated at multiple levels, among which the translation of mRNA into proteins represents one of the most critical. For many genes, mRNA levels within a cell do not correlate with corresponding protein abundance, reflecting the high variability in translational efficiency[1]. Unlike transcriptional regulation, translational control of pre-existing mRNAs enables rapid adjustments in the cellular levels of encoded proteins[2], thereby playing an essential role in cellular growth and proliferation, by shaping the proteome[3]. Moreover, since mRNA translation requires a substantial amount of cellular metabolic energy and consumes a high share of amino acids, cells must carefully adjust protein synthesis rates according to nutrient availability[3].
A central mechanism of translational regulation involves the reversible phosphorylation of key components of the initiation and elongation machinery. Protein kinases such as the mechanistic Target of Rapamycin (mTOR), Mitogen-Activated Protein Kinases (MAPKs), and various stress-activated kinases phosphorylate specific translation factors, altering their activity, interactions, or localization[3]. Through these modifications, cells can dynamically regulate both global protein synthesis and selective translation of specific mRNAs, ensuring flexible and appropriate responses to environmental changes and supporting long-term adaptations in cell physiology and fate[2].

In addition to its role in controlling the translational machinery, phosphorylation also contributes to the regulation of ribosome biogenesis, a highly energy-demanding process that must be finely tuned according to cellular growth demands and nutrient availability[4]. The synthesis and assembly of ribosomal subunits require the concerted production and processing of ribosomal RNA, ribosomal proteins, and assembly factors. Several kinases and phosphatases modulate these steps by phosphorylating nucleolar and ribosome-associated proteins, thereby influencing rRNA transcription, pre-ribosomal particle maturation, and nuclear export[5,6]. This level of regulation ensures that ribosome production is synchronized with cellular growth demands and metabolic conditions.

### 1.1.1. Translation intiation and eukaryotic initiation factors regulated by phosphorylation

Translation consists of four main steps – initiation, elongation, termination, and ribosome recycling[7] - and most translational control is exerted during the initiation phase, when the ribosome is recruited to the mRNA and precisely positions the initiator methionyl tRNA (Met-tRNAi) at the start codon (AUG) within the P site[2].

In prokaryotes, translation initiation relies on the base-pairing between the Shine–Dalgarno (SD) sequence located upstream of the start codon in the mRNA and the complementary anti-SD sequence at the 3′ end of the 16S rRNA of the small (30S) ribosomal subunit[8]. This interaction allows precise positioning of the ribosome on the mRNA, facilitating start codon recognition. Only three initiation factors (IF1, IF2, and IF3) are required to assemble a competent initiation complex[9], reflecting a relatively streamlined process that is largely constitutive and less dependent on extensive regulatory input[9,10].

In contrast, eukaryotic translation initiation is considerably more complex, involving the interplay of numerous structural features of the mRNA – most notably the 7-methylguanosine ($m^7G$) 5′ cap, the poly(A) tail, and long, structured 5′ untranslated regions (5′ UTRs)[11] – and the action of at least twelve eukaryotic initiation factors (eIFs)[7] (**Table 1)**. Many of these eIFs are large, multidomain or multisubunit complexes that serve scaffolding, regulatory, or catalytic roles[12]. Another fundamental difference between prokaryotes and eukaryotes lies in the spatial and temporal organization of transcription and translation. In prokaryotic cells, transcription and translation are tightly coupled both spatially and temporally: ribosomes can begin translating nascent mRNAs even as they are being synthesized by RNA polymerase, through the RNAP-ribosome expressome, recently revealed at the 7.6 Å resolution[13]. This physical and functional coupling enables rapid and efficient gene expression with minimal post-transcriptional regulation.

| Name | Number of subunits and their molecular mass (kDa) | | Function |
|---|---|---|---|
| | Yeast | Higher eukayotes | |
| *Initiation factors* | | | |
| eIF1 | 1 (12.3) | 1 (12.7) | Facilitates recognition of the initiator codon, modulates translation accuracy at the initiation phase |
| eIF1A | 1 (17.4) | 1 (16.5) | Stimulates eIF2–GTP–Met-$tRNA_i^{Met}$ binding to 40S subunits and promotes ribosome scanning and initiation codon selection together with eIF1 |
| eIF2 | α (34.7)<br>β (31.5)<br>γ (57.8) | α (36.1)<br>β (38.4)<br>γ (51.1) | Forms an eIF2–GTP–Met-$tRNA_i^{Met}$ ternary complex and delivers Met-$tRNA_i^{Met}$ to the 40S subunit |
| eIF3 | a (110.3)<br>b (88.1)<br>c (93.2)<br>g (30.5)<br>i (38.7) | a (166.6), b (92.5)<br>c (105.3), d (64)<br>e (52.2), f (37.6)<br>g (35.6), h (39.9)<br>i (36.5)<br>j (29.1)<br>k (25.1), l (66.7)<br>m (42.5) | Is involved in the preinitiation complex assembly and start codon selection, stimulates the binding of mRNA and Met-$tRNA_i^{Met}$ to the ribosome |
| eIF4A | 1 (44.6) | 1 (46.1) | DEAD-box ATPase and ATP-dependent RNA helicase |
| eIF4B | 1 (48.5) | 1 (69.3) | RNA-binding protein that enhances eIF4A helicase activity |
| eIF4E | 1 (24.2) | 1 (24.5) | mRNA cap-binding protein |
| eIF4F | A (24.2)<br>E (44.6)<br>G (103.9) | A (24.5)<br>E (46.1)<br>G (175.5) | Cap-binding complex that unwinds the 5′ UTR of mRNA, mediates the binding of 43S complexes and assists the ribosomal complexes during scanning |
| eIF4G | 1 (103.9) | 1 (175.5) | Platform protein that binds eIF4E, A, 3; PABP; and mRNA, and enhances the helicase activity of eIF4A |
| eIF4H | None | 1 (27.4) | RNA-binding protein that enhances eIF4A helicase activity; is homologous to a fragment of eIF4B |
| eIF5 | 1 (45.2) | 1 (49.2) | GTPase-activating protein that induces hydrolysis of eIF2-bound GTP upon initiation codon recognition |
| eIF5B | 1 (112.2) | 1 (138.9) | Mediates ribosomal subunit joining in a GTP-dependent manner |
| eIF2B | α (34)<br>β (42.5)<br>γ (65.6)<br>δ (70.8)<br>ε (81.1) | α (33.7)<br>β (39)<br>γ (50.2)<br>δ (59.7)<br>ε (80.3) | Guanosine nucleotide exchange factor that promotes GDP–GTP exchange on eIF2 |

**Table 1. List of the most studied eukaryotic translation initiation factors.**

Differently, in eukaryotes, transcription and translation are physically separated within distinct cellular compartments[14]. Transcription and initial mRNA processing occur in the nucleus, after which mature mRNAs are exported to the cytoplasm where translation takes place[14]. This compartmentalization introduces additional layers of regulation absent in prokaryotes, allowing for greater complexity and versatility in translational control.

Most eukaryotic mRNAs are translated by a scanning mechanism, wherein the initiation begins with the formation of the 43S pre-initiation complex (PIC), comprising the 40S ribosomal subunit, the ternary complex (eIF2–GTP–Met-tRNA$_i^{Met}$), and the initiation factors eIF1, eIF1A, eIF3 and eIF5[15] (**Figure 1**). The PIC is recruited to the mRNA through interactions with the eIF4F complex, which includes the cap-binding protein eIF4E, the RNA helicase eIF4A, and the large scaffolding protein eIF4G[11]. eIF4G also interacts with poly(A)-binding protein (PABP), which associates with the poly(A) tail at the 3′ end of mRNA. PABP promotes efficient translation by increasing the affinity of the eIF4F complex for the 5′ cap and is therefore considered a translation initiation factor[16]. Through its interaction with PABP, eIF4G bridges the 5′ cap and the 3′ poly(A) tail, leading to the topological circularization of the mRNA in a closed-loop structure formed by eIF4F–mRNA–PABP[17].

Binding of the 43S PIC at the 5′ cap of the mRNA leads to formation of the 48S PIC, which scans the 5′ UTR in a 5′→3′ direction. During scanning, the helicase activity of eIF4A, stimulated by eIF4B, unwinds secondary structures to allow the ribosome to inspect each codon. Recognition of an AUG start codon within an optimal Kozak consensus sequence triggers GTP bound to eIF2, resulting in the release of most initiation factors[14]. For the efficient scanning of mRNAs with long or highly structured 5′ UTRs, additional helicases are often required, including mammalian DHX29 and DDX3, or the yeast homolog Ded1[11]. Subsequently, eIF5B binds to the ribosome, promoting the joining of the 60S large ribosomal subunit[11]. This final step yields the elongation-competent 80S initiation complex (80S IC), poised to enter the translation elongation phase[7].

This scanning-based mechanism, while more energetically demanding, confers enhanced regulatory capacity. Unlike the relatively static SD-directed initiation of prokaryotes, eukaryotic initiation is highly responsive to cellular signals, stress, and nutrient availability. Selective engagement of different eIFs and their regulators allows for dynamic modulation of translation efficiency across specific mRNA subsets. Central to this translational plasticity is the reversible phosphorylation of initiation factors and their associated regulatory proteins. This post-translational modification serves as a rapid and reversible mechanism to modulate the activity, subcellular localization, and intermolecular interactions of key components of the initiation machinery, thereby coupling

translational output to a wide array of environmental and intracellular cues, including growth factors, cytokines, nutrient availability, and diverse forms of cellular stress.

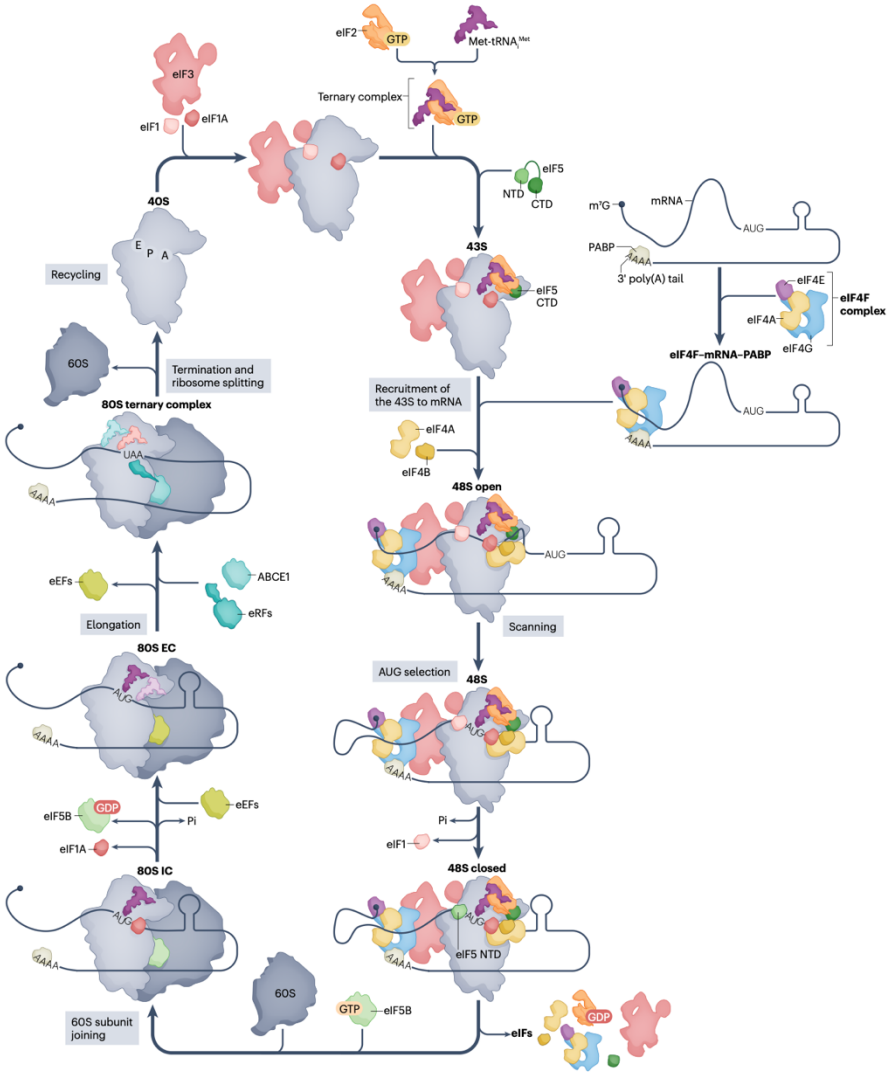


**Figure 1. Schematic overview of eukaryotic translation.** Translation initiation begins with the assembly of the 43S pre-initiation complex, composed of the 40S subunit, eIF1, eIF1A, eIF3, eIF5, and the eIF2–GTP–Met-tRNAi complex. Activated mRNAs, marked by the cap-binding complex eIF4F and PABP, recruit the 43S to form the scanning-competent 48S complex. Start-codon recognition triggers GTP hydrolysis, release of initiation factors, and recruitment of eIF5B, which promotes 60S joining to form the 80S initiation complex. GTP hydrolysis on eIF5B finalizes initiation and enables elongation, where eEF1A delivers aminoacyl-tRNAs and eEF2 drives translocation. Termination occurs when eRFs recognize a stop codon, leading to peptide release. ABCE1 then splits the 80S ribosome and, together with recycling factors, clears mRNA and tRNA, making the 40S subunit available for a new round of translation[11].

### 1.1.1.1 eIF2α

The first initiation factor identified as being regulated through phosphorylation was the α-subunit of the heterotrimeric eukaryotic initiation factor 2 (eIF2). Phosphorylation of eIF2α on Ser51[18] acts as a potent inhibitor of global protein synthesis by blocking the recycling of eIF2–GDP to eIF2–GTP, a step essential for ternary complex reformation[19]. In the canonical initiation pathway, recognition of the start codon and the base-pairing of Met-tRNA$_i^{Met}$ with the AUG codon in the P site of the 40S ribosomal subunit lead to cessation of scanning and GTP hydrolysis on eIF2. Following the release of eIF2-GDP, the 60S ribosomal subunit joins the complex to form the elongation-competent 80S ribosome[19] (**Figure 2**). For subsequent rounds of initiation, GDP bound to eIF2 must be exchanged for GTP, a reaction catalyzed by the guanine nucleotide exchange factor eIF2B. P-eIF2α-GDP binds

with high affinity to a regulatory domain of eIF2B, sequestering it and thereby preventing the GDP-to-GTP exchange. This results in a depletion of active eIF2-GTP, reduced delivery of Met-tRNA$_i^{Met}$ to ribosomes, and a consequent strong inhibition of global translation initiation[20].

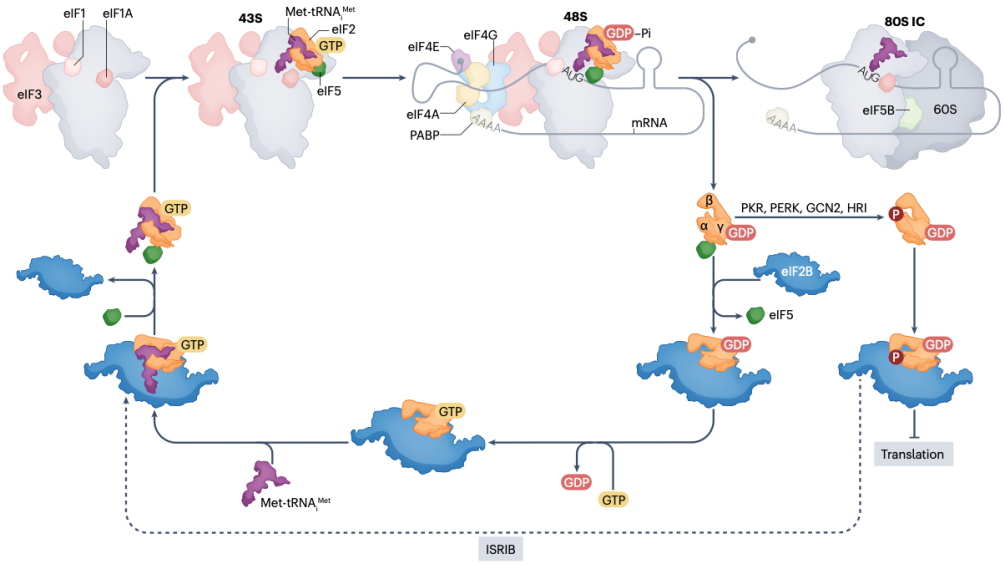


**Figure 2. Inhibition of translation initiation by eIF2 phosphorylation.** eIF2 (in orange) delivers the initiator Met-tRNA$_i$Met to the P site of the ribosome and represents a major control point in translation. Scanning of the 5′ UTR triggers GTP hydrolysis by eIF2, in a process regulated by eIF5 (in green), which acts as a GTPase activator. GTP hydrolysis and the release of inorganic phosphate (Pi) greatly reduce the affinity of eIF2 for Met-tRNA$_i$Met, promoting its release from the 48S complex. To initiate a new round of translation, GDP bound to eIF2 must be exchanged for GTP, a reaction catalyzed by the guanine nucleotide exchange factor eIF2B (in blue). This step is a key target of translational regulation: when eIF2 is phosphorylated, it forms a stable complex with eIF2B, preventing GDP–GTP exchange. As a result, active eIF2 is depleted, leading to inhibition of translation initiation and global protein synthesis[11].

The regulatory serine of the subunit α is highly conserved from yeast to humans[21] and its phoshorylation represents a pivotal adaptive response that enables cells to cope with diverse forms of stress. By repressing global translation initiation, this modification conserves cellular energy and nutrient resources[19], while simultaneously biasing the translational machinery toward the selective synthesis of proteins encoded by stress-responsive mRNAs[22]. This process, collectively known as the integrated stress response (ISR), is mediated by a family of eIF2α kinases whose composition varies among species. In mammals, four kinases have been identified: GCN2, activated by amino acid starvation or stalled ribosomes; HRI, triggered in erythroid cells by haem deficiency; PKR, induced by cytoplasmic double-stranded RNA during viral infection; and PERK, which responds to unfolded proteins in the endoplasmic reticulum. In *Saccharomyces cerevisiae*, by contrast, GCN2 is the sole eIF2α kinase[11].

The global reduction in protein synthesis promotes polysome disassembly and the assembly of stress granules – cytoplasmic aggregates containing untranslated mRNAs, 40S ribosomal subunits, and associated RNA-binding proteins – which serve as sites for mRNA triage and storage during stress. In parallel, the rapid depletion of labile proteins as a consequence of reduced synthesis can lead to significant proteome remodeling[19]. A well-characterized example is the activation of the transcription factor NF-κB: diminished production of its inhibitor, IκBα, combined with the inherently short half-life of this protein, results in the release and nuclear translocation of NF-κB, thereby initiating

transcriptional programs involved in inflammation, proliferation, and apoptosis[23]. Through these coordinated effects, eIF2α phosphorylation not only preserves cellular resources but also reconfigures gene expression and signaling pathways to enhance stress resilience[19]. Notably, recent studies have identified ISRIB, a small molecule capable of binding to eIF2B and restoring its activity even in the presence of phosphorylated eIF2α, thus counteracting the ISR and reopening translation[24].

Through this multilayered regulation, eIF2α phosphorylation functions as a molecular switch that preserves cellular resources while redirecting gene expression and signaling pathways toward stress adaptation and survival.

#### 1.1.1.2. eIF4E

Regulation of eukaryotic translation initiation also occurs at the level of initiation complex assembly, with the formation of the eIF4F complex at its core[25]. In this context, eIF4E plays an essential role, being the cap-binding protein that recognizes the $m^7G$ cap structure at the 5′ end of eukaryotic mRNAs, thereby facilitating their recruitment to the translation initiation machinery via the eIF4F complex[2]. In quiescent cells or stressed cells, eIF4E activity is primarily restrained through its sequestration by inhibitory binding proteins such as 4E-binding protein 1 (4EBP1). Mitogenic stimulation promotes phosphorylation of 4EBP1, leading to its dissociation from eIF4E and enabling assembly of the active eIF4F complex[26].

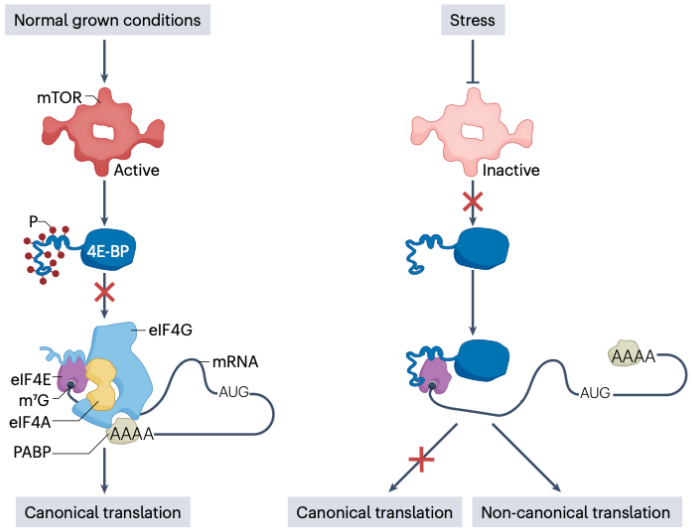


**Figure 3. 4E-BPs inhibit eIF4F formation under stress conditions.** The interaction between eIF4E and eIF4G can be blocked by eIF4E-binding proteins (4E-BPs), which inhibit the formation of the eIF4F complex and canonical translation. Under favorable growth conditions, 4E-BPs are phosphorylated by the kinase mTOR, preventing their binding to eIF4E and allowing eIF4E to associate with both the mRNA 5′ cap ($m^7G$) and eIF4G, thereby promoting canonical translation initiation. In contrast, under stress or nutrient deprivation, mTOR activity is reduced, 4E-BPs remain bound to eIF4E, block eIF4F assembly, and inhibit canonical translation, enabling non-canonical translation of specific mRNAs *(*Modified from[11]*)*.

A second layer of regulation involves direct phosphorylation of eIF4E on Ser209, a modification induced by mitogenic and stress signals and catalyzed *in vivo* by the MAP kinase-interacting serine/threonine-protein kinase 1 (Mnk1). Mnk1 interacts with the scaffolding protein eIF4G, positioning it in proximity to eIF4E within the initiation complex. Phosphorylation at Ser209 has been associated with enhanced affinity for the $m^7G$ cap and for eIF4G, potentially modulating the

selective translation of specific mRNA subsets, particularly those with complex 5′ untranslated regions (UTRs) that are more dependent on cap recognition[27].

#### 1.1.1.3. eIF4G

Another key component of the cap-binding complex subject to regulation by phosphorylation is eIF4G, the large scaffolding protein that bridges eIF4E, eIF4A, and the 43S pre-initiation complex via interaction with eIF3. More than 30 serine and threonine phosphorylation sites have been identified on eIF4G, collectively contributing to the fine-tuning of translation initiation. Among them, phosphorylation at Ser1108, Ser1148, and Ser1192 is stimulated by serum and inhibited by rapamycin treatment in human embryonic kidney (HEK) 293 cells[25]. In particular, nutrient stimulation enahnces phosphorylation at Ser1108, reinforcing eIF4E-eIF4G interaction in skeletal muscle and promoting cap-dependent translation[28]. eIF4G can also associate with mitogen-activated kinases (MNKs) in its C-terminal region near Ser1108. Phosphorylation at Ser1186 by protein kinase Cα (PKCα) enables the binding of MNK1 to eIF4G, thereby facilitating subsequent phosphorylation of eIF4E on Ser209[29]. Conversely, under conditions of skeletal muscle atrophy, MNK2 acts as a negative regulator of this process, counteracting Ser1108 phosphorylation and ultimately dampening translation[25]. Further within the C-terminal domain, additional critical phosphorylation sites orchestrate the assembly of the eIF4G–eIF4A–eIF4B helicase complex. Specifically, phosphorylation of Ser1232 by CDK1–cyclin B1 weakens the interaction of eIF4G with eIF4A and RNA, leading to reduced helicase activity and contributing to the global repression of translation observed during mitosis[30]. A nearby site, Ser1239, is a target of CKα, and its phosphorylation induces local conformational changes in the C-terminal region of eIF4G, enabling Erk1/2 binding and stimulating subsequent phosphorylation of Ser1232 by Erk1/2[31]. Finally, eIF4G can also be targeted by stress-activated kinases, such as Pak2 (p21-activated kinase 2). While its activity is relatively low under normal proliferative conditions, Pak2 can be rapidly activated in response to moderate cellular stress, thereby contributing to the reprogramming of translation initiation. Pak2 interacts with the region of eIF4G that encompasses the eIF4E-binding site (aa 610–643), thereby competing with eIF4E and preventing stable association of the cap-binding factor. This competition inhibits formation of the eIF4F complex and consequently reduces translation. In addition, Pak2-mediated phosphorylation of Ser896, located within the eIF3/eIF4A-binding site of eIF4G, further impairs the recruitment of eIF3 and eIF4A, thereby reinforcing the block on translation initiation at the level of scaffold assembly. Through this mechanism, stress-activated signaling pathways selectively suppress global cap-dependent translation, while leaving alternative, non-canonical initiation routes – such as IRES-driven – available to ensure the synthesis of stress-response proteins[32].

#### 1.1.1.4. eIF4B

Another member of the eIF4 group whose activity is regulated by phosphorylation is eIF4B. This factor plays a major role in translation initiation, primarily by enhancing eIF4A helicase activity and facilitating the recruitment of mRNA to the initiation complex through its interactions with both eIF3 and 18S ribosomal RNA[33]. In particular, eIF4B supports the translation of mRNAs with highly structured 5′ UTRs, which often encode proteins involved in proliferation (e.g., Cdc25C, c-Myc, ODC) or survival (e.g., Bcl-2, XIAP). Notably, recombinant eIF4B purified from bacteria shows limited ability to substitute for the native protein, indicating that its activity depends on post-

translational modifications specific to eukaryotic cells. Among these, phosphorylation at Ser406 and Ser422 has been most extensively studied. These sites are targeted by two major proto-oncogenic signaling pathways: Ras–MAPK and PI3K–mTOR, via ribosomal S6 kinase (RSK) and S6 kinase 1 (S6K1), respectively. Phosphorylation at Ser422 enhances the interaction of eIF4B with eIF3, thereby stabilizing its recruitment to the initiation complex and promoting ATPase activity of eIF4A, while phosphorylation at Ser406 is essential to achieve full translational activity[34].
More recently, phosphorylation of Ser504 has been identified as a neuron-specific modification. This event is rapidly induced through casein kinase and mGluR-dependent signaling, enhancing the recruitment of eIF4B to the pre-initiation complex and selectively promoting the translation of structured mRNAs, such as PKMζ[33].

#### 1.1.1.5. eIF3

The largest initiation factor is eIF3, which plays an essential role in translation by binding directly to the 40S ribosomal subunit and promoting the formation of the 43S pre-initiation complex. This factor also facilitates the recruitment of 5′-m$^7$G-capped mRNAs through its interaction with eIF4G. eIF3 is a multiprotein complex composed of 13 different subunits which are named IF3a to eIF3m in order of decreasing molecular weight. Mass spectrometry-based studies have identified a total of 29 phosphorylation sites across the different subunits[35]. Validation studies demonstrated that CK2 phosphorylates the eIF3j subunit at Ser127, a modification that stabilizes its association with other eIF3 components and promotes proper assembly of the pre-initiation complex. Disruption of this phosphorylation, for example via the S127A mutation or CK2 inhibition, reduces eIF3j incorporation into the complex and markedly impairs protein synthesis, indicating that CK2-mediated regulation of eIF3 is critical for overall translation efficiency[36]. In addition, eIF3f is directly phosphorylated by the cyclin-dependent kinase CDK11p46 during apoptosis. This modification facilitates its incorporation into a nuclear micro-complex with eIF3b and eIF3c, supporting the hypothesis that nuclear localization and phosphorylation of eIF3f may confer functions beyond translation initiation, potentially contributing to mRNA metabolism, including splicing, transport, and ribosomal RNA synthesis and maturation[37]. Crucially, eukaryotic initiation factor 3d (eIF3d), one of the key component of the eIF3 complex and an established cap-binding protein, emerged as a novel regulator for cellular survival and translational adaptation, particularly under chronic stress. Its function is tightly controlled by a phosphorylation switch that dictates its cap-binding activity[38]. eIF3d's activity shifts from:

- "OFF" State (phosphorylated): under normal conditions or acute endoplasmic reticulum (ER) stress, eIF3d is phosphorylated at residues like Ser528 and Ser529 by the enzyme Casein Kinase 2 (CK2). This modification keeps its cap-binding function inhibited, essentially acting as an "RNA gate" that occludes the cap-binding pocket[38].
- "ON" State (de-phosphorylated): when cells encounter sustained or chronic ER stress (e.g., after 16 hours of thapsigargin treatment), this phosphorylation is lost. In this context, eIF3d de-phosphorylation acts as a translational switch, immediately increasing eIF3d's cap-binding activity to target specific messenger RNAs[38].

Thus, the activation of eIF3d is a critical, "life-or-death" cellular decision point. When cells face prolonged stress (e.g., sustained ER stress), eIF3d undergoes de-phosphorylation, switching its cap-

binding activity to the "ON" state. This activated eIF3d then orchestrates the sustained ISR via two synergistic pathways:

- Kinase activation: eIF3d drives the translation of the kinase GCN2. GCN2 is crucial for maintaining the phosphorylation of eIF2α (p-eIF2α), which sustains the general protein synthesis shutoff required for the ISR[38].
- Epitranscriptome remodeling: In parallel, eIF3d increases the translation of the demethylase ALKBH5. The resulting demethylation of the ATF4 mRNA 5' UTR ensures robust production of the ATF4 protein.[38]

Essentially, the eIF3d phosphorylation switch translates chronic stress into a multi-layered, adaptive gene program, ensuring cellular survival.

#### 1.1.1.6. eIF5

Phosphorylation of eukaryotic initiation factor 5 (eIF5) is mediated primarily by casein kinase II (CK2) and targets a cluster of serine residues near the C-terminus of the protein, specifically Ser387 and Ser388. CK2-dependent phosphorylation enhances eIF5's functional interactions: it increases eIF5's affinity for eIF2, thereby promoting efficient GTP hydrolysis during ternary-complex formation, and also strengthens binding to eIF1A, modulating pre-initiation complex assembly[39].

#### 1.1.1.7. eIF6

In mammalian cells, eIF6 plays a central role in ribosome biogenesis within the nucleolus and contributing to 80S ribosome assembly in the cytoplasm[40,41]. Three potential phosphorylation sites have been identified, with Ser174 and Ser175 phosphorylated *in vitro* by the nuclear isoforms of casein kinase (CK1α and CK1δ)[42]. This phosphorylation promotes the export of eIF6 to the cytoplasm, facilitating the formation of pre-60S ribosomal particles[42]. Conversely, dephosphorylation by the $Ca^{2+}$/calmodulin-dependent phosphatase calcineurin enables eIF6 to return to the nucleolus and continue 60S subunit maturation[42]. Collectively, these findings indicate that CK1-mediated phosphorylation controls the subcellular distribution and activity of eIF6, linking its localization to ribosome assembly. Additional phosphorylation sites are located within the C-terminal tail of eIF6 and are believed to modulate its ability to associate with the 60S ribosomal subunit[42].

### 1.1.2. Phosphorylation as a mechanism to control ribosome biogenesis

The human 80S ribosome is composed of a small (40S) and a large (60S) subunit. The 40S subunit contains a single 18S rRNA strand and 33 ribosomal proteins (RPs) and is primarily responsible for binding, unwinding, and scanning messenger RNAs, whereas the 60S subunit, which mediates peptide bond formation and quality control of nascent peptides, comprises three rRNA species (5S, 5.8S, and 28S) together with 47 RPs. Ribosome biogenesis occurs mainly in the nucleolus, a membraneless nuclear compartment that assembles around nucleolar organizer regions (NORs), which harbor several hundred ribosomal DNA (rDNA) repeats. These rDNA repeats, located on the short arms of acrocentric chromosomes 13, 14, 15, 21, and 22, encode the 47S pre-rRNA, a polycistronic precursor that is co-transcriptionally processed into the 18S, 5.8S, and 28S rRNAs, while the 5S rRNA is transcribed independently within the nucleoplasm by RNA polymerase III from

a distinct locus on chromosome 1 (**Figure 4**). Notably, the number of rDNA repeats varies among individuals, although the functional implications of this variability remain unclear[43].

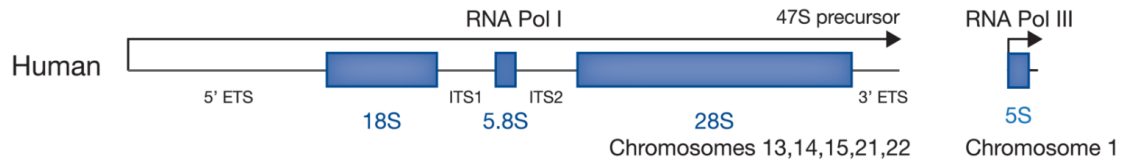


**Figure 4. Organization of human ribosomal RNA (rRNA) genes (modified from[44]).** The 47S rRNA precursor, transcribed by RNA polymerase I from rDNA clusters on chromosomes 13, 14, 15, 21, and 22, gives rise to the 18S, 5.8S, and 28S rRNAs through processing of the internal (ITS) and external (ETS) transcribed spacers. The 5S rRNA is independently transcribed by RNA polymerase III from a separate locus on chromosome 1. Together, these rRNAs form the core structural and functional components of the ribosome.

Assembly of ribosomal subunits requires the concerted deposition of numerous RPs onto the nascent pre-rRNAs in parallel with transcription, folding, modification, and processing events, in a hierarchical and energy-demanding process[45]. This compartmentalized pathway begins in the nucleolus with transcription of the 47S precursor by RNA polymerase I and the co-transcriptional formation of a 90S processome. Critical endonucleolytic cleavage of the pre-rRNA separates the pre-40S and pre-60S particles, which subsequently undergo extensive nuclear maturation steps, including incorporation of the 5S rRNA into the pre-60S subunit[44]. During the transition of the 90S processome into pre-40S and pre-60S ribosomal subunits, the precursor rRNA undergoes extensive processing and chemical modification mediated by roughly 200 small nucleolar RNAs (snoRNAs). Most of these snoRNAs are generated from intronic regions of Pol II–transcribed genes within the nucleoplasm.

Foundational research in budding yeast, a highly conserved model system, has demonstrated that this processing is regulated by a group of non-ribosomal "assembly factors" that are essential for recruiting key enzymes, such as the 5' exonuclease Rat1, which is critical for precise pre-rRNA cleavage[46]. Several studies revealed that these factors are also required for the structural folding of the pre-rRNA, ensuring the RNA adopts the correct conformation before final maturation[46]. This complex pathway is further safeguarded by quality-control mechanisms that eliminate defective precursors. A central role is played by the nuclear exosome, a 3′→5′ exoribonuclease complex that degrades aberrant pre-rRNAs[47]. Its degradative activity requires activating cofactors such as the TRAMP complex, which includes a poly(A) polymerase (Trf4p) and an RNA helicase (Mtr4p)[47]. This complex can stimulate the exosome's degradation of structured RNA substrates and polyadenylate nuclear RNA precursors, which helps to target them for destruction[47].

Following these early maturation events, a subset of ribosomal proteins is incorporated into the pre-40S and pre-60S subunits[43]. Both subunits are then exported to the cytoplasm, where final maturation occurs through the release of remaining RBFs, incorporation of late-joining RPs, and remodeling events that complete the formation of functional ribosomal subunits competent for translation[44] (**Figure 5**). Once assembled, ribosomes engage in translation. Individual ribosomes (monosomes) move along mRNAs, decoding codons and catalyzing peptide bond formation during elongation, whereas multiple ribosomes can simultaneously translate a single mRNA to form polysomes. Translation elongation generally occurs at a conserved rate of ~5.6± 0.5 codons per second[48] but can be modulated by stress[49], in response to signaling pathways such as mTORC1 and ERK, or phosphorylation of elongation factors such as eEF2 by eEF2 kinase, which slow down translation and

enhances fidelity[50]. Codon usage, amino acid sequence [51–53], and ribosome quality-control pathways triggered by stalled ribosomes[54,55] further contribute to the fine-tuning of protein synthesis, with implications for development, stress adaptation, and disease.

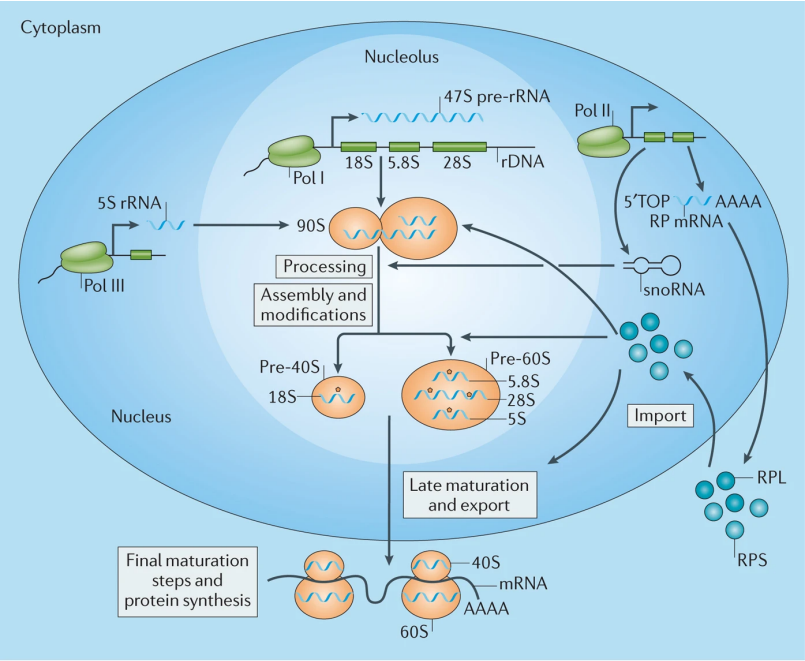


**Figure 5. Ribosome biogenesis requires the activity of all three RNA Polymerases**. The mature 80S ribosome consists of a 40S subunit, containing 18S rRNA and 33 ribosomal proteins (RPs), and a 60S subunit, containing 5S, 5.8S, and 28S rRNAs together with 47 RPs. Ribosome biogenesis largely takes place in the nucleolus, where RNA Pol I transcribes the 47S precursor rRNA, which encodes 18S, 5.8S, and 28S rRNAs. This precursor is co-transcriptionally assembled into the 90S processome together with 5S rRNA (transcribed by Pol III) and RPs (encoded by Pol II–derived mRNAs, translated in the cytoplasm, and re-imported into the nucleus). Maturation of the 90S into pre-40S and pre-60S subunits requires extensive rRNA processing and modification, driven by ~200 snoRNAs and numerous accessory factors. Final maturation occurs in the nucleoplasm and cytoplasm, where additional RPs are incorporated, yielding the functional 80S ribosome[43].

Ribosome biogenesis is among the most energy-demanding processes in eukaryotic cells, consuming up to 60% of total transcriptional activity and a large fraction of cellular energy resources.[56] Given this enormous metabolic investment, it is tightly controlled to ensure that ribosome production is coordinated with cellular growth, nutrient availability, and stress conditions and phosphorylation in this context plays a crucial role.

A central target for coordinating growth signals with ribosome production is TIF-IA (the mammalian ortholog of yeast Rrn3), that senses nutrient and growth-factor availability. Its phosphorylation status determines its ability to recruit RNA polymerase I to rDNA promoters and its regulated by mTOR pathway. Inhibition of this signalling, causes hypophosphorylation of Ser44 and hyperphosphorylation of Ser199. Phosphorylation at these sites affects TIF-IA activity in opposite ways, as phosphorylation of Ser44 activates while Ser199 inactivates TIF-IA[57].

Cell cycle progression is driven by the periodic activation of cyclin-dependent kinases (Cdks), which regulate not only DNA replication but also key biosynthetic pathways. Among their metabolic targets, Pol I transcription of rRNA is critical because it determines the rate of ribosome production and, consequently, the proliferative capacity of the cell[58]. In this context, differential phosphorylation of

the upstream binding factor (UBF), an important activator of Pol I transcription, has emerged as a key mechanism underlying cell cycle–dependent oscillations of rRNA synthesis. Early studies demonstrated that UBF activity is modulated by post-translational modifications, with hypophosphorylation correlating with transcriptional silencing in quiescent or serum-deprived cells. Sequential phosphorylation events link UBF activity to cell cycle progression: phosphorylation at Ser484 by $G_1$-specific cyclin-dependent kinase (cdk)/cyclin complexes G1 initiates rDNA transcription, while subsequent phosphorylation at Ser388 cdk2/cyclin E and A is indispensable for full transactivation. Mutational analyses confirm that Ser388 is critical, as its substitution with glycine abolishes UBF activity, whereas an aspartate substitution enhances it[59]. Beyond initiation, phosphorylation within UBF's HMG-box domains promotes promoter escape and productive elongation by relieving UBF-imposed DNA bending/looping at rDNA promoters, thereby helping Pol I transition from initiation to elongation[60].

Conversely, during mitosis, the activity of Cdks contributes to the transient shutdown of rRNA transcription, ensuring proper coordination with cell-cycle progression. At mitotic entry, Cdk1/cyclin B – the kinase orchestrating early events such as chromosome condensation, nuclear envelope breakdown, and spindle formation – phosphorylates the SL1 subunit $TAF_I110$ at threonine 852. This modification, togheter with the deacetylation of $TAF_I68$ by SIRT1, disrupts SL1's association with UBF, thereby preventing pre-initiation complex assembly at rDNA promoters. Following mitotic exit, dephosphorylation restores SL1 function and reactivates rDNA transcription[58]. Collectively, these events illustrate how phosphorylation serves as a versatile regulatory switch, linking ribosome production to cellular proliferation, metabolism, and stress adaptation in mammals.

### 1.1.3. Phosphorylation-dependent signaling networks in eukaryotic protein synthesis and ribosome biogenesis

The ability of eukaryotic cells to finely tune their anabolic capacity is central to maintaining homeostasis and responding to a variety of environmental and developmental cues[1]. This balance is particularly evident in the regulation of two highly demanding cellular processes: protein synthesis and ribosome biogenesis[4].

#### 1.1.3.1 mTOR signalling pathway

The mTOR signaling cascade consists of two distinct multi-subunit complexes named mTOR complex 1/2. mTORC1 is a protein complex that integrates signals from growth factors, intracellular nutrients, cellular energy status, and oxidative stress. It comprises the catalytic mTOR subunit and the regulatory protein Raptor, along with other components such as mLST8, DEPTOR, and PRAS40[61]. mTORC1 activity is acutely inhibited by rapamycin, which binds to FKBP12, forming a complex that interacts with mTORC1's FKBP12-rapamycin-binding (FRB) domain, thereby blocking its activation[62]. The mTOR complex 1 (mTORC1) integrates a diverse range of signals, including those from growth factors, hormones, and, crucially, intracellular nutrient levels like amino acids[4]. Its primary function is to promote cell growth and proliferation by upregulating anabolic processes, such as protein, lipid, and organelle biosynthesis, while simultaneously repressing catabolic pathways like autophagy[4]. mTORC2, composed of mTOR, Rictor, mSIN1, mLST8, and DEPTOR, is primarily involved in regulating cell survival, metabolism, and cytoskeletal

organization. Unlike mTORC1, mTORC2 is generally resistant to acute rapamycin inhibition; however, prolonged exposure can disrupt its assembly[63].

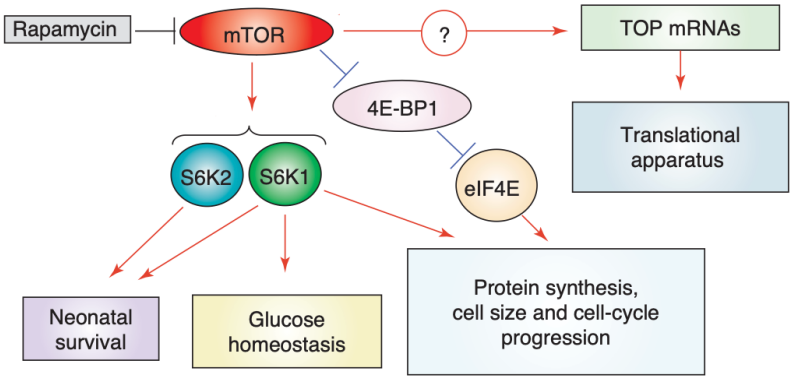


**Figure 6. mTOR-dependent regulation of protein synthesis.** mTOR promotes protein synthesis, cell growth, and cell-cycle progression by phosphorylating and inhibiting 4E-BP1, which releases eIF4E, and by activating S6K1/2. S6Ks regulate translation, cell size, glucose metabolism, and survival. TOP mRNAs, which encode ribosomal proteins and elongation factors, are translationally induced by growth factors and amino acids. Arrows denote activation, bars inhibition, and question marks uncertain pathways (modified from[64]).

The mTORC1 pathway primarily controls protein synthesis by phosphorylating two key downstream effectors: p70 S6 Kinase 1 (S6K1) and the eukaryotic initiation factor 4E-binding protein 1 (4E-BP1)[65](**Figure 6**).

- **The S6K1 Axis:** In response to growth factor and nutrient signals, mTORC1 directly phosphorylates S6K1 at a key site, threonine 389, leading to its activation[6]. Activated S6K1 promotes mRNA biogenesis, cap-dependent translation, and elongation through the phosphorylation of multiple downstream targets. Its best-characterized substrate is ribosomal protein S6 (rpS6), phosphorylated at five conserved serine residues (Ser235, Ser236, Ser240, Ser244, Ser247), a modification linked to cell size regulation and glucose metabolism[64]. S6K1 also phosphorylates and inhibits eEF2K at Ser366, thereby sustaining eEF2 activity and facilitating translation elongation, and modifies eIF4B, enhancing its recruitment to the initiation complex and boosting the translation of specific mRNAs[64]. Additional cytoplasmic substrates include the pro-apoptotic protein BAD, whose phosphorylation promotes cell survival, insulin receptor substrate (IRS), and possibly mTOR itself[64] (**Figure 7**). This axis is counter-regulated by protein phosphatase 2A (PP2A), which dephosphorylates S6K1, an essential step for signal termination and proper metabolic control[66].
- **The 4E-BP1 Axis:** Under conditions of low growth stimulation, the protein 4E-BP1 binds to and inhibits the eukaryotic initiation factor 4E (eIF4E)[65].When the cell receives anabolic signals and mTORC1 is active, it phosphorylates 4E-BP1, leading to its release from eIF4E[67]. This release is the critical step that allows eIF4E to bind to the scaffolding protein eIF4G and form the eIF4F complex, which is essential for recruiting the ribosome and initiating the translation of most cellular proteins[67].

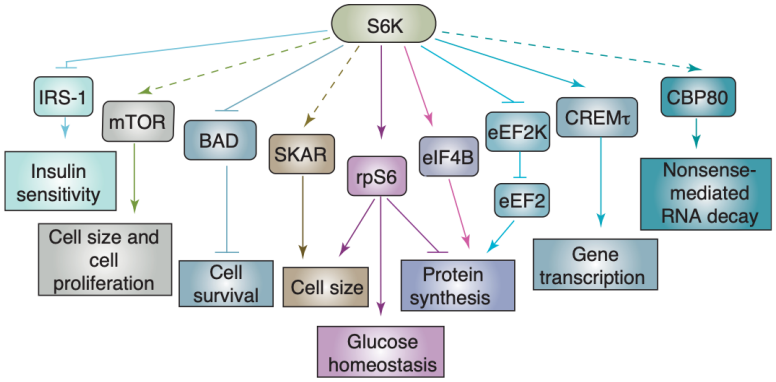


**Figure 7. S6K exerts its function through multiple downstream effectors**. Its phosphorylation activity promotes the activation of rpS6, the transcription factor CREMt, and likely eIF4B, while it inhibits IRS-1, the pro-apoptotic protein BAD, and eEF2K, whose activity normally suppresses eEF2. By contrast, no definitive regulatory effect has been assigned to S6K on mTOR, SKAR, or CBP80[64].

mTORC1, through phosphorylated rpS6, also regulates the production of new ribosomes to match the cell's synthetic demands. A key mechanism involves the regulation of a class of transcripts, know as 5' terminal oligo-pyrimidine tract (TOP) mRNAs[68]. These mRNAs are fundamental for the assembly of translation machinery since they code for all of the ribosomal proteins, many translation factors, in addition to some RNA-binding proteins[68]. When mTORC1 is inactive due to nutrient or growth signaling shortage, La-Related Protein 1 (LARP1) acts as a repressor of TOP mRNA translation, displaces eIF4E from the $m^7$Gppp cap moiety of TOP mRNAs, impeding the assembly of the eIF4F complex on these transcripts[67,68]. Upon activation, mTORC1 phosphorylates LARP1 at specific serine and threonine residues, causing its dissociation from TOP mRNAs and rescuing their translation[68]. This is an example of how phosphorylation events can act as a molecular switch to coordinate the production of new ribosomal components with the cell's energetic and nutritional status.

### 1.1.3.2. Extracellular Signaling Pathways

The mTORC1 pathway is not a stand-alone regulator but is intricately linked to other major signaling cascades that respond to a variety of extracellular stimuli (**Figure 8**)[8].

- **The PI3K/Akt Pathway:** The phosphatidylinositol 3-kinase (PI3K)/protein kinase B (Akt) pathway is activated by the binding of growth factors and hormones to their cell surface receptors[69].This cascade, which promotes cell growth, proliferation, and survival, is a powerful upstream activator of mTORC1[69].The activation of Akt, for instance, leads to the inhibition of the tuberous sclerosis complex (TSC), which in turn removes a brake on the mTORC1 activator Rheb, thereby activating mTORC1 and downstream anabolic processes[3]. This connection provides a direct molecular link between external growth signals and internal metabolic regulation[3].
- **The MAPK/ERK Pathway:** The Mitogen-Activated Protein Kinase (MAPK) cascade, particularly the extracellular signal-regulated kinases (ERK1/2), transmits diverse extracellular signals, such as those from mitogens and growth factors like EGF, into a coordinated cellular response[3]. The MAPK/ERK pathway contributes to the regulation of protein synthesis through both indirect and direct mechanisms.

- **Indirect activation of mTORC1:** The MAPK/ERK pathway can activate mTORC1 by phosphorylating TSC, similar to the PI3K/Akt pathway, providing an important layer of redundancy and signal convergence[3].
- **Direct regulation of translation:** The ERK pathway directly regulates the translational machinery by activating kinases like MAP kinase-interacting kinases (MNKs)[8]. MNKs, in turn, phosphorylate the initiation factor eIF4E at Ser209[3]. Furthermore, the MAPK pathway inhibits eukaryotic elongation factor 2 kinase (eEF2K), which removes a rate-limiting step for translational elongation, thus promoting overall protein synthesis[3]. The RSK kinase, a downstream effector of MAPK/ERK, also directly phosphorylates eukaryotic initiation factor 4B (eIF4B) and eEF2K, showcasing a multi-layered control system[3].

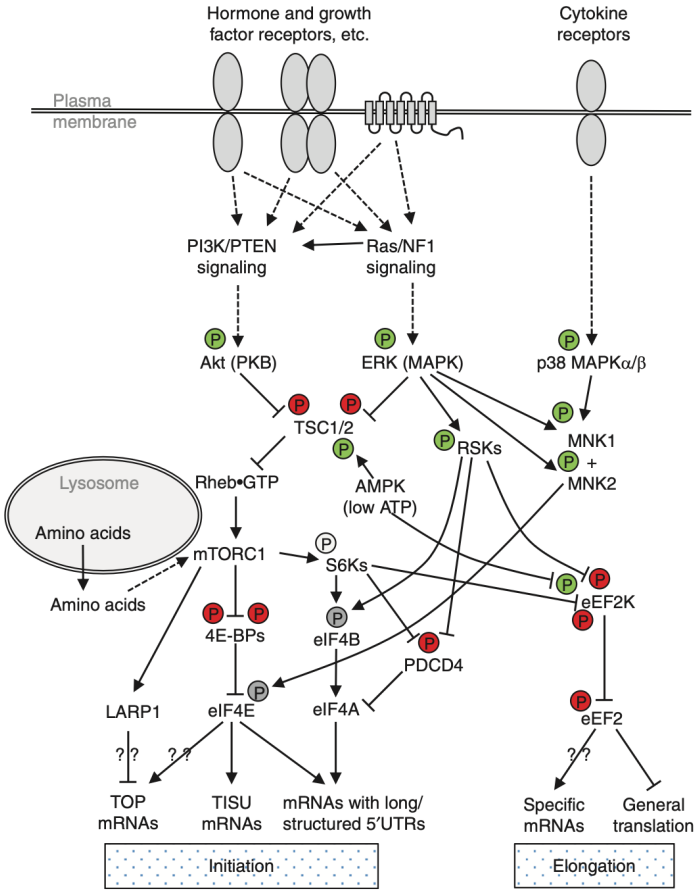


**Figure 8. Overview of the principal signaling pathways affecting the translational machinery**. The schematic highlights major regulatory connections, with solid lines indicating direct interactions and dashed lines representing indirect links (e.g., involving multiple intermediates). Phosphorylation events are marked as (P); activating modifications are shown in green, inhibitory phosphorylations in red, and gray denotes cases where the functional outcome remains unresolved[3].

### 1.1.3.3. Control of ribosome biogenesis by PI3K/Akt and MAPK/ERK

The production of new ribosomes can be influenced by:

- **PI3K/Akt:** Nuclear Akt contributes to ribosome biogenesis primarily by regulating rRNA synthesis. It stabilizes and activates transcription initiation factor I (TIF-I) via CK2α, thereby promoting the recruitment of RNA polymerase I to rDNA promoters[70]. Akt also engages in interactions with nuclear PI(3,4,5)P3 and with the nucleolar protein B23, in part through

nuclear PI3K activity[71,72]. Importantly, Akt protects B23 from proteolytic cleavage, and B23 itself is crucial for c-Myc–dependent regulation of rDNA transcription and nucleolar localization. c-Myc plays a central role in malignancy, in part by driving ribosome biogenesis[71]. Within the nucleus, it regulates UBF expression, binds directly to rDNA, and supports the assembly of transcriptional machinery at rDNA promoters, including SL1, UBF, and TBP[73] (**Figure 9**).

- **MAPK/ERK:** The MAPK pathway regulates post-transcriptional ribosome maturation. A study found that the RSK kinase, activated by the MAPK pathway, phosphorylates RIOK2, a pre-40S particle assembly factor, at Ser483[74]. This phosphorylation event is critical for the release of RIOK2 from the pre-40S particle and its subsequent nuclear recycling, which is a necessary step for the final maturation of the 40S ribosomal subunit in the cytoplasm[74].

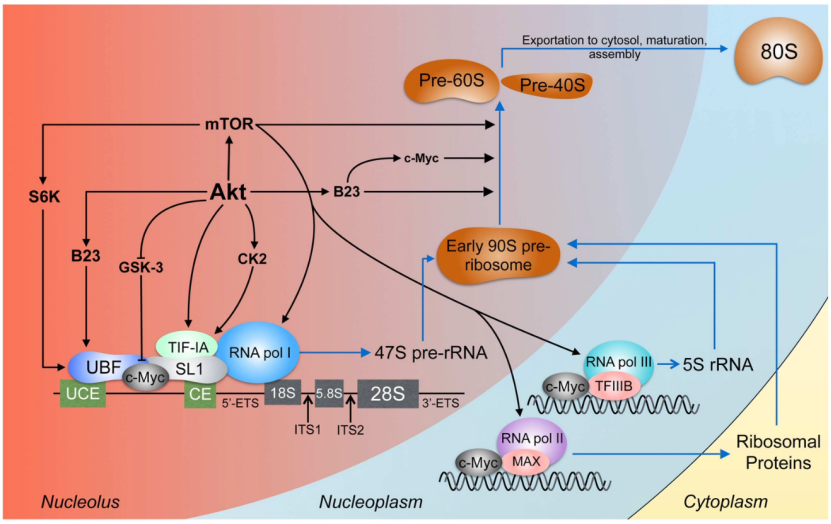


**Figure 9. Akt in ribosome biogensis control**. Akt promotes rDNA transcription by stabilizing c-Myc, B23, and TIF-IA, the latter directly interacting with SL1 and RNA Pol I. In parallel, mTOR, through S6K1, enhances UBF–SL1 interaction and can also bind 5S rDNA promoters. c-Myc further amplifies transcription by all three RNA polymerases through direct rDNA binding and association with SL1, MAX, and TFIIIB.

### 1.1.3.4. The Integrated Stress Response (ISR)

In contrast to the anabolic pathways that promote protein synthesis, the Integrated Stress Response (ISR) acts as a global, rapid "emergency brake" on translation in response to various forms of cellular stress[20,75]. This response is primarily mediated by the phosphorylation of eIF2α at the residue Ser51. This phosphorylation inhibits the nucleotide exchange factor eIF2B, thereby preventing the recycling of the eIF2 complex and leading to a sharp reduction in the supply of the Met-tRNAiMet to the ribosome[2].

In mammalian cells, the ISR is activated by a family of distinct eIF2α kinases, each acting as a specific stress sensor[76]:

- General control nonderepressible 2 (GCN2): responds to nutritional stress, such as amino acid or glucose deprivation[19,77].
- PKR-like endoplasmic reticulum kinase (PERK): activated by endoplasmic reticulum (ER) stress, often caused by an accumulation of misfolded proteins[76].
- Heme-regulated eIF2α kinase (HRI): activated by heme deprivation[19].
- Protein kinase R (PKR): part of the antiviral defense, activated by double-stranded RNA[19].

A remarkable feature of this global repression is the paradoxical selective translation of specific mRNAs, such as the one encoding the transcription factor ATF4. The translation of ATF4 is regulated by upstream open reading frames (uORFs) that act as switches depending on the cell's condition. The translation of ATF4 is controlled by upstream open reading frames (uORFs) located before the ATF4 coding sequence (CDS). Mouse Atf4 mRNA contains two uORFs (uORF1 and uORF2), while human ATF4 mRNA has three (uORF1-3)[78]. Under basal conditions, translation starts at uORF1 and reinitiates at uORF2 (or uORF3 in humans), which overlaps out-of-frame with the ATF4 CDS, thereby blocking its translation[78]. When cells are exposed to stress, however, eIF2α is phosphoryated and the availability of the ternary complex is reduced, which slows down the process of reinitiation[52]. Because of this delay, ribosomes are able to bypass the inhibitory uORF and instead initiate translation at the ATF4 coding sequence[79]. In this way, ATF4 expression is selectively turned on in response to stress signals.

#### 1.1.3.5. The role of phosphatases as signal terminators

The dynamic nature of phosphorylation-dependent signaling is balanced by the action of protein phosphatases, which are responsible for removing phosphate groups and terminating signals[80]. While kinase-dependent events are often well-defined, the specific phosphatases that counteract them are frequently less characterized[80]. The protein phosphatase 2A (PP2A) is a major serine/threonine phosphatase that plays a crucial counter-regulatory role[81]. It has been identified as the key phosphatase that inactivates the S6K kinase by dephosphorylating it, effectively antagonizing the activation induced by mTOR[81]. PP2A can form approximately 100 different heterotrimeric complexes with various regulatory subunits, which confers substrate specificity and allows it to precisely control specific processes, such as the inactivation of S6K, without non-specifically deactivating entire signaling networks[82].

#### 1.1.3.6. Pathophysiological implications

The tight regulation of these signaling networks is essential for health, and their dysregulation is a central feature of many diseases, particularly cancer[83]. Cancer cells are characterized by uncontrolled growth and proliferation, which are driven by a sustained increase in protein synthesis and ribosome biogenesis[69]. The hyperactivation of the mTOR, MAPK, and PI3K/Akt pathways is a common feature in many malignancies. This hyperactivation drives "oncogenic translational programs" that increase global protein synthesis and, importantly, selectively translate mRNAs that are critical for tumor cell survival, invasion, and metastasis[84]. Genetic studies in mouse models have elegantly demonstrated that limiting the ability of oncogenic signals to increase protein synthesis is sufficient to block tumorigenesis, underscoring the central role of translational control in cancer development[69].

## 1.2. Experimental strategies to study protein phosphorylation and phospho-site mapping

Phosphorylation is among the most widespread post-translational modifications (PTMs), first described by Phoebus Levene in 1906[85]. In proteins, the addition of a phosphate group to hydroxyl-containing amino acids introduces negative charges into residues that are otherwise neutral. This chemical change can alter the three-dimensional conformation of a protein, thereby modulating its

function. Phosphorylation typically involves the transfer of the terminal (γ) phosphate from adenosine triphosphate (ATP) to specific residues, most commonly serine, threonine, or tyrosine, although other amino acids can also serve as substrates[86]. The reaction is mediated by two major enzyme superfamilies: protein kinases, which catalyze phosphorylation, and protein phosphatases, which remove phosphate groups[86]. Given its central role in regulating protein activity, the balance between these opposing enzymatic activities is essential for cellular homeostasis.

The enzymatic transfer of phosphate groups by protein kinases was first discovered in the 1950s by Edmond Fischer and Edwin Krebs[87], and has since become a major focus of research. It is estimed that 70% of human proteins are phosphorylated at least once[88], with over 240,000 phosphorylation sites cataloged in PhosphoSitePlus as of July 2024[89]. The human genome encodes 538 kinases and 226 phosphatases, together representing about 2.5% of protein-coding genes. These enzymes drive reversible phosphorylation, enabling complex signal transduction cascades, as kinases often modify multiple substrates and are themselves regulated by other kinases[89].

Given the central role of phosphorylation in cellular regulation, the ability to study post-translational modifications with precision is essential. Several methodological advances, ranging from antibody-based detection to large-scale mass spectrometry, have enabled researchers to map and quantify these modifications, providing critical insights into their functional significance.

### 1.2.1 MS-based phosphoproteomics

Mass spectrometry (MS) has long been a key tool for studying protein modifications, initially applied to purified proteins and more recently to large-scale proteomic studies of post-translational modifications (PTMs) across organelles or entire cells[90]. PTM analysis presents unique challenges compared with standard proteome profiling: each modified peptide must be individually detected and localized, and many modifications occur at substoichiometric levels or are labile, making their identification technically demanding[91]. These difficulties are particularly evident in phosphoproteomics. Unlike conventional proteomic workflows, phosphoproteomic analyses require substantially more starting material – often 100- to 200-fold higher – because phosphorylated peptides represent less than 1% of the total peptide population[89].

To overcome this limitation, phosphoproteomic workflows incorporate additional steps aimed at reducing peptide complexity and selectively enriching phosphorylated species from a vast excess of non-phosphorylated peptides prior to mass spectrometry (MS) analysis[89]. Although established strategies have enabled broad coverage of the phosphoproteome, they often necessitate further optimization depending on experimental parameters such as sample type, available material, and the number of conditions under investigation[89].

A typical phosphoproteomic workflow involves cell lysis and protein extraction, followed by enzymatic digestion (commonly with trypsin) to generate peptides for MS analysis. After initial cleanup to remove contaminants, a crucial enrichment step is performed to selectively isolate phosphorylated peptides from the overwhelming background of unmodified species. The enriched sample is then desalted and prepared for LC-MS/MS analysis[89].

#### 1.2.1.1. Enrichment strategies

In mass spectrometry (MS)-based phosphoproteomics, enrichment of phosphopeptides is essential due to their low abundance and labile nature[92]. The main enrichment approaches are categorized as either affinity strategies or chemical enrichment strategies.

Affinity enrichment strategies rely on the specific interaction of phosphorylated amino acids with binding reagents or on their unique physicochemical properties.

- Chromatography-Based Methods: These techniques take advantage of the chemical properties of phosphopeptides.
    - Immobilized Metal Ion Affinity Chromatography (IMAC) uses positively charged metal ions like $Fe^{3+}$or $Ti^{4+}$ to capture the negatively charged phosphate groups on peptides. However, IMAC can also bind to other negatively charged, non-phosphorylated peptides[92].
    - Metal Oxide Affinity Chromatography (MOAC) relies on the affinity of phosphate groups for metal oxides like $TiO_2$. This method is more robust than IMAC, as it can tolerate low pH and detergents[92].
- Ion-exchange chromatography separates peptides based on their overall charge. Strong cation exchange (SCX) works by isolating phosphopeptides due to their weaker interaction with the column at acidic pH[92]. Conversely, strong anionic exchangers (SAX) attract the negatively charged phosphate groups[92].
- Antibody/Protein Domain-Based Methods: These strategies use specific biological molecules to capture modified peptides.
    - Anti-pTyr antibodies are used for enriching tyrosine phosphorylations (pTyr), which are less common than other phosphorylation events[92].
    - Protein domains, such as the Src homology 2 (SH2)-domain-derived super-binder protein, can also be used to pull down pTyr-containing peptides[92]. This method offers a more comprehensive coverage of pTyr sites compared to antibody-based methods.

Chemical strategies were developed to overcome the limitations of affinity methods, such as non-specific binding or the lack of suitable antibodies.

- The photo-pTyr-scaffold is a trifunctional probe designed to selectively capture native pTyr signaling complexes. It includes an engineered SH2 domain, a photoreactive group for covalent cross-linking, and a biotin tag for enrichment[92].
- For the analysis of fragile phospho-aspartate (pAsp) sites, a desthiobiotin-containing hydroxylamine (DBHA) probe has been used to capture these modifications[92]. A more recent probe, hydroxylamine alkyne (HA-yne), has been shown to be even more effective due to its lower steric hindrance[92].

Since no single enrichment method can capture all phosphopeptides, combining complementary strategies is often recommended for a deeper phosphoproteome analysis[92]. Future advancements in this field are expected to focus on new sorbent materials, such as magnetic and mesoporous materials, and on combining both affinity-capture and chemical labeling strategies to push the boundaries of

PTM analysis[92]. The ultimate goal is to optimize workflows to handle the limited sample amounts from clinical samples, paving the way for personalized medicine.

#### 1.2.1.2 Advancements in sample sensitivity

Recent advancements in phosphoproteomics have focused on overcoming challenges related to sample sensitivity, particularly for low-input samples such as single cells. Traditional sample preparation methods often lead to significant material loss due to extended processing times and multiple transfer steps. To address this, miniaturized strategies have been developed to enhance the recovery and analysis of limited phosphorylated peptides. These approaches include the use of miniaturized analytical systems that reduce sample loss through direct sample injection, and integrated platforms like Phospho-SISPROT, which simplify the workflow from protein digestion to enrichment by coupling specialized pipette tips in tandem[89]. Additionally, high-throughput automated platforms such as EasyPhos[93] and R2-P2[94] leverage magnetic particles and 96-well formats to efficiently process multiple low-input samples. These innovations are crucial as they enable the reliable mapping of phosphorylation events from minimal starting material, opening new avenues for single-cell phosphoproteomics and clinical research with precious tissue samples[89].

#### 1.2.1.3. Fragmentation methods and data acquisition

Once enriched, peptides are analyzed by mass spectrometry and subjected to advanced fragmentation methods to determine their sequence and locate modifications. Peptide fragmentation is an indispensable step, as the mass of the whole peptide (precursor) is insufficient for its unique identification[95]. Fragmentation generates a series of fragment ions whose combined mass and unique bond-breaking patterns can be matched to databases to deduce the original peptide's amino acid sequence and determine the exact phosphorylation site[95]. Techniques such as higher-collisional dissociation (HCD)**,** multistage activation (MSA)**,** and electron transfer dissociation (ETD) are widely used. HCD accelerates ions to collide with a gas, generating fragment ions that allow precise sequence reading and modification localization, particularly useful for multiphosphorylated peptides. MSA, often used in ion trap instruments, fragments large peptide ions in multiple stages, increasing the chances of detecting modification-containing fragments. ETD is a "gentle" method that transfers electrons to peptide ions, breaking peptide bonds while preserving labile modifications such as O-GlcNAc or other glycopeptides. The combination of these methods allows confident peptide identification and site localization, typically achieving >99% localization probability in large datasets.

The mass spectrometry analysis workflow is based on two main data acquisition strategies: Data-Dependent Acquisition (DDA) and Data-Independent Acquisition (DIA). Data-independent acquisition (DIA) has become a widely adopted strategy for large-scale proteomic studies, offering both broad proteome coverage and robust quantitative accuracy. This approach involves the systematic fragmentation of all analyte ions within a sample, followed by measurement of their respective mass-to-charge (m/z) ratios. This process generates a spectrum of fragment ions, or "mass spectrum," which can then be used to identify the different components present in the sample[96]. For instance, Collins et al. successfully applied DIA to quantify over 9,000 proteins in the mouse brain, underscoring its unmatched capacity for comprehensive proteome profiling[97]. In contrast, DDA is the

traditional approach, where a full mass scan (MS1) identifies the most abundant precursor ions, which are then isolated and fragmented (MS2) for peptide identification. It remains the preferred method for smaller-scale investigations that prioritize sensitivity, particularly in the detection of post-translational modifications. A study by Mehar Un Nissa et al., which employed DDA to characterize the proteome and post-translational modifications of a widely farmed tropical fish species, illustrates the method's strength in capturing fine-grained molecular details[98].

#### 1.2.1.4 Quantification strategies

Beyond identification, a central goal of phosphoproteomics is the quantitative analysis of phosphorylation events. This can focus on two primary objectives: measuring relative changes in phosphorylation at specific sites or determining phosphorylation stoichiometry, defined as the fraction of a given protein phosphorylated at a particular residue relative to the total protein amount. Most studies focus on tracking dynamic, site-specific phosphorylation events that often do not correlate directly with protein expression levels, thereby providing insights into transient signaling responses. The latter approach, quantifying stoichiometry, offers a more absolute measure of site occupancy and is essential for understanding functional impact on protein activity[90].

Most quantitative phosphoproteomic studies rely on the use of stable isotopes, introduced through either metabolic or chemical labeling strategies. The simplest alternative is label-free quantification, although this method is more susceptible to inaccuracies arising from sample preparation compared with label-based techniques.

Metabolic labeling, such as Stable Isotope Labeling with Amino acids in Cell culture (SILAC), involves the incorporation of stable isotope-labeled amino acids directly into newly synthesized proteins in living cells[99]. In this approach, cells are grown in media containing either normal ("light") or isotopically labeled ("heavy") amino acids, most commonly lysine and arginine $^{13}C$ or$^{15}N$ (**Figure 10b**). SILAC enables direct comparison between experimental conditions by distinguishing labeled from unlabeled peptides via mass spectrometry, allowing for relative quantification through peak area ratios[99]. During MS analysis, peptides appear as pairs separated by the isotopic mass difference, and relative quantification is achieved by comparing the peak area ratios of the extracted ion chromatograms[99]. While highly accurate and conceptually straightforward, SILAC can be costly, particularly for *in vivo* applications[89].

Chemical labeling approaches have expanded the toolkit for quantitative studies using a variety of chemical tags or reagents to label peptides or proteins (**Figure 10c**). Stable isotope dimethylation offers a simple, cost-effective method for comparing two samples, especially when a relatively large amount of material is available[100]. Isobaric labeling strategies – including TMT (Tandem Mass Tags) and iTRAQ – are extensively used due to their improved sensitivity, higher sample throughput, and greater quantitative accuracy and reproducibility[101]. Compared with dimethyl labeling or SILAC, isobaric tags also offer significantly higher multiplexing capacity, allowing the simultaneous analysis of up to 18 samples[102].

Label-free quantification provides an alternative approach that does not require chemical or metabolic labeling. In this strategy, each sample is processed and analyzed independently by mass spectrometry,

and phosphosite quantification is achieved by comparing the peak areas of precursor or fragment ions across conditions[103] (**Figure 10a**). While a theoretically unlimited number of samples can be compared, accuracy critically depends on reproducible sample handling, enrichment, and chromatography [89].

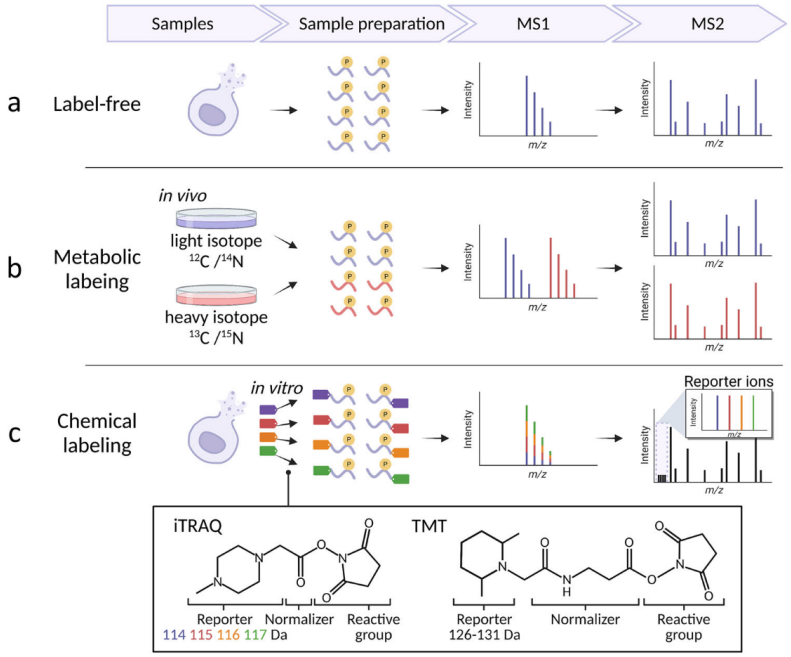


**Figure 10. Overview of quantitative proteomics strategies.** (a) Label-free quantification: protein abundance is inferred directly from MS signal intensity or spectral counts without isotope labeling. (b) Metabolic labeling (e.g., SILAC): cells are cultured with light ($^{12}C/^{14}N$) or heavy ($^{13}C/^{15}N$) isotope-labeled amino acids, allowing relative quantification of peptides based on mass differences. (c) Chemical labeling (e.g., iTRAQ, TMT): peptides are derivatized in vitro with isobaric tags consisting of a reporter, normalizer, and reactive group. Quantification is achieved through reporter ion intensities generated in MS2 spectra[89].

## 1.2.2. Complementary approaches for validation

Functional characterization of identified phosphorylation sites typically combines *in vitro* and *in vivo* approaches. Kinase–substrate relationships can be probed using purified kinases with radiolabeled ATP, or via chemical-genetic strategies employing analog-sensitive kinases to selectively label target residues[104]. Validation in cells is often achieved with phospho-specific antibodies, enabling detection by immunoblotting or immunoprecipitation. Site-directed mutagenesis, substituting phosphorylatable residues with phospho-dead or phospho-mimetic amino acids, allows assessment of functional consequences on protein activity or interactions. Furthermore, modern techniques like proximity labeling and interactomics can further explore these protein interactions[89]. Dynamic and *in vivo* monitoring of phosphorylation includes metabolic labeling with radioactive phosphate, mobility shifts in Phos-tag gels, or genetically encoded FRET-based biosensors, providing temporal and spatial resolution of kinase activity in live cells. Together, these complementary strategies enable the identification, quantification, and functional dissection of phosphorylation events within complex signaling networks[89].

Looking ahead, the future of phosphoproteomics is poised for transformative change. It is anticipated that advancements in miniaturized platforms and microfluidic tools will make single-cell

phosphoproteomics more accessible, providing unprecedented insights into signaling dynamics and cellular heterogeneity[89]. Concurrently, the integration of artificial intelligence and deep learning is expected to improve sensitivity, site localization, and quantification precision, enabling the field to overcome persistent challenges in data analysis and move toward a more comprehensive understanding of the "dark phosphoproteome"—the vast majority of phosphosites with unknown functions[90].

## 1.3. The Eukaryotic Initiation Factor 6 (eIF6): A translation factor at the crossroads of ribosomal biogenesis and protein synthesis

Eukaryotic intiation factor 6 (eIF6) was first identified in wheat germ[105] and calf liver[106] based on its anti-association activity, whereby it binds to the 60S subunit and blocks its premature association with the 40S subunit. eIF6, also known as integrin β4 binding protein, p27BBP or β4 integrin interactor, is a remarkably conserved protein of 245 amino acids and is 77% identical between humans and yeast[40,107]. Its primary sequence is evolutionarily unique, with no identifiable homologs or conserved motifs[107]. The absence of gene duplication events suggests strong selective pressure to maintain tight regulation of protein abundance[107].

In humans, eIF6 is constitutively expressed *in vitro* but subject to stringent modulation *in vivo*, with expression levels differing across organs[107]. In general, eIF6 protein levels reflect the demand for ribosome production and the overall rate of translation. Proliferating cells display higher amounts of eIF6 compared to post-mitotic cells[108]. A rapid increase in eIF6 occurs during processes such as mast cell activation, disruption of the epidermal barrier, or liver regeneration[108]. However, there are exceptions – for example, neurons exhibit high eIF6 levels despite being post-mitotic[108]. Over the past three decades, cumulative research has progressively delineated eIF6 as a fundamental regulator of translation, endowed with multiple and context-dependent roles in cellular physiology.

### 1.3.1 eIF6 properties, structure and functions

The definitive cloning of eIF6 was achieved in 1997[40,109] . Biffo's group identified the protein through its ability to bind β4 integrin, naming it p27BBP (β4 Binding Protein)[40]. Subsequent studies revealed that eIF6 is a remarkably stable protein that associates with intermediate filaments *in vivo* [41] and can contribute to nuclear matrix formation *in vitro*[110].

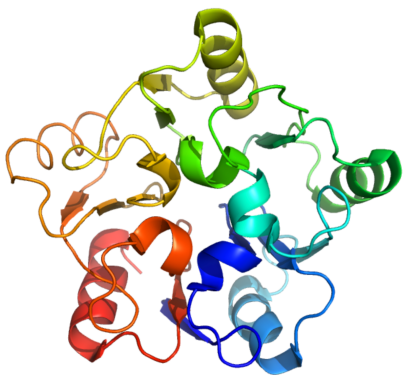

**Figure 11. X-ray crystallography-based model of eIF6 structure from S. cerevisiae**. A model of the eIF6 structure based on the X-ray crystallography results deposited at RCSB PDB under the identifier 1G62, from the work of Groft et al.[111] . Notably, the structure lacks the the aa 224-245 of the C-terminal tail.

Further mechanistic insights were reached thanks to X-ray crystallography that resolved its structure. It revealed a highly rigid protein organized into a cyclic fold, termed a pentein or *star-like* structure, composed of five α/β subdomains arranged around a five-fold pseudosymmetric axis[111]. The architecture encloses a cavity containing sixteen well-ordered water molecules with limited mobility[111] (**Figure 11**). In contrast, the semi-conserved carboxy-terminal region of eIF6 was not resolved in the crystal structure[111]; its structural flexibility suggests that it may contribute to regulatory functions. Supporting this view, the C-terminal region in mammalian cells harbors multiple phosphorylation sites, although their precise functional roles remain to be fully elucidated[108].

#### 1.3.1.1. Nucleolar eIF6 in ribosome biogenesis

Ribosome biogenesis takes place in the nucleolus, leading to the production of mature large and small subunits that are subsequently exported to the cytoplasm. The nucleolar localization of eIF6 supports its role in this process in both yeast and mammalian cells[41]. Three independent studies demonstrated that deletion of the yeast eIF6 homolog, Tif6, results in loss of 60S ribosomal subunits, a defect rescued by ectopic expression of human eIF6[41,112,113]. Supporting this genetic evidence, biochemical and morphological analyses identified eIF6 within complexes spanning from the 60S pre-ribosome to the nearly mature 60S subunit[114,115]. The molecular mechanism by which eIF6 regulates 60S biogenesis remains unclear. rRNA pulse-chase experiments revealed that depletion of Tif6 in yeast impairs pre-rRNA processing, resulting in reduced maturation of 25S and 5.8S rRNAs relative to 18S rRNA[116]. These findings suggest that eIF6 functions in 60S subunit biogenesis rather than solely in its stabilization. In mammals, most eIF6 is found in the cytoplasm, yet maintenance of a nuclear pool is essential to sustain ribosome biogenesis[41]. Partial downregulation of eIF6 (to ~50%) does not cause evident defects, as the nuclear pool is preserved, whereas complete depletion results in severe defects in ribosome biogenesis and the lethal pre-implantation phenotype of eIF6$^{-/-}$ knockout mice[117].

The nucleocytoplasmic shuttling of eIF6/Tif6 is regulated by phosphorylation. Two conserved C-terminal residues, Ser-174 and Ser-175, are critical for this process: substitution of both residues with alanine abolishes Tif6 phosphorylation, impairs cell viability, and results in constitutive nuclear localization of the mutant protein[116]. Consistently, casein kinase I was identified as the kinase responsible for phosphorylating eIF6 at Ser174/175[118]. However, it should be noted that no nuclear localization signal or nuclear export signal has been identified. Thus, phosphorylation of eIF6/Tif6 may regulate its interaction with partner proteins rather than directly controlling nuclear–cytoplasmic shuttling[72].

#### 1.3.1.2. Cytoplasmic eIF6 in translation

During canonical translation, 80S ribosomes terminate protein synthesis at stop codons, dissociate from the mRNA, and are recycled for subsequent rounds of translation. In the absence of mRNA, however, free 40S subunits may aberrantly associate with 60S subunits, giving rise to inactive 80S particles. These complexes are non-productive, suggesting the existence of dedicated factors that prevent inappropriate subunit joining. In this context, eIF6 was initially proposed to have an anti-

association activity necessary for the protein synthesis in the cytoplasm[71]. Consistently, biochemical assays demonstrated that eIF6 prevents the joining of 40S and 60S subunits in the absence of mRNA, thereby avoiding the accumulation of inactive 80S complexes and maintaining free ribosomal subunits available for for translation initiation[119]. Structural studies mapped the binding site of eIF6 on the 60S ribosomal subunit to the intersubunit face, at the 40S–60S interface, in *Archaea*[120], *S. cerevisiae*[121], and *Tetrahymena thermophila*[122]. Because eIF6 and the 40S subunit compete for the same binding region, their interactions with 60S are mutually exclusive. In fact, eIF6 interacts near the sarcin–ricin loop (SRL) and ribosomal proteins rpL23 and rpL24, creating a steric hindrance that blocks 40S recruitment[121,122]. This structural mechanism explains its ability to prevent de novo 80S formation, while leaving pre-assembled complexes[121] (**Figure 12**).

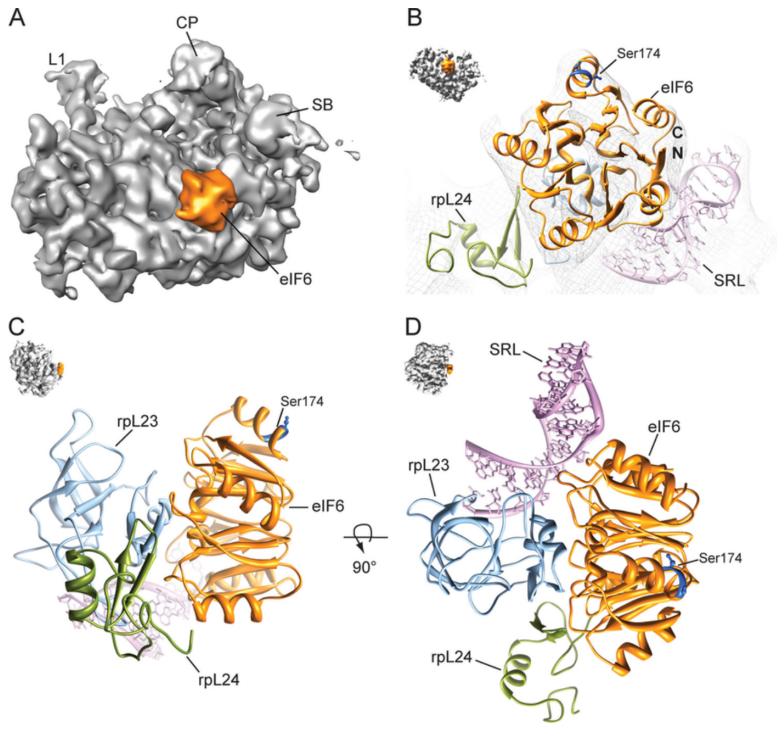


**Figure 12. Localization of eIF6 within the cryo-EM reconstruction of the 60S–eIF6 complex**. (**A**) Overall crown view of the 60S–eIF6 cryo-EM map, highlighting the position of eIF6 on the large ribosomal subunit. (**B**) Close-up view showing the atomic model of eIF6 fitted into the EM density (mesh), illustrating the accuracy of the structural assignment. (**C**, **D**) Detailed representation of the molecular environment at the eIF6 binding site on the 60S subunit, with interacting ribosomal proteins and RNA elements indicated. Thumbnails depict the respective orientations of each panel for reference. Color code: eIF6, orange; sarcin–ricin loop (SRL), magenta; ribosomal protein L23 (rpL23), blue; ribosomal protein L24 (rpL24), green; 60S ribosomal subunit, gray. Abbreviations: CP, central protuberance; L1, L1 stalk; SB, stalk base; N/C, N- and C-termini of eIF6, respectively[121].

Although early studies in yeast supported a role for eIF6 primarily in ribosome biogenesis[112,113], evidence in mammals points to a distinct and essential function in translation initiation. Complete loss of eIF6 results in embryonic lethality at the preimplantation stage, highlighting its indispensability[117]. In heterozygous mice, where eIF6 levels are reduced by half across all tissues, liver and adipose tissue mass is markedly decreased due to a reduced cell number and impaired progression through the $G_1$/S phase of the cell cycle[117]. Importantly, $eIF6^{+/-}$ cells retain sufficient nucleolar eIF6 to sustain normal ribosome biogenesis, indicating that the observed defects are not linked to ribosome assembly[117]. Instead, polysome profiling of hepatocytes revealed an accumulation of 80S monosomes and defective insulin-stimulated translation, while embryonic fibroblasts from

heterozygous mice recapitulated the impaired translation phenotype alongside delayed cell-cycle progression[117].

Together, these findings establish eIF6 as a key initiation factor associated with the 60S ribosomal subunit. By coupling extracellular cues, such as growth factors and insulin signaling, to the control of translation initiation, eIF6 emerges as a pivotal regulator at the interface between ribosome function, cell growth, and proliferation.

### 1.3.2. Models for eIF6 release

The central question in understanding eIF6's function is how it is released from the 60S subunit to permit translation. Two distinct models try to exaplain the molecular mechanisms for eIF6's release from the 60S subunit:

The primary and most comprehensively validated mechanism for eIF6 release is a GTP-dependent catalytic pathway involving the Shwachman-Bodian-Diamond syndrome (SBDS) protein and the GTPase Elongation factor-like 1 (EFL1). Cryo-EM and biochemical analyses suggest that SBDS and EFL1 cooperate to mediate the release of eIF6 from the 60S ribosomal subunit through a cofactor-dependent conformational switching mechanism[123]. Initially, EFL1 binds the ribosome in a GTP-bound, low-affinity state, forming direct contacts with both SBDS and eIF6[123]. In this configuration, EFL1 is inactive and cannot displace eIF6. Its subsequent interaction with SBDS induces conformational changes in both proteins facilitating the transition of EFL1 into a high-affinity, SRL-bound accommodated state[123]. In this conformation, EFL1 effectively competes with eIF6 for an overlapping binding site on the SRL, leading to eIF6 displacement from the ribosome. Following eIF6 eviction, GTP hydrolysis by EFL1 drives a conformational shift from the high-affinity accommodated state to a low-affinity state, promoting the dissociation of both EFL1 and SBDS from the 60S subunit and leaving it free for participation in translation[123].

Recent work has investigated how eIF6-bound 60S subunits are recycled into the pool of active ribosomes[124]. Under normal conditions, translation termination involves recognition of the stop codon by eRF1 and eRF3, followed by peptide release and dissociation of the 80S ribosome by the ATPase ABCE1, generating free 40S and 60S subunits[125]. While most 60S subunits can directly participate in new rounds of translation, those re-bound by eIF6 require an additional mechanism to be released. Evidence demonstrates that SBDS and the GTPase EFL1 serve this function as general eIF6 release factors, acting not only during the final cytoplasmic maturation of 60S but also during post-termination recycling[124]. Loss of either protein leads to persistent eIF6 retention on the intersubunit surface of 60S, blocking subunit joining and reducing global protein synthesis[124]. These findings support a model in which SBDS and EFL1 maintain ribosome homeostasis by coupling late 60S maturation with the recycling of post-termination subunits[124].

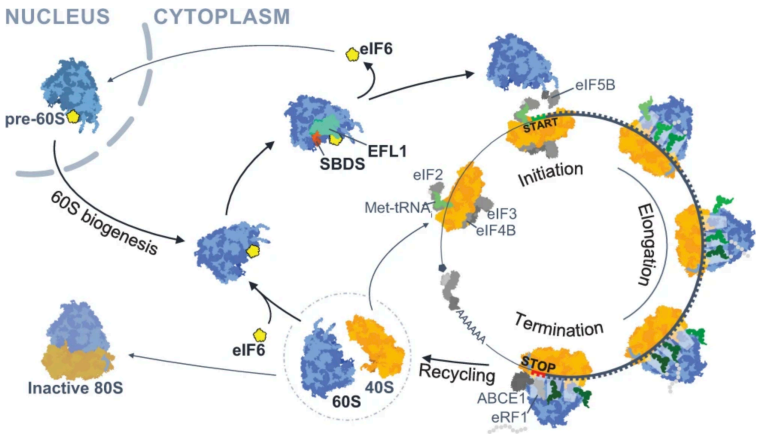


**Figure 13. Model of eIF6 rebinding as a bridge between ribosome maturation and translation.** eIF6 acts as a ribosome anti-association factor, maintaining both nascent pre-60S and recycled post-termination 60S subunits in a translationally inactive state. The coordinated action of SBDS and EFL1 promotes eIF6 release, thereby coupling 60S subunit maturation with ribosome recycling[124].

An alternative model proposes a phosphorylation-dependent mechanism for eIF6 release mediated by the Receptor for Activated C Kinase 1 (RACK1) and Protein Kinase C (PKC). This model suggests that RACK1, positioned on the head of the 40S subunit near the mRNA exit channel[126], functions as a scaffold that recruits active PKC to the small ribosomal subunit[119,127]. Upon activation, PKC translocates from endomembranes to the ribosome, where it comes into proximity with eIF6 bound to the 60S subunit and phosphorylates it on Ser235, thereby promoting its release[128]. Supporting this model, PMA-stimulated translation correlates with the phosphorylation of eIF6 at Serine 235. Notably, an eIF6 mutant in which Ser235 is replaced with alanine (Ser235Ala) cannot be released from the 60S subunit *in vitro*[119], thereby impairing growth factor–stimulated translation. This pathway links eIF6 release to cellular signaling, suggesting a mechanism for rapid, on-demand modulation of translation.

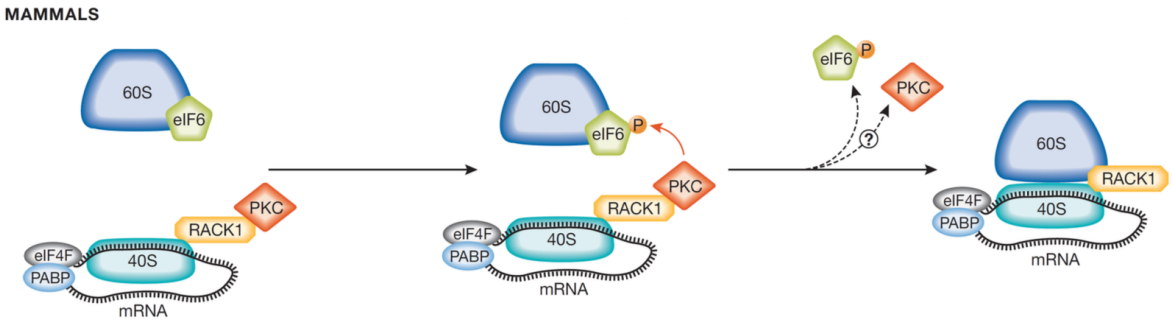


**Figure 14. Phosphorylation-mediated release of eIF6**. In this model, the dissociation of eIF6 from the 60S subunit is controlled by the RACK1–PKC complex. RACK1 recruits PKC to the 40S ribosomal subunit, where PKC phosphorylates eIF6 at Ser235, thereby promoting its release[107].

A recent work has identified a distinct, stress-responsive regulatory mechanism for eIF6 involving the kinases GSK3α and GSK3β. This pathway operates primarily during conditions of serum or nutrient starvation, and it differs from other regulatory mechanisms by its sequential phosphorylation pattern. Specifically, GSK3 acts on a multisite motif within the C-terminus of eIF6. The process begins with the phosphorylation of a key priming site, Serine 239 (Ser239). This initial

phosphorylation is crucial because it creates a binding site for GSK3, allowing the kinase to then phosphorylate other serine residues located just upstream of Ser239[129]. This sequential cascade of phosphorylation events modulates the properties of the eIF6 protein. The result is a functional shift in eIF6 dynamics: this multisite phosphorylation facilitates the protein's accumulation in the cytoplasm, where it can contribute to a global attenuation of protein synthesis. This inhibitory effect is a critical part of the cell's adaptive response to stress, enabling it to conserve energy and resources[129].

### 1.3.3. eIF6 in physiological and pathological contexts

In its physiological role, eIF6 is essential for coordinated ribosomal biogenesis and translation, which are fundamental for cell growth and proliferation[117]. In mammals, eIF6 is required for efficient translation initiation *in vivo*[117]. Studies in mice have shown that eIF6 deficiency impairs insulin-stimulated translation, leading to a metabolic shift that reduces lipid accumulation and preserves insulin sensitivity[117]. Specifically, eIF6 is a key regulator of glycolysis and fatty acid synthesis, acting in a cell-autonomous manner by controlling the translation of specific lipogenic transcription factors like C/EBPβ, C/EBPδ, and ATF4, which contain G/C-rich or uORF sequences in their 5' UTRs[130].

This translational regulation of metabolism appears to be a stable and coordinated response, resulting in a transcriptional program that favors reduced lipogenesis[130]. Interestingly, eIF6 haploinsufficient ($eIF6^{+/-}$) mice are leaner and have lower blood levels of cholesterol and triglycerides, without affecting glucose control or glycogen synthesis[117]. These mice are also protected from diet-induced obesity and hepatic steatosis[130]. The protective effect of eIF6 depletion on metabolism is, at least in part, mediated by maintaining an active mTORC1-eIF4F translational pathway that increases the expression of the transcription factor YY1, which is important for mitochondrial biogenesis and function[131].

The function of eIF6 extends beyond metabolism. During mouse embryonic development, eIF6 is essential for proper pre-implantation and is expressed early in blastocysts[117]. Mice lacking eIF6 ($eIF6^{-/-}$) are pre-implantation lethal while heterozygous ($eIF6^{+/-}$) mice are viable, but display a 50% reduction in eIF6 levels across all tissues, leading to reduced mass of hepatic and adipose tissues, fewer cells, and impaired G1/S cell cycle progression[117]. This indicates that a certain level of eIF6 is critical for normal development and proliferation.

The dysregulation of eIF6 is implicated in pathological conditions, including a rare genetic disorder and various cancers. Shwachman-Diamond Syndrome (SDS) is a recessive disorder characterized by bone marrow failure and a predisposition to hematological malignancies[132]. While most cases are caused by mutations in the SBDS gene, biallelic mutations in the EFL1 gene have also been identified[132]. The SBDS protein cooperates with the EFL1 GTPase to catalyze the release of eIF6 from the nascent 60S ribosomal subunit, a crucial step for activating translation[132]. In SDS patients with EFL1 mutations, eIF6 release is impaired, leading to a defect in ribosomal subunit joining and attenuated global protein synthesis[132]. This results in a clinical phenotype consistent with SDS, including hematological abnormalities, short stature, and exocrine pancreatic insufficiency. A key aspect of eIF6's role in this disease is its function as a ribosome anti-association factor that forms a physical barrier to subunit joining[132].

eIF6 is frequently overexpressed in a wide range of cancers, and its levels correlate with poor prognosis and advanced disease stages[133–135]. This is particularly true for highly invasive, high-grade tumors rather than early-stage cancers, suggesting that eIF6 upregulation is often a consequence of tumor progression rather than an initiating event[136]. For example, in oral squamous cell carcinoma (OSCC), high eIF6 expression enhances cell proliferation, migration, and invasion both in vitro and in vivo[134]. The pro-tumorigenic effects of eIF6 are linked to its role in regulating translation. In OSCC, eIF6 promotes tumor progression by activating the AKT signaling pathway[134]. Co-immunoprecipitation experiments revealed a direct physical interaction between eIF6 and the AKT protein in the cytoplasm of OSCC cells. This eIF6/AKT axis enhances the expression of cell cycle proteins (CDK2, CDK4, cyclin D1, D3, E1) and EMT markers, while decreasing epithelial markers like E-cadherin[134]. Similarly, in gastric carcinoma (GC), eIF6 knockdown inhibits cell proliferation, invasion, and promotes apoptosis[133].

In ovarian cancer and melanoma cell lines, eIF6 overexpression increases cell motility and invasiveness by modulating a network of membrane-associated proteins[133,135]. In this context, a key effector is cdc42, a small GTPase, whose protein levels and active form are increased upon eIF6 overexpression, without a corresponding increase in its mRNA levels[135]. This suggests that eIF6 primarily regulates cdc42 at a post-transcriptional level. Inhibiting cdc42 activity with a specific inhibitor, ML-141, significantly decreases eIF6-induced cell migration[135].

A recent study employed the eIF6-N106S mutation to dissect the role of eIF6's anti-association activity and its impact on cancer[136]. This mutation disrupts the interaction of eIF6 with the 60S subunit, thereby allowing premature 60S–40S joining and resulting in an accumulation of inactive 80S ribosomes[136]. Notably, while the anti-association function is impaired, 60S biogenesis remains largely unaffected, as total 60S levels are preserved. The excess of vacant 80S particles leads to a global reduction in translation, with particularly severe effects during mitosis. Functionally, the eIF6-N106S mutation markedly restricts the invasive capacity of cancer cells in vitro and in xenograft models[136]. This anti-invasive effect correlates with reduced translational efficiency of key pro-metastatic transcripts, including *VASP* and *NFIB*, whose protein levels are nearly abolished in mutant cells compared to wild type[136].

Moreover, eIF6 levels significantly increase throughout the progression from normal liver to Non-Alcoholic Fatty Liver Disease (NAFLD) and, subsequently, to hepatocellular carcinoma (HCC)[131]. High eIF6 levels are positively correlated with lipid accumulation, disease progression, and decreased patient survival in NAFLD and HCC[131]. In a mouse model of diet- and chemical-induced HCC, eIF6 haploinsufficiency delayed the formation and growth of tumor nodules, reduced liver damage (lower ALT/AST levels), and decreased fibrosis and proliferation markers (Ki-67)[131]. In vitro, eIF6 depletion in hepatocytes reduces de novo fatty acid synthesis and intracellular lipid content while increasing mitochondrial fatty acid oxidation (FAO)[131]. Additionally, eIF6 depletion or treatment with pharmacological inhibitors of eIF6-60S binding, such as eIFsixty-1, eIFsixty-4, and eIFsixty-6, significantly reduced the growth of HCC spheroids[137]. Clinically, high eIF6 mRNA levels are correlated with reduced overall survival in patients with primary liver cancer, and tumors from patients with metastases show even higher eIF6 mRNA levels. This suggests that eIF6 can serve as a prognostic biomarker for HCC[131].

Overall, current evidence indicates that eIF6 is a promising therapeutic target in several cancers[133,134,137]. Notably, mice with eIF6 haploinsufficiency display resistance to tumor development while maintaining normal growth, pointing to a potentially favorable therapeutic window. Developing selective eIF6 inhibitors that fine-tune its activity rather than fully suppressing it represents an attractive direction for future research[137].

## 1.4. Phosphatases: understudied regulators of translational control

Protein phosphatases (PPs) are a class of essential enzymes that catalyze the removal of phosphate groups from protein substrates, a process known as dephosphorylation[138]. This mechanism, along with the opposing activity of protein kinases (PKs) which add phosphate groups, constitutes a reversible molecular switch that regulates almost all cellular processes. The dynamic equilibrium between phosphorylation and dephosphorylation is fundamental for maintaining proper cellular functions and signaling pathways and it is estimated that up to a third of the cellular proteome is regulated by this post-translational modification at any given time[138].

From a genomic perspective, the human genome encodes roughly 500 kinases, including about 90 tyrosine kinases and more than 400 serine/threonine kinases.[139]Despite their diversity, they share a conserved three-dimensional architecture consisting of an N-terminal lobe, primarily composed of β-sheets, that binds ATP, and a predominantly α-helical C-terminal lobe that interacts with the peptide substrate. [140] Upon substrate binding, kinases undergo conformational changes, and the rate-limiting step is typically the rapid phosphotransfer and product release[140]. This structural and mechanistic uniformity makes the biochemistry of the kinase superfamily relatively straightforward. Unlike protein kinases, which derive from a common evolutionary ancestor, protein phosphatases have emerged from several independent families that differ both in structure and catalytic mechanism[141].Approximately 140 phosphatase genes have been identified, including ~30 catalytic subunits of the protein serine/threonine phosphatase (PSP) family and 107 members of the protein tyrosine phosphatase (PTP) superfamily[142]. The apparent disparity between the number of protein kinases and protein serine/threonine phosphatases can be partly explained by looking at how many genes encoding PSP regulatory subunits, which generates a comparable complexity of phosphatase holoenzymes relative to the serine/threonine kinase superfamily[141]. Far from being simple housekeeping enzymes, phosphatases are subject to regulatory mechanisms as precise and stringent as those controlling kinases[141].

Historically, research in the field of signal transduction has focused predominantly on kinases, which were perceived as the main “switches” of cellular signaling[143]. Phosphatases, in contrast, were mistakenly considered simple “housekeeping enzymes” with limited specificity and a role of indiscriminate signal deactivation. Advances over the last decades have overturned this perspective, demonstrating that phosphatases are not merely negative regulators but active players – and in some contexts even drivers – in diverse physiological and pathological processes[144]. This shift has been reinforced by the discovery of disease-associated mutations in phosphatase genes, which has sparked renewed interest in their study and positioned them as promising therapeutic targets[145].
Despite progress, studying phosphatases remains challenging. Differently from kinases, whose activity can be readily assayed using radiolabeled ATP, phosphatase assays require purified, phosphorylated substrates that are often difficult to obtain in sufficient quantity and quality. Early

work was further hindered by heterogeneous enzyme preparations, susceptibility to proteolysis, and reliance on artificial substrates, which were hampered by poor solubility, low phosphorylation stoichiometry, and non-linear kinetics of dephosphorylation[140].

### 1.4.1. Classification of protein phosphatases

The human protein phosphatase superfamily is classified based on the amino acid residue they dephosphorylate.The two main macro-families are the Serine/Threonine (Ser/Thr) phosphatases and the Tyrosine (Tyr) phosphatases[140].In turn, these are divided into distinct subfamilies, based on sequence, structure and catalytic function[140] (**Figure 16**). The PSPs are divided in three families: the phosphoprotein phosphatase (PPP) family, the $Mg^{2+}$/$Mn^{2+}$-dependent phosphatases (PPM), and the aspartate-based protein phosphatase (FCP/SCP)[146]. Representative members of the PPP family include PP1, PP2A, PP2B (PP3 or calcineurin), PP4, PP5, PP6 and PP7; PPM family include PP2C and pyruvate dehydrogenase phosphatase; and FCP/SCP family include Scp1 and Fcp1[146].

In contrast, the PTP superfamily is classified into four major classes (I–IV), primarily based on domain architecture and catalytic domain homology (Figure). Among these, Class I is the largest and encompasses both the classical PTPs and the dual-specificity phosphatases (DUSPs). DUSPs include enzymes that act on serine, threonine, and tyrosine residues, as well as specialized members that target carbohydrates and lipids[147].

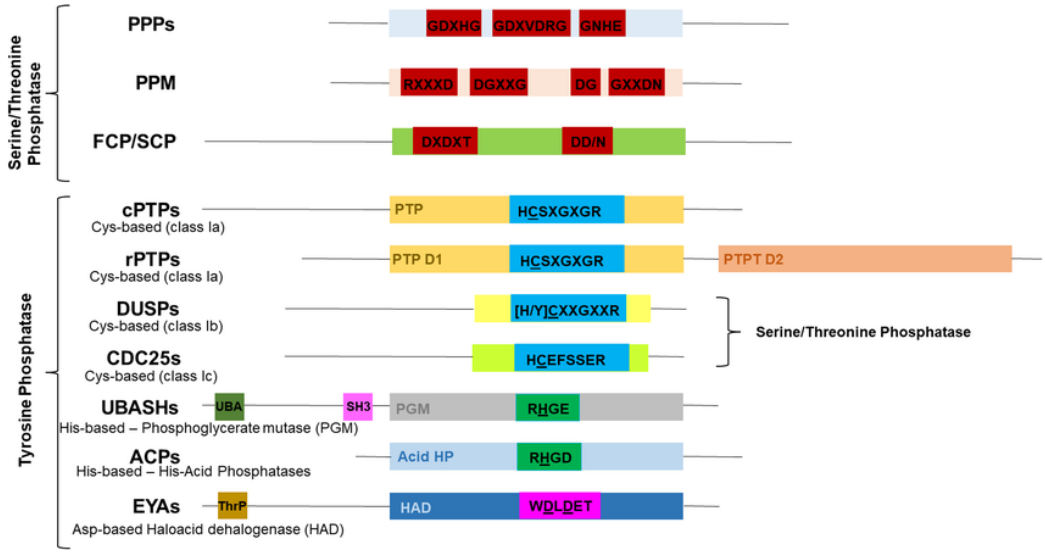


**Figure 15. Schematic representation of the domain architecture of major serine/threonine and tyrosine phosphatase families.** Serine/threonine phosphatases (PPPs, PPMs, FCP/SCP) and tyrosine phosphatases (cPTPs, rPTPs, DUSPs, CDC25s, UBASHs, ACPs, EYAs) are shown with their characteristic catalytic and regulatory domains highlighted in different colors. Conserved sequence motifs within each domain are indicated (e.g., DXDXT, HCSXGXXGR, RHGD), illustrating the structural basis for substrate specificity and catalytic activity[146].

### 1.4.2. Phosphatases in translational control

Although translational control has classically been attributed to kinase-driven phosphorylation events, the opposing activity of phosphatases have long remained underexplored. Neverthless, studies on the serine/threonine phosphatases PP1 and PP2A have revealed that these enzymes exert pivotal functions in modulating translation dynamics.

One of the most studied mechanisms for translation regulation is the phosphorylation of eukaryotic initiation factor 2α. Under stress conditions (e.g., amino acid deprivation, heat shock, viral infections), specific kinases (GCN2, HRI, PKR, PERK) phosphorylate eIF2α on Ser51, inhibiting global protein synthesis[21]. This leads to energy conservation and the reprogramming of gene expression to alleviate stress[19].

The reversal of this process is crucial for restoring homeostasis. The dephosphorylation of eIF2α is catalyzed by PP1, which is recruited by specialized targeting subunits: the GADD34 protein (Growth Arrest and DNA Damage-inducible protein 34) and the CReP protein (constitutive repressor of eIF2α phosphorylation)[19]. The expression of GADD34 is induced precisely by the eIF2α phosphorylation it reverses, creating a fundamental negative feedback loop that restores normal protein synthesis once stress subsides[19].This mechanism is more than a simple switch off; it represents a biological "restorative brake," where the cell not only stops in response to stress but actively builds the system needed to release the brake and return to a basal state.

The connection between eIF2 and PP1 is further highlighted by *in vitro* experiments that demonstrated an interaction between eIF2β and PP1. It has been suggested that eIF2β may be a PP1 substrate or function as a substrate-specifier, bringing the phosphatase into proximity with the 43S preinitiation complexes to dephosphorylate other components, though this hypothesis requires further validation[148].
The activity of the eIF2B complex, a key guanine exchange factor, is negatively regulated by phosphorylation on its ε-subunit (eIF2Bε) at Ser535 and Ser539. While early studies suggested PP1 was responsible for dephosphorylating these sites[149], more recent evidence points to PP2A as an eIF2B phosphatase[150].

A key control point in translation initiation is the eIF4F complex, whose components are regulated by phosphatases.

- **eIF4E:** The cap-binding protein eIF4E is phosphorylated at Ser209 by MAP kinase-interacting kinases (MNK1/MNK2).While not essential for normal development[151], this phosphorylation enhances the transformation potential of eIF4E in cancers, highlighting its functional importance under pathological conditions[152]. Evidence suggests that PP2A acts as the phosphatase for eIF4E. Treatment with the PP2A activator FTY720 strongly decreased Ser209 phosphorylation, and *in vitro* assays showed that PP2A can directly dephosphorylate both MNK1 and eIF4E[153].
- **eIF4B:** The activity of eIF4B, which unwinds mRNA secondary structures, is regulated by phosphorylation on several residues, including Ser406. In the brain, neuronal stimulation triggers the rapid dephosphorylation of eIF4B at Ser406 by PP2A. This dephosphorylation frees eIF4B from non-protein-coding RNAs, promoting neuron-specific translation[154].
- **4E-BP:** A major repressor of cap-dependent translation is 4E-BP, which, in its hypo-phosphorylated form, sequesters eIF4E. Its phosphorylation occurs in a hierarchical manner: Thr37 and Thr46 are phosphorylated first, followed by Thr70 and finally Ser65[155]. Only fully phosphorylated 4E-BP is unable to bind eIF4E[155]. Some evidence points to PP2A as the primary phosphatase for 4E-BP, though a direct interaction has yet to be demonstrated[156]. However,

other phosphatases, such as the PPM1 family member PPM1G, have also been implicated in 4E-BP dephosphorylation[157].

A growing body of evidence suggests they also act as a "speed control" mechanism during the later stages of protein synthesis. For instance, PP2A can counteract the phosphorylation of eukaryotic elongation factor 2 (eEF2), which is responsible for slowing down the elongation rate of protein synthesis[158]. Similarly, PP1 has been shown to dephosphorylate another elongation factor, eEF1BδL, in response to cellular stress, which not only regulates elongation but also links this process to transcriptional activity, demonstrating a sophisticated coordination between different cellular functions[159].

In a less understood but emerging area of research, phosphatases may also play a role in the final stage of protein synthesis: termination. The eukaryotic release factor 1 (eRF1), which recognizes stop codons, has been found to physically associate with PP2A and target it to ribosomes. While the exact functional consequence of this interaction is still under investigation, it suggests that PP2A may dephosphorylate a key ribosomal or termination factor that is brought into close proximity by eRF1, a process that is crucial for the ribosome's recycling and for starting new rounds of translation[160]. This indicates a complex and still largely unexplored role for phosphatases in the final steps of protein synthesis.

In addition to their regulatory influence on translation, phosphatases may also directly contribute to ribosome biogenesis regulation. Despite the limited number of studies exploring phosphatases in ribosome biogenesis, current evidence highlights a particularly significant role for PP1, one of the major serine/threonine phosphatases. A significant pool of PP1, particularly the β and γ isoforms, accumulates in the nucleolus, where it accounts for a large fraction of the Serine/Threonine phosphatase activity in this structure[161]. The RRP1B protein acts as a nucleolar targeting subunit for PP1, binding specifically to the PP1β and PP1γ isoforms and localizing to the pre-60S ribosomal subunit processing complex[161]. This positions PP1 in a prime location to modulate the structural assembly of these particles through reversible phosphorylation events[161]. Similarly, the nucleolar protein Nom1 interacts with and directs PP1α into the nucleolus. Studies in zebrafish demonstrated that defects in the Nom1 gene lead to severe alterations in pre-rRNA processing and impaired proliferation of progenitor cells, underscoring the vital, site-specific role of PP1 in this process[162].

Moreover, studies on the yeast *Saccharomyces cerevisiae* have established that Yvh1, a dual-specificity phosphatase (capable of acting on tyrosine, serine, and threonine residues) plays a critical role in the final stage of 60S ribosomal subunit maturation. Specifically, Yvh1 is essential for the release of the accessory factor Mrt4 from pre-60S ribosomes in the nucleus. This step is mandatory to allow for the subsequent loading of the ribosomal protein P0, which is a fundamental component of the ribosomal stalk. The absence of Yvh1 leads to a defect in Mrt4 release, which in turn causes problems in rRNA processing and the export of pre-ribosomes from the nucleus, compromising the production of functional ribosomes[163,164]. Its human homologue, hYVH1 or DUSP12, is highly conserved and has been shown that it associates with the 60S ribosomal subunit. Further mechanistic evidence revealed how the phosphorylation of hYVH1 by the Src kinase influences its cellular localization, promoting its binding to the 60S subunit. This interaction not only increases translational efficiency but also helps reduce the formation of "stalled intermediates" in ribosomal biogenesis[165].

## 1.5. DUSP12: A pleiotropic and understudied Dual-Specificity Phosphatase

The dual specific phosphatase 12 (DUSP12) was first identified through the cloning and characterization of the yeast VH1-related phosphatase (YVH1) by Guan and Dixon in 1992[166]. Early studies revealed that YVH1 mRNA levels were strongly upregulated under conditions of nitrogen deprivation and low temperature stress. Functional analyses further demonstrated that deletion of the *yvh1* gene led to slow growth, impaired glycogen accumulation, and defects in spore maturation, underscoring its physiological significance in yeast[166]. Building on these findings, the human ortholog, commonly referred to as hYVH1, was subsequently identified and shown to share approximately 31% sequence identity with yeast YVH1[167]. Notably, this gene is highly conserved across eukaryotes, from yeast to humans, with only a single copy present in most species[168]. Beyond its evolutionary conservation, hYVH1 gained additional interest when gene amplification events were reported in several cancers, including retinoblastoma[169], liposarcoma[170], and intracranial ependymoma[170]. Taken together, the genetic evidence from yeast and the emerging links to human disease emphasized the importance of investigating the structural features and biological functions of DUSP12.

### 1.5.1. DUSP12 structural domains and enzymatic activity

DUSP12 belongs to dual-specificity phosphatases family, a subgroup within the type I cysteine-based PTP superfamily, whose members have the ability to remove phosphate groups from both tyrosine and serine/threonine residues on the same substrate[143]. The DUSP subfamily, comprising 63 genes, encompasses several distinct classes, including the phosphothreonine (pThr)/phosphotyrosine (pTyr)-specific mitogen-activated protein kinase phosphatases (MKPs); the phosphoserine (pSer)-targeting slingshots; and the pTyr-specific phosphatases of regenerating liver (PRLs). Additional members include the pSer/pThr-directed CDC14 phosphatases, the PTEN family, the myotubularins, which act on phosphatidylinositol-3-phosphate and the inositol 4-phosphatases[143]. Within the DUSP family, the atypical DUSPs represent a intriguing subgroup; they share some features with MKPs but notably lack the N-terminal CH2 (Cdc25-homology 2) domain which contains kinase interaction motifs (KIMs) essential for binding MAPKs and facilitating substrate recognition and efficient dephosphorylation[143,171] (**Figure 17**).

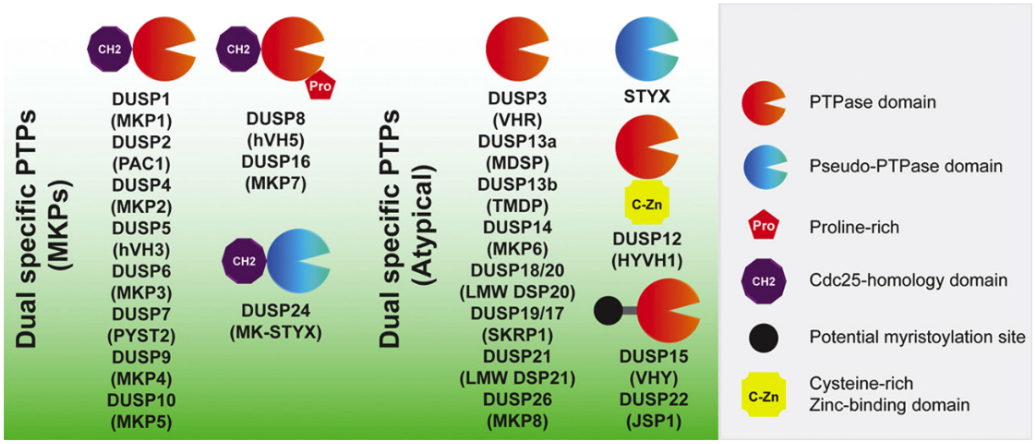

**Figure 16. Schematic view rapresentig the main differences between typical and atypical DUSPs.** Atypical DUSPs contain the consensus DUSP catalytic domain, but lack the N-terminal CH2 domain found in MKPs[172].

DUSP12 is composed of two distinct functional domains: a catalytic N-terminal phosphatase domain and a C-terminal zinc-binding domain (ZBD). The catalytic domain, which spans residues 1-175, contains the highly conserved H**CX$_5$R**(S/T) motif, a hallmark of Class I protein tyrosine phosphatases (PTPs). This conserved sequence establishes a defined microenvironment that lowers the pKa of the catalytic cysteine, thereby enabling it to act as a nucleophile on the phosphorylated substrate. A catalytic acid subsequently donates a proton to the leaving group, promoting the release of the dephosphorylated product from the active site of the phosphatase and leading to the formation of a thiol–phosphate enzyme intermediate[173]. In the second step of the reaction, an ordered water molecule is deprotonated by a catalytic base, generating a hydroxide ion that performs a nucleophilic attack on the thiol–phosphate[173] intermediate. This results in the release of phosphoric acid as the second product and the regeneration of the PTP[173].
The ZBD, located at the C-terminus (residues 220-340), is a unique and defining feature of the protein, making DUSP12 the only known PTP to contain such a domain[167]. These two domains are connected by an intrinsically disordered region (residues 176-219)[174]. The ZBD contains 7 cysteins and 1 histidine conserved residues and is capable of binding 2 moles of zinc per mole of protein[167] (**Figure 18**). It has been established to be a redox sensor, capable of forming intramolecular disulfide bonds under oxidative stress[175]. This unique capacity allows the ZBD to protect the catalytic cysteine from irreversible inactivation during severe cellular stress, a key survival mechanism[175]. Notably, only the phosphatase domain of hYVH1 has had its crystal structure solved[174].

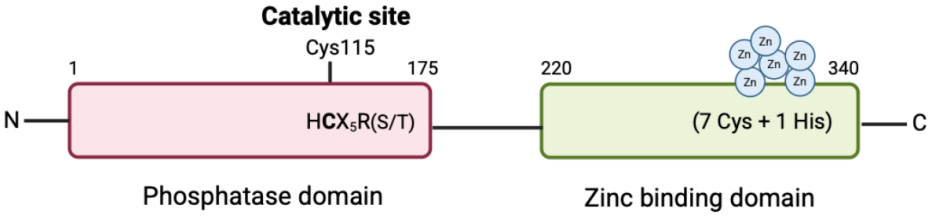


**Figure 17. Schematic illustration of the dicotomic structure of DUSP12.** The N-terminal phosphatase domain (residues 1-175) contains the highly conserved CX5R motif, where the catalytic Cystein is in position 115. The C-terminal zinc-binding domain (residues 220-340) indicates the 7 cysteines and 1 histidine residue, capable of binding 2 moles of zinc/mole of protein (Created with biorender.com).

Early functional studies have identified DUSP12 as a binding partner of glucokinase and demonstrated that it can dephosphorylate glucokinase *in vitro*[176]. Interestingly, while GST-tagged DUSP12 shows specificity for phosphotyrosine residues, glucokinase dephosphorylation occurs predominantly on phosphoserine residues. Moreover, efficient dephosphorylation *in vitro* requires high concentrations of DUSP12[176], suggesting that additional protein partners may be necessary *in vivo* to enhance its phosphatase activity. However, it should be noted that no direct substrate has been firmly established to date.

### 1.5.2. Early characterization in yeast and evolutionary conservation

Yvh1 was first identified in *Saccharomyces cerevisiae* in 1992 based on its sequence homology to the vaccinia virus VH1 phosphatase, representing one of the earliest characterized eukaryotic dual-specificity phosphatases (DSPs)[166]. By 1996, Yvh1 had been described as a nitrogen-starvation–responsive phosphatase[177], and deletion of YVH1(yvh1Δ) was associated with a broad spectrum of

phenotypes, including slow growth, defective glycogen accumulation, impaired sporulation, heat sensitivity, and difficulties entering stationary phase[178]. These pleiotropic defects initially suggested a role in stress-response regulation, potentially linked to cAMP–PKA signaling or sporulation-associated kinases such as Mck1, implying that Yvh1 influenced nutrient-sensing and kinase-based pathways[178].

A major breakthrough in the field occurred in 2009, when two independent studies demonstrated that Yvh1 functions as a dedicated ribosome biogenesis factor, essential for a late cytoplasmic maturation step of the 60S ribosomal subunit[163,179]. Specifically, Yvh1 mediates the release of the placeholder protein Mrt4 and facilitates the incorporation of the ribosomal P-stalk base protein P0 (uL10)[179]. This exchange is indispensable for assembly of the complete P-stalk, which serves as docking hub that recruits and activates translational GTPases such as elongation factor 2 (eEF2)[180]. Without a properly assembled P-stalk, ribosomes cannot engage efficiently with the translation machinery, producing widespread defects in growth, metabolism, and stress response. In *Δyvh1* cells, Mrt4 remains abnormally bound to cytoplasmic pre-60S particles, P0 incorporation fails, and halfmer polysomes accumulate[179].

Crucially, a gain-of-function Mrt4 mutant (G68D or G68E) fully restores normal growth and polysome profiles in *Δ*yvh1 cells. This single amino-acid substitution, which maps to the Mrt4–25S rRNA interaction surface, is predicted to weaken Mrt4's affinity for the pre-60S particle, thereby enabling its spontaneous dissociation and allowing P0 incorporation. The rescued phenotype induced by this Mrt4 mutation provided compelling evidence that Yvh1's essential role is to promote Mrt4 release[179]. Domain-mapping studies showed that the C-terminal zinc-binding domain (ZBD) of Yvh1 is required for its function in 60S maturation, whereas the N-terminal DSP domain is dispensable[163,179].

Building on these discoveries, Sugiyama et al. proposed that all previously reported *Δyvh1* phenotypes –including impaired growth, sporulation failure, glycogen dysregulation, and stress sensitivity– are indirect consequences of a single primary defect: the failure to assemble translationally competent 60S subunits due to defective P-stalk formation. The complete suppression of all *Δyvh1* phenotypes by the Mrt4-G68D mutation strongly supported this unified "ribosome-assembly-first" model[181]. As translational competency is required for most cellular processes, and life itself, it is not surprising that defects in ribosome assembly would display pleiotropic phenotypes on many cellular pathways.

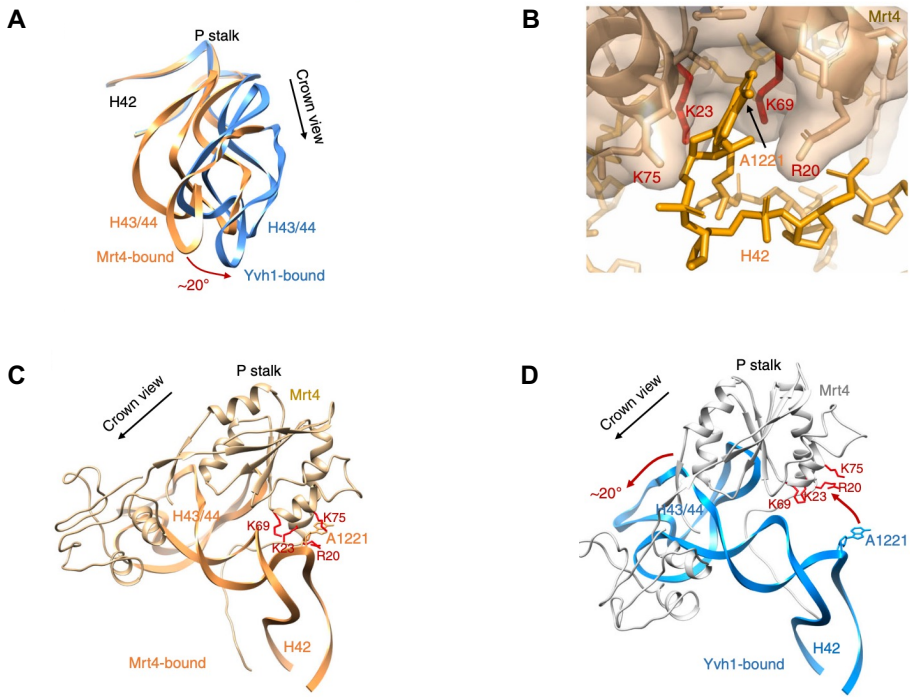


**Figure 18. Yvh1 forces the release of Mrt4 via allosteric rearrangement of the P-stalk.** Structural mechanism of Mrt4 displacement revealed by cryo-EM analysis of ribosomal pre-subunits. (**A**) Comparison of the P-stalk rRNA helices (H42−H44) in the Mrt4-bound state (shown in orange) and the Yvh1-bound state (shown in blue). The Yvh1-induced bending of H42 and the ~20° rotation of the H43/H44/Rpl12 tip are visible. (**B**) Close-up view of Mrt4 (cartoon and transparent surface) docked onto the P-stalk rRNA. The critical contact residue A1221 of H42 is shown inserted into a complementary pocket within Mrt4. (**C**) Mrt4 bound to the P-stalk RNA in the initial state. Key Mrt4 residues involved in the stabilizing interaction with H42 (including A1221) are indicated. (**D**) Mrt4 from the initial state is docked onto the structure of the Yvh1-bound particle. The visualization highlights the significant spatial retraction of the Mrt4 binding pocket away from the anchor point A1221 on H42 due to the Yvh1-induced conformational change, explaining the loss of affinity and subsequent dissociation (Modified from Zhou et al., 2019[182]).

Subsequent structural and biochemical studies further refined the mechanistic model. The Yvh1 ZBD binds near the base of the P-stalk, engaging rRNA helices H43/H44 and contacting the sarcin–ricin loop (SRL)[1], a universally conserved rRNA element essential for stimulating the GTPase activity of translational factors[180]. Upon binding, the ZBD inserts between the nascent P-stalk and the pre-60S core, inducing an allosteric rearrangement on the surrounding rRNA helices. This conformational change specifically bends helix H42 –the stem of the stalk– which propagates a ~20° rigid-body rotation of the H43/H44 region and its associated protein, Rpl12 (uL11)[182], a conserved component of the stalk base (**Fig. 18A**). This coordinated movement effectively destabilizes the Mrt4-rRNA interface by retracting the Mrt4 binding pocket from critical contacts, including A1221 on H42 (**Fig. 18B**), thereby weakening Mrt4's affinity for the pre-60S particle[182]. The resulting loss of stabilizing interactions promotes Mrt4 dissociation, thereby enabling the subsequent loading of the permanent stalk proteins, P0, zP1 and P2. Thus, Yvh1 acts as a structural "molecular wedge" that triggers a key remodeling event by allosterically reshaping the the Mrt4 binding site to license P-stalk assembly[182] (**Fig. 18C, D**).

Notably, earlier findings introduced an additional layer of complexity to this model. Yvh1 was shown to physically interact with the nucleolar assembly factor Nop7 (Yph1), with the interaction mapping to the Yvh1 DSP domain and the BRCT domain of Nop7[183]. This led to the proposal that Nop7 might be a Yvh1 substrate or a regulatory partner modulating its activity[183]. Although this model has largely

been superseded by the established Mrt4-release mechanism, this interaction suggests that Yvh1 may engage early nucleolar assembly factors transiently or under specific physiological conditions.

The Mrt4–P0 exchange is also highly conserved. Evidence produced in HeLa cells shown that the Yvh1 orthologue DUSP12 localizes to late pre-60S particles and is required for the release of human Mrt4 orthologue MRTO4 and subsequent incorporation of P0. DUSP12 depletion causes cytoplasmic retention of MRTO4-bound intermediates, reduced levels of mature 60S subunits, and defective polysome formation[179]. Remarkably, human DUSP12 can complement *Δyvh1* yeast cells, demonstrating strong functional conservation across eukaryotes[179]. Like Yvh1, DUSP12 possesses a dispensable DSP domain and an essential ZBD; however, evidence suggests that DUSP12 may itself be subject to regulatory phosphorylation[165], raising the possibility that higher eukaryotes modulate P-stalk maturation in response to signaling states, stress conditions, or developmental cues.

### 1.5.3. Open questions in Yvh1/DUSP12-mediated ribosome assembly

Despite significant progress in defining the role of Yvh1/DUSP12 in ribosome assembly, several important questions remain unresolved. The precise timing and subcellular location of the Mrt4–P0 exchange are still debated, with evidence supporting both cytoplasmic[163] and nuclear contributions[179], consistent with the fact that Yvh1 is a shuttling protein. Moreover, Yvh1 fails to displace Mrt4 in simplified *in vitro* systems[179], suggesting that additional cofactors or specific pre-60S conformations are required, *in vivo*. Recent cryo-EM analyses further reveal unexpected heterogeneity among late pre-60S particles, implying that multiple, condition-dependent routes to P-stalk assembly may exist. This hypothesis is reinforced by stechiometric challenges in the current model. Given that a yeast cell produces an estimated 200,000 ribosomes per generation, but contains only ~ 4,000 Yvh1 molecules and ~14,000 Mrt4 molecules, a purely Yvh1-dependent mechanism for the removal of every single Mrt4 molecule appears kinetically limiting[184]. This numerical disparity suggests that other factors or less Yvh1-intensive pathways must contribute significantly to the overall efficiency of P-stalk assembly in the cell.

In this context, in mammalian systems, an additional regulatory layer – possibly involving phosphorylation-dependent DUSP12 recruitment – may couple ribosome assembly to broader signaling and physiological states[165]. This places DUSP12 at the intersection between ribosome biogenesis and the emerging concept of ribosomal heterogeneity, the idea that ribosomes with distinct protein or rRNA compositions and modifications can preferentially translate specific mRNAs[185]. Increasing evidence suggests that such compositional diversity can arise in response to environmental cues, stress, or developmental programs, and that heterogeneous ribosomes may exhibit differential translational output in both yeast and human cells[186]. The biomedical implications of this possibility are substantial; since all steps of protein synthesis are susceptible to dysregulation during tumorigenesis, compositionally altered ribosomes resulting from impaired DUSP12 function may influence oncogenic translation programs. Supporting this idea, DUSP12 overexpression has been identified as a candidate oncogenic event in human liposarcomas[170]. Moreover, given that many ribosomopathies arise from alteration in the structure or function of ribosomal components[187], even partial impairment of DUSP12 activity could exacerbate or modulate existing pathogenic mutations. Thus, a deeper mechanistic understanding of Yvh1/DUSP12 not only advances fundamental ribosome biology but also provides a framework for exploring how targeted alterations in ribosomal

composition contribute to human disease. Collectively, these unresolved issues make Yvh1/DUSP12 a compelling target for ongoing structural, biochemical, and cell-biological investigation.

### 1.5.4. DUSP12 functions in human cells

Building on the established conservation of the Mrt4-release mechanism, studies in human cells have revealed that the Yvh1 orthologue DUSP12 not only retains its central role in large ribosomal subunit biogenesis[188], but has also acquired additional layers of regulation and functions that extend beyond P-stalk assembly.

A defining feature of DUSP12 function is its ability to shuttle between nucleus and cytoplasm. Recent work by DaDalt et al. showed that Src phosphorylates DUSP12 at Tyr179, and this modification drives its relocalization toward the nucleus, increasing its association with nascent 60S subunits, thereby promoting translational fitness under pro-growth conditions[189]. Conversely, when Src activity is low and – thus DUSP12 is less phosphorylated – DUSP12 remains predominantly cytoplasmic, where it associates with stress granules and contributes to their disassembly during recovery from stress. Through this bidirectional localization, DUSP12 effectively links growth signals to translational homeostasis: phosphorylation promotes its nuclear engagement in ribosome production, whereas reduced phosphorylation permits its involvement in stress-granule–mediated mRNA handling[189].

In the cytoplasm, DUSP12 can interact with a broad spectrum of messenger ribonucleoprotein particles (mRNPs) and, under arsenite-induced stress, co-localizes with translational regulators such as Y-box-binding protein 1 (YB-1) and fragile X mental retardation protein (FMRP), both key players in translational repression and stress-granule dynamics. DUSP12 depletion delays stress-granule disassembly during recovery, indicating a central role in restoring translation after stress[188]. This cytoprotective role is further supported by DUSP12's interaction with the chaperone Hsp70, which enhances DUSP12-mediated resistance to cell death triggered by heat shock and redox-sensitive pathways, including Fas signaling and hydrogen peroxide exposure [190]. Notably, this prosurvival activity depends on both the catalytic domain and the zinc-binding domain (ZBD) and is specific to redox-driven apoptotic pathways, as DUSP12 fails to protect against cisplatin-induced, DNA-damage–mediated apoptosis[191]. Together with evidence of *yvh1* amplification in several tumors, these observations suggest that DUSP12 may help cancer cells endure adverse microenvironmental conditions and sustain uncontrolled growth.

Beyond its role in stress responses, DUSP12 actively regulates cell cycle. Its overexpression increases the percentage of cells in the $G_2$/M phase, whereas its silencing causes cells to arrest in the $G_0/G_1$ phases[192]. A recent study identifies ZPR9 as a DUSP12-interacting protein and clarify a mechanistic link between DUSP12, mitotic control, and cell survival[193]. Functionally, DUSP12 dephosphorylates ZPR9 at Ser143, a modification required to prevent ZPR9-driven mitotic defects and apoptosis. Loss of DUSP12 results in pre-metaphase arrest and stress-induced cell death, while overexpression of ZPR9 alone triggers apoptosis. Strikingly, co-expression of DUSP12 mitigates ZPR9-induced cytotoxicity, highlighting a coordinated regulatory axis that integrates mitosis and cell fate. These findings also provide a rationale for the recurrent amplification and overexpression of DUSP12 observed in several cancers, where its presence often correlates with disease progression. Consistent

with this, DUSP12 overexpression was shown to protect cells from taxol-induced apoptosis, raising the possibility that tumors exploit DUSP12 to resist chemotherapeutic stress. Accordingly, the generation of selective DUSP12 inhibitors will be instrumental in testing whether disrupting this survival node can tilt the balance toward apoptosis in malignant cells, potentially augmenting the efficacy of established anticancer regimens[193].

The indispensable nature of DUSP12 in higher eukaryotes is underscored by phenotypic data: in yeast, *yvh1* deletion is non-lethal and results only in slow-growth[166], which can be rescued by human hYVh1[167], whereas homozygous *Dusp12* loss in mice triggers embryonic lethality prior to organogenesis[194], highlighting the acquisition of essential, non-redundant functions in mammalian development. Interestingly, heterozygous animals display additional phenotypic alterations, including defects in sensorimotor gating, abnormal adrenal morphology, and changes in hematopoietic cell populations[194], further suggesting a broader role for DUSP12 in physiological regulation beyond ribosome biogenesis.

### 1.5.5. DUSP12 involvement in disease contexts

DUSP12 has been linked to several disease contexts, particularly in metabolic disorders and various cancers. DUSP12 gene is significantly amplified in various cancers, including retinoblastoma and liposarcomas that have progressed to advanced stages[188]. This gene amplification, which leads to DUSP12 overexpression, might provide a selective advantage to cancer cells, because of its pro-survival functions. In this context, the protein's gain of function appears to be a driver of tumor progression, supporting the uncontrolled cell growth that is a hallmark of cancer.

Recent studies on chordoma, a rare notochord-derived tumor with limited therapeutic options and poor prognosis, have uncovered a novel role for DUSP12 in ribosomal signaling. DUSP12 was shown to act on ribosomal protein S6, specifically dephosphorylating p-S6 at Ser235/236[195]. This finding is particularly relevant given the central role of S6 phosphorylation in controlling mRNA translation and protein synthesis downstream of mTORC1 signaling[195]. Importantly, the oncogenic GTPase RAB3B was shown to interact with both S6 and DUSP12, thereby impairing DUSP12-mediated dephosphorylation and sustaining S6 phosphorylation. In this way, RAB3B indirectly suppresses DUSP12 activity, enhancing mTORC1-driven tumorigenic signaling in chordoma cells[195]. These observations highlight DUSP12 as a regulatory checkpoint within the mTORC1–S6 axis, where its loss of function contributes to sustained oncogenic signaling.

DUSP12 has a complex and context-dependent role in liver pathology and metabolic disorders. In hepatocellular carcinoma (HCC), its expression is markedly upregulated in tumor tissues compared to normal liver tissues, and high levels correlate with a shorter overall survival for patients[196]. Loss-of-function experiments have shown that a knockdown of DUSP12 expression can decrease the proliferation and migration of HCC cells[196]. In contrast, in nonalcoholic fatty liver disease (NAFLD), DUSP12 acts as a protective regulator against steatosis, insulin resistance, and inflammation. Mechanistically, it binds to and inhibits apoptosis signal-regulating kinase 1 (ASK1), thereby preventing activation of its downstream effectors JNK and p38 MAPK. This regulation dampens lipogenesis and inflammatory signaling under high-fat conditions and it seems to be dependent on phosphatase activity, as a catalytically inactive DUSP12 mutant lost its ability to inhibit ASK1[197].

A similar mechanism extends to diabetes and its complications. Genome-wide linkage analyses have implicated DUSP12 in susceptibility to type 2 diabetes (T2D), while functional studies highlight its cytoprotective capacity[198]. DUSP12 expression is upregulated in hyperglycemic cell models and in mice exposed to a high-fat diet (HFD). In the context of diabetic cardiomyopathy (DCM), heart-specific DUSP12 deficiency leads to severe cardiac dysfunction, remodeling, oxidative stress, and apoptosis under HFD conditions, whereas DUSP12 overexpression alleviates these defects. These effects, as in NAFLD, are mediated through suppression of ASK1 signaling and its downstream JNK and p38 MAPK pathways[198].

DUSP12 has been also identified as an endogenous protective signal against hepatic ischemia-reperfusion injury (IRI). Consistent with its role in NAFLD, IRI significantly decreases DUSP12 expression in the liver. Overexpression of DUSP12 in hepatocytes protects against IRI, and its deletion in DUSP12 knockout mice exacerbates the injury. The protective mechanism involves the inhibition of the pro-inflammatory and pro-apoptotic ASK1/JNK-p38 MAPK pathway[199].

Collectively, these data indicate that DUSP12 is a multifunctional regulator implicated in diverse pathological contexts. In cancer, its amplification or overexpression has been linked to enhanced survival signaling and tumor progression, including in retinoblastoma, liposarcoma, chordoma, and hepatocellular carcinoma. In contrast, in metabolic and liver-related disorders such as NAFLD, diabetes, and ischemia–reperfusion injury, DUSP12 exerts cytoprotective effects by restraining ASK1/JNK–p38 MAPK signaling and limiting inflammation, steatosis, and apoptosis. These findings underscore the context-dependent nature of DUSP12 biology, whereby it can act either as a facilitator of oncogenic processes or as a protective factor against metabolic and inflammatory stress. Further elucidation of the molecular mechanisms underlying these opposing roles will be essential for a comprehensive understanding of its function in disease.

### 1.5.6. From eIF6 to DUSP12: A hypothesis-driven shift in focus

Interestingly, DUSP12 has recently been identified as a putative interactor of eIF6 through a proximity-labeling–based approach[200]. Consistently, the two proteins display spatial overlap: both are enriched in the nucleolus, yet can shuttle to the cytoplasm under specific conditions[107,165,188]. This shared localization points to a possible functional connection.

A second line of convergence arises from their roles in ribosome biogenesis. Complete loss of eIF6 severely impairs ribosome formation and causes embryonic lethality[117], while in yeast the DUSP12 homolog has been shown to be essential for 60S subunit maturation[164]. These parallels raise the hypothesis that DUSP12 might influence translation directly or indirectly, potentially in cooperation with eIF6.

Finally, evidence of their relationship also emerges in pathological contexts, particularly in non-alcoholic fatty liver disease (NAFLD), where DUSP12 overexpression[197] and eIF6 downregulation[131] both confer protective effects during disease progression.

Taken together, these three elements – shared localization, complementary roles in ribosome biogenesis, and coherent involvement in disease – provided the rationale to further investigate the relationship between DUSP12 and eIF6.

## 1.6. Aim of thesis

Translational control and ribosome biogenesis are essential determinants of cell growth and adaptation, and their deregulation is a hallmark of human disease, including cancer. A central player in this process is the eukaryotic initiation factor 6 (eIF6), whose activity is tightly regulated by phosphorylation of Ser235. Despite the critical nature of this modification, the upstream signaling mechanisms that govern it remain largely undefined. Addressing this gap is crucial to understanding how translational output is fine-tuned under physiological and pathological conditions.

The primary aim of this thesis was to identify and characterize upstream regulators of eIF6 phosphorylation at Ser235 and to define their functional impact on translational control. While unbiased biochemical approaches failed to identify stable regulatory candidates, integrative analysis of proximity-labeling datasets highlighted the atypical dual-specificity phosphatase DUSP12 as a high-confidence interactor of eIF6. On this basis, the project focused on a comprehensive functional characterization of DUSP12 as a regulatory node linking translational control to broader aspects of cellular physiology.

Specifically, this thesis aimed to (i) define the role of DUSP12 in global translational output, (ii) identify direct and indirect substrates of DUSP12 using quantitative phosphoproteomics, and (iii) dissect the contribution of its catalytic domain and C-terminal Zinc-Binding Domain to substrate specificity and functional outcomes. Finally, these mechanistic insights were integrated at the cellular level to explore how DUSP12-dependent signaling influences proteostasis, metabolic remodeling, and stress-adaptive responses.

# 2. Materials and Methods

## 2.1 Molecular cloning and plasmid generation

### 2.1.1. Generation of eIF6 expression constructs

For cellular overexpression studies, human eIF6 cDNA (RefSeq: NM_001007252.3) was cloned in-frame with either an N-terminal FLAG or Strep affinity tag to generate tagged wild-type (WT) eIF6 constructs. The eIF6 open reading frame was amplified by PCR using AmpliTaq Gold™ DNA Polymerase (Thermo Fisher Scientific, Cat. # N8080245), which produces 3′ A-overhangs suitable for TA cloning. The following primers were used:

- **Forward FLAG:** 5′-GGTGGTGGATCCGCGACCATGGACTACAAAGACGATGACGACAAGGCGGTCAGAGCGTCG-3′
- **Forward Strep:** 5′-GGTGGTGGATCCGCCACCATGGCGTGGAGCCACCCGCAGTTCGAAAAGGGTGCAGCGGTCAGAGCGTCG-3′
- **Reverse:** 5′-TATAGGGTCGACTCATGTGAGGCTG-3′

PCR reactions contained 1× PCR Buffer II, 1.5 mM $MgCl_2$, 200 µM dNTPs (Thermo Fisher Scientific, Cat. #R0191), 0.5 µM of each primer, and 1 U Taq DNA polymerase. PCR products were resolved on a 2% (w/v) agarose gel and subsequently purified using the QIAquick Gel Extraction Kit (Qiagen, Cat. #28106) before ligation into the pCR™2.1-TOPO® TA vector (Invitrogen, Cat. #K450002). Transformations were performed in One Shot® TOP10 chemically competent *E. coli* (Thermo Fisher, Cat. #C404010). Positive clones were selected on LB/Kanamycin plates (50 µg/mL) and screened by blue/white colony selection (X-Gal/IPTG system). Recombinant plasmids were confirmed by colony PCR, and plasmid DNA was isolated using the QIAprep Spin Miniprep Kit (Qiagen, Cat. #12123).

TOPO-intermediate plasmids were digested with *BamHI*-HF® (NEB, Cat. # R3136) and *SalI*-HF® (NEB, Cat. #R3138). The final recipient vector, pCCL-sin-PPT.hPGK.Wpre[201] (kindly provided by Prof. Luigi Naldini), was digested with the same restriction enzymes and purified in parallel. Ligation reactions were performed using T4 DNA Ligase (NEB, Cat. #M0202), and ligation products were transformed into *E. coli* TOP10 chemically competent cells (Thermo Fisher Scientific, Cat. #C737303).

Individual colonies were cultured in 3 mL LB broth containing ampicillin (50 µg/mL) at 37 °C with shaking at 180 rpm for ~8 h (overday). Plasmid DNA was isolated using the QIAprep Miniprep Kit (Qiagen, Cat. #27104) and screened by diagnostic restriction digestion and Sanger sequencing (Eurofins Genomics). Verified constructs were subsequently amplified in 500 mL LB broth containing ampicillin (50 µg/mL) overnight at 37 °C, 180 rpm. Bacterial pellets were harvested by centrifugation (5000 rpm, 15 min at 4 °C) in a Beckman Coulter JA-10 rotor and plasmid DNA was purified using the QIAprep Spin Maxiprep Kit (Qiagen, Cat. #12162).

### 2.1.2. Site-Directed mutagenesis for eIF6 constructs

Site-directed mutagenesis was performed to generate *eIF6* expression plasmids containing either the S235A (non-phosphorylatable) or S235E (phosphomimetic) point mutation. Mutagenesis reactions were carried out using the Phusion Site-Directed Mutagenesis Kit (Invitrogen, Cat. # F541). Each reaction contained 1× PCR buffer, 0.5 µM of each primer, and 50 ng of plasmid template (FLAG- or Strep-tagged *eIF6* constructs).

To generate the S235A mutant, site-directed mutagenesis was performed using either pCCL-FLAG-eIF6 WT or pCCL-Strep-eIF6 WT as template, with the following primers:

- **Forward:** 5′-TGCCACCGCAATGCGGGATTCCCTCATTG-3′
- **Reverse:** 5′-CCGCATTGCGGTGGCAATGGTACTTGG-3′

To generate the S235E mutant, mutagenesis was performed using the pCCL-Strep-eIF6 S235A plasmid as template, with the following primers:

- **Forward:** 5′-TGCCACCGAAATGCGGGATTCCCTCATTG-3′
- **Reverse:** 5′-CCGCATTTCGGTGGCAATGGTACTTGG-3′

PCR amplification products were treated with *DpnI* restriction enzyme for 1 h at 37 °C to selectively digest methylated parental DNA. The *DpnI*-treated mixtures were directly transformed into *E. coli* One Shot® TOP10 chemically competent cells (Thermo Fisher Scientific, Cat. # C404010). Colonies were screened by colony PCR, and plasmid DNA was purified using the QIAprep Spin Miniprep Kit (Qiagen, Cat. # 27104). Successful introduction of the S235A and S235E mutations was verified by Sanger sequencing (Eurofins Genomics). Verified constructs were subsequently amplified in 500 mL LB broth containing ampicillin (50 µg/mL) overnight at 37 °C, 180 rpm. Bacterial pellets were harvested by centrifugation in a (5000 rpm, 15 min at 4 °C) and plasmid DNA was purified using the QIAprep Spin Maxiprep Kit (Qiagen, Cat. #12162).

This cloning strategy yielded the following *eIF6* expression constructs for subsequent functional studies:

- pCCL-FLAG-eIF6 WT
- pCCL-FLAG-eIF6 S235A
- pCCL-Strep-eIF6 WT
- pCCL-Strep-eIF6 S235A
- pCCL-Strep-eIF6 S235E

### 2.1.3 Generation of ΔZBD DUSP12 mutant constructs

For the generation of ΔZBD DUSP12 mutant constructs, PCR amplification was performed using the following primers:

- **Forward**: 5′-GTTGTAGGATCCGCCACCATGTTGGAGGCTCCG-3′
- **Reverse**: 5′-GCAACGCGTCTCTGTAACCTTTTGTAAACGATATTGC-3′

containing *BamHI* and *MluI* restriction sites, respectively. The PCR reaction was designed to amplify the region of DUSP12 encoding the first 130 amino acids, thereby generating a truncated variant

lacking the C-terminal zinc-binding domain (ΔZBD, amino acids 192–340), using the pCMV-DUSP12 expression plasmid (OriGene, Cat. #RC202411) as DNA template.

PCR reactions were performed as previously described. PCR products were resolved on a 2% (w/v) agarose gel and purified using the QIAquick Gel Extraction Kit (Qiagen, Cat. #28106). The purified insert was subsequently digested with BamHI-HF® (NEB, Cat. #R3136) and MluI-HF® (NEB, Cat. #R3198) and re-purified from a 2% (w/v) agarose gel using the same kit. In parallel, the parental plasmid vector was digested with the same restriction enzymes and purified from a 1% (w/v) agarose gel.

Ligation reactions were carried out using T4 DNA Ligase (NEB, Cat. #M0202) according to the manufacturer's instructions. Ligation products were transformed into One Shot® TOP10 chemically competent *E. coli* (Thermo Fisher Scientific, Cat. #C404010). Transformants were selected on LB agar plates supplemented with kanamycin (50 µg/mL). Positive colonies were expanded in LB broth containing kanamycin (50 µg/mL), and plasmid DNA was purified using the QIAprep Spin Miniprep Kit (Qiagen, Cat. #27104) and confirmed by Sanger sequencing (Eurofins Genomics). Verified clones were further amplified as previously described, and plasmid DNA was isolated using the QIAprep Spin Maxiprep Kit (Qiagen, Cat. #12162).

## 2.2. Cell culture and transient transfection

### 2.2.1. Cell culture

HEK 293T (ATCC® CRL-3216™) and HeLa (ATCC® CCL-2™) cells were maintained under standard culture conditions (37 °C, 5% $CO_2$). HEK 293T cells were cultured in Iscove's Modified Dulbecco's Medium (IMDM, Euroclone, Cat # ECB2072L), and HeLa cells in Dulbecco's Modified Eagle's Medium (DMEM, Euroclone, Cat. #ECB7501L), each supplemented with 100 mM Penicillin/streptomycin (Euroclone, Cat. #ECB3001D) and 10% (v/v) fetal bovine serum (FBS; Euroclone, Cat. #ECS5000L, Lot. EUS00QV). Cultures were routinely tested for mycoplasma contamination on a monthly basis.

For puromycin incorporation assays, cells were treated with 10 µg/mL puromycin (Sigma-Aldrich, Cat. #P8833) for 10 min at 37 °C prior to harvesting. For polysome profiling experiments, culture medium was replaced with fresh medium 4 h before harvest; cells were then stimulated with 5 µg/mL insulin for 30 min immediately before collection.

### 2.2.2. Cellular transient transfection

For cellular overexpression experiments, mammalian expression vectors encoding the constructs described above were used, along with control plasmids including the pCMV empty vector (OriGene, Cat. # PS100001) and the pCMV-DUSP12 expression plasmid (OriGene, Cat. # RC202411). Cells were seeded in 6-well plates or 10-cm dishes and transfected upon reaching ~50% confluence using the calcium phosphate precipitation method.

Briefly, plasmid DNA was mixed with 2 M $CaCl_2$ and added dropwise to sterile-filtered 2× HBS buffer (50 mM HEPES, pH 7.05; 10 mM KCl, 280 mM NaCl; 1.5 mM $Na_2HPO_4$). The mixture was

vortexed briefly and incubated for 20 min at room temperature to allow precipitate formation. The resulting suspension was then added dropwise to the culture medium. After 12–16 h, the medium was replaced to remove residual precipitates, and cells were harvested 36–48 h post-transfection, depending on the downstream application. Under these conditions, transient expression of experimental and control constructs was consistently achieved, yielding material suitable for subsequent biochemical and functional analyses.

## 2.3. Purification and testing of recombiant eIF6 protein

### 2.3.1. Bacterial colture

Recombinant human eIF6 (full-length, residues 1–245) containing an N-terminal His-tag was expressed in Escherichia coli BL21(DE3) cells[202]. This strain lacks the *lon* and *ompT* proteases, thereby reducing proteolytic degradation of heterologous proteins, and harbors a lysogenic λ prophage encoding T7 RNA polymerase under control of the lacUV5 promoter, enabling IPTG-inducible expression from T7 promoter-driven constructs. To enhance folding and solubility of recombinant eIF6 and reduce inclusion body formation associated with high T7 transcriptional activity, BL21(DE3) cells were co-transformed with plasmids encoding bacterial molecular chaperones DnaK, DnaJ, GrpE, ClpB, and GroESL[203].

For pre-inoculum preparation, a single colony was isolated from LB agar plates containing chloramphenicol (25 µg/mL; Sigma-Aldrich, Cat. #C0378-100G), spectinomycin (50 µg/mL; Sigma-Aldrich, Cat. #S9007-SG), and kanamycin (50 µg/mL; Sigma-Aldrich, Cat. #6061S-SG), and used to inoculate a 10 mL starter culture in LB medium. Cultures were grown overnight (O/N) at 37 °C with agitation at 130 rpm.

The pre-inoculum was then diluted into 3 L of fresh LB medium containing the same antibiotics and incubated at 37 °C, 130 rpm until an optical density at 600 nm ($OD_{600}$) of 0.4 was reached. Protein expression was induced by adding isopropyl β-D-1-thiogalactopyranoside (IPTG) to a final concentration of 0.1 mM, after which the culture was incubated at 20 °C with shaking at 130 rpm until $OD_{600}$ reached 6.0–7.0.

### 2.3.2. Bacterial lysis

Bacterial cells were harvested by centrifugation at 5,000 rpm in a Beckman Coulter JA-10 rotor for 15 min at 4 °C. The pellet was resuspended in lysis buffer containing 50 mM Tris-HCl pH 8.0; 300 mM NaCl; 1 mM β-mercaptoethanol (Sigma-Aldrich, Cat. #M-R148100ML); 10 mM Imidazole (Sigma-Aldrich, Cat. #I0125); 1 mg/mL lysozyme; 2 µg/mL DNase; 10 µg/mL RNase (Promega, Cat. #A7973); and protease inhibitor cocktail (Sigma-Aldrich, Cat. #P8340-1ML)) and incubated for 30 min at 4 °C with agitation. The suspension was then sonicated at 80% intensity for 45 seconds and clarified by centrifugation at 15,000 g for 1 hour at 4 °C. The supernatant was filtered through a 0.2 µm filter (Life Science, Cat. #4652) prior to chromatography.

### 2.3.3. His-Trap affinity purification and quality control

Purification was performed at 4 °C. The sample was loaded onto a His-Trap affinity column and incubated for 1 hour. The column was washed sequentially with resuspension buffer (50 mM Tris-HCl pH 8.0; 300 mM NaCl; 1 mM β-mercaptoethanol; 10 mM imidazole) and wash buffer (50 mM Tris-HCl pH 8.0; 300 mM NaCl; 1 mM β-mercaptoethanol; 30 mM imidazole). The protein of interest was eluted using elution buffer (50 mM TrisHCl pH 8.0; 300 mM NaCl; 1 mM β-mercaptoethanol; 300 mM Imidazole). Elution peaks were monitored by absorbance at λ=280 nm.

The pooled fractions were then concentrated and loaded onto a second column, a Superose 12 10/300 gel filtration column (GE Healthcare). Size-Exclusion Chromatography (SEC) was performed to isolate the active eIF6 monomers from aggregates. Elution was monitored at λ=280 nm. Fractions containing active monomers were pooled. Fractions were analyzed by 12% SDS-PAGE (30% Acrylammide/Bis Solution 29:1 Biorad 1610156), followed by staining with EZBlue Gel Staining Reagent (Sigma-Aldrich, Cat. #G1041) for 1 hour and subsequent overnight destaining. The eIF6 band (approximately 27 kDa) was confirmed using a protein standard marker (Blue Plus2 Pre-stained Protein Standard, Thermo Fisher, cat #LC5925). The final purified protein was stored at −20 °C.

### 2.3.4. Ribosome purification

Ribosomes were purified from *Artemia* cysts following a protocol previously optimized for subunit integrity[204]. Briefly, 50 g of *Artemia* cysts were suspended in 100 mL of ice-cold 20% sodium hypochlorite for 5 min with gentle agitation every minute. Cysts were filtered through 0.4 µm membranes, washed twice with cold sterile water, and subjected to six additional washing cycles (500 mL each) by sedimentation (~15 min per wash) to remove debris and non-viable material. After a final filtration, viable cysts were ground in a pre-chilled mortar with 37.5 g of glass beads, gradually adding 20 mL of buffer A (70 mM KCl, 1 mM DTT, 9 mM $MgCl_2$, 0.1 mM EDTA, 5% glycerol, 20 mM Tris-HCl, pH 7.5) until a fine paste was obtained. An additional 60 mL of buffer A were added, and the suspension was filtered through four layers of sterile cheesecloth.

The retained material was re-ground with 40 mL of buffer A and filtered again; both filtrates were combined and centrifuged in Beckman centrifuge with Allegra 2IR 30 ml corex at 10,733 × *g* for 30 min at 4 °C. The resulting supernatant was filtered through poly-prep chromatography columns (Bio-Rad) to remove lipid contaminants and sequentially centrifuged using Beckman 50.2 Ti rotor at 71,256 × *g* for 30 min and 145,421 × *g* for 2.5 h at 4 °C. The ribosomal pellet was gently washed with buffer A and resuspended in 0.5 mL of buffer B (700 mM KCl, 4 mM $MgCl_2$, 2 mM DTT, 20 mM Tris-HCl, pH 7.5).

The suspension was layered onto 15–30% linear sucrose gradients prepared in 20 mM Tris-HCl (pH 7.5), 2 mM DTT, 11 mM $MgCl_2$, and 700 mM KCl, and ultracentrifuged at 49,392 × *g* for 16 h at 4 °C (Beckman SW41 Ti rotor). Fractions corresponding to 40S and 60S subunits were pooled, diluted to a final concentration of 100 mM KCl, and concentrated using Centricon YM-100 filters (2,500–3,000 × *g*). Ribosomal subunits were quantified spectrophotometrically at 260 nm, adjusted to 50% glycerol, aliquoted, and stored at −80 °C, remaining stable for at least one year.

### 2.3.5. 60S Binding Assay

For eIF6-60S binding assays, 96-well plates were coated with fixed concentrations of ribosomes diluted in 50 µL of PBS 1× + 0.01% Tween-20, O/N at 4 °C in a humid chamber. The coating solution was removed and unspecific sites were blocked with 5% BSA powder in PBS 1× + 0.01% Tween-20 for 30 min at 37 °C. The plate was washed with 100 microliters/well with PBS-Tween. His-tagged eIF6 was resuspended in a reaction mix to the final concentration of 2 nM with 5 mM $MgCl_2$, 0.5% BSA, PBS-Tween 0.01% pH 7.4, to reach 50 µL of final volume/well. The reaction mix was added in the well and was incubated for 1 h at room temperature. To remove unbound proteins, each well was washed 3 times with PBS-Tween. HRP-conjugated HisTag antibody was diluted 1:5000 in PBS-Tween, and 50 µL were incubated in the well for 30 min at room temperature. Binding was revealed with addition of 100 uL of TMB Liquid Substrate (Sigma-Aldrich T0440) and was blocked with the addition of an equivalent volume of stopping solution (2M $H_2SO_4$). The signal was then measured at 450 nm on a multiwell plate reader (Microplate Bio-Rad model 680).

# 2.4 Functional Translation Assays

## 2.4.1. Rabbit Reticulocyte Lysate (RRL) Assay

The effect of purified eIF6 constructs on translational efficiency was assessed using a Rabbit Reticulocyte Lysate (RRL) system (Promega, Cat. #L4960) supplemented with exogenous luciferase mRNA as a reporter. Reactions were assembled according to the manufacturer's instructions, with recombinant eIF6 WT or S235A proteins added at a fixed concentration. Samples were incubated for 90 min at 30 °C, and luciferase activity was subsequently measured using a luminometer. Data were normalized to control reactions containing RRL supplemented with the recombinant protein elution buffer only.

## 2.4.2. Preparation of translationally active lysates and *in vitro* translation

Translationally active cytoplasmic lysates were prepared using an optimized dual-centrifugation protocol[205] with a Zentrifugen 380R centrifuge (Hettich). Briefly, cells were harvested and subjected to two consecutive centrifugation steps to remove intact nuclei and cellular debris, yielding a clarified cytosolic fraction containing ribosomes and translation factors. Lysate integrity and purity were assessed by measuring absorbance at 260 nm ($OD_{260}$) and by Western blot analysis.
For *in vitro* translation assays, control and DUSP12-overexpressing lysates were incubated with exogenous luciferase mRNA. Luminescence was subsequently quantified, and results were expressed as normalized relative luciferase units (RLU), corrected for total protein concentration in each lysate.

# 2.5. Molecular and biochemical techniques

## 2.5.1. Protein extraction and quantification

Total protein extracts were prepared from HEK293T cells for Western blot analysis. Cell pellets were resuspended in RIPA lysis buffer (10 mM Tris-HCl, pH 7.2; 1% sodium deoxycholate; 1% Triton X-100; 0.1% SDS; 150 mM NaCl; 1 mM EDTA) supplemented with protease inhibitor cocktail (Sigma-Aldrich, Cat. #P8340) and phosphatase inhibitor cocktail (Sigma-Aldrich, Cat. #P2850). The buffer

volume was adjusted according to pellet size. Lysates were incubated on ice for 15 min and clarified by centrifugation at 14,000 rpm for 15 min at 4 °C.

Total protein concentration in the resulting supernatants was determined using the BCA Protein Assay Kit (Thermo Scientific, Cat. #23225) following the manufacturer's instructions. A six-point standard curve was generated using serial dilutions of bovine serum albumin (BSA; 2 mg/mL stock). Absorbance was measured at 595 nm using a Biophotometer Plus (Eppendorf), and protein concentrations were calculated by interpolation from the BSA standard curve.

### 2.5.2. Western Blotting

For standard protein analysis, 30 µg of total protein per sample was denatured in Laemmli sample buffer (62.5 mM Tris-HCl, pH 6.8; 20% glycerol; 2% SDS; 2% β-mercaptoethanol) for 5 min at 99 °C. Samples were resolved by SDS–PAGE using polyacrylamide gels of appropriate concentration (10%, 12%, or 15%, depending on the molecular weight of the target protein). Each gel consisted of a 5% acrylamide stacking layer (130 mM Tris-HCl, pH 6.8; 0.1% SDS; 0.1% APS; TEMED) and a 10–15% acrylamide resolving layer (390 mM Tris-HCl, pH 8.8; 0.1% SDS; 0.1% APS; TEMED). Electrophoresis was carried out at 120–130 V for approximately 2–3 h in running buffer (144 g/L glycine, 30 g/L Tris base, 10 g/L SDS).

Proteins were transferred onto PVDF membranes (Thermo Fisher Scientific) pre-activated in methanol and equilibrated in transfer buffer (GenScript) using the eBlot Protein Transfer System (GenScript) for ~20 min at room temperature. Membranes were blocked with 5% (w/v) BSA in PBS containing 0.1% Tween-20 (PBS-T) for 1 h at room temperature to prevent non-specific antibody binding.

Following blocking, membranes were incubated overnight at 4 °C with gentle agitation in primary antibodies diluted in PBS-T containing 5% BSA. The following primary antibodies were used: eIF6 (in-house, mouse monoclonal antibody, clone 8D10[206]), p-eIF6 (in-house, unpublished, 1:200), anti-β-Actin (Cell Signalling, Cat. #3700S; 1:4000), anti-GAPDH (Cell Signalling, Cat. #2118S; 1:3000), anti-β-Tubulin (Cell Signalling, Cat. #2128S; 1:3000), anti-FLAG (Sigma-Aldrich, Cat. #F1804; 1:3000), anti-StrepII (Invitrogen, Cat. #MA5-42540; 1:4000), anti-DUSP12 (Abnova, #H00011266-B01P; 1:2000), and anti-LaminB1 (Sigma-Aldrich; Cat. #MABS492; 1:3000). After incubation, membranes were washed three times in PBS-T and subsequently incubated for 1 h at room temperature with the appropriate HRP-conjugated secondary antibody diluted in PBS-T: mouse anti-rabbit IgG-HRP (Santa Cruz, Cat. #sc-2357; 1:3000), m-IgGκ BP-HRP (Santa Cruz, Cat. #sc-516102; 1:3000), and goat anti-chicken IgY HRP (Abcam, Cat. #ab6877; 1:3000). Protein bands were visualized using the SuperSignal™ West Pico PLUS Chemiluminescent Substrate (Thermo Scientific, Cat. #34577) and detected with the ChemiDoc™ MP Imaging System (Bio-Rad). Signal intensity was quantified using Image Lab software (Bio-Rad).

### 2.5.3. Nucleus-Cytoplasm fractionation

HEK293T were harvested by scraping, washed once with ice-cold PBS, and then centrifuged at 1,000 x g for 5 minutes at 4 °C. The pellet was gently resuspended in an appropriate volume of Cytoplasmic

Lysis Buffer (10 mM Hepes pH 7.9; 10 mM KCl; 1.5 mM $MgCl_2$; 0.5% Nonidet P-40 [NP-40]), supplemented with protease and phosphatase inhibitors. The suspension was incubated on ice for 10 minutes to allow cell membrane lysis. Following cytoplasmic lysis, the suspension was centrifuged at 1,000 x g for 10 minutes at 4 °C. The resulting supernatant was collected as the Cytoplasmic Fraction. This fraction was then clarified by a second, high-speed centrifugation step at 14,000 x g for 15 minutes at 4 °C to remove cellular debris and residual insoluble material. The final supernatant was stored at −80 °C. The remaining pellet (containing intact nuclei) was washed once with Cytoplasmic Lysis Buffer without NP-40 and then resuspended in Nuclear Extraction Buffer (20 mM Hepes pH 7.9; 420 mM NaCl; 1.5 mM $MgCl_2$; 0.2 mM EDTA; 25% Glycerol), also supplemented with protease and phosphatase inhibitors. The nuclear suspension was incubated on ice for 30 minutes, with periodic vortexing, to extract nuclear proteins. The resulting mixture was centrifuged at 14,000 x g for 15 minutes at 4 °C. The supernatant was collected as the Nuclear Fraction and stored at −80 °C. Protein concentrations for both fractions were determined using the BCA Assay. Fraction purity was validated by Western blotting using specific markers: Lamin B1 (nuclear) and β-Tubulin (cytoplasmic). Densitometric quantification was performed using ImageJ to calculate the percentage of target protein localized in each compartment, normalized to the respective compartment marker.

### 2.5.4. Polysome profiling

Polysome profiling was performed 48 h post-transfection using HEK 293T cells seeded in 100-mm culture dishes and grown to 70–80% confluence. Actively proliferating, subconfluent cultures in the logarithmic growth phase were used, as translational activity closely correlates with cell proliferation, and excessive confluence results in reduced polysomal signal intensity[207]. Four hours before harvesting, culture medium was replaced with fresh medium.

For experimental treatments, cells were incubated for 30 min at 37 °C with insulin (Sigma-Aldrich, Cat. #91077C; 1:5000 dilution) and 100 µg/mL cycloheximide (Sigma-Aldrich, Cat. #81K1749). Following treatment, cells were washed once with ice-cold PBS supplemented with 10 µg/mL cycloheximide and lysed directly on the plate in ice-cold lysis buffer containing 20 mM Tris-HCl (pH 7.5), 50 mM NaCl, 10 mM $MgCl_2$, 100 µg/mL cycloheximide, 1 mM DTT, and 0.1% NP-40, supplemented with 0.2 mg/mL heparin and 40 U/mL RNasin® Plus RNase Inhibitor (Promega, Cat. #N261A). Plates were incubated on ice for at least 10 min before collecting lysates.

Cell lysates were clarified by centrifugation at 14,000–20,000 × *g* for 10 min at 4 °C. The supernatant was either flash-frozen and stored at −80 °C or immediately loaded onto prechilled 15–50% (w/v) sucrose gradients prepared in gradient buffer (50 mM Tris-acetate, pH 7.5; 50 mM $NH_4Cl$; 12 mM $MgCl_2$; 1 mM DTT). Gradients were centrifuged in an SW41Ti rotor (Beckman Coulter) at 39,000 rpm for 3 h 30 min at 4 °C. Absorbance profiles at 254 nm were continuously recorded using a BioLogic LP system and software (Bio-Rad).

### 2.5.5. RNA extraction and quality assessment

Total RNA was extracted using the TRIzol/chloroform method followed by purification with Zymo RNA Clean & Concentrator columns (Zymo Research, Cat. #R1054). Briefly, cell pellets were resuspended in an appropriate volume of TRIzol reagent (Invitrogen, Cat. # 15596018), and 1/5

volume of chloroform was added. Samples were vortexed for 15 s and centrifuged at 12,000 × g for 15 min at 4 °C to achieve phase separation. The upper aqueous phase containing RNA was carefully collected and mixed with an equal volume of 70% ethanol. The resulting mixture was loaded onto Zymo RNA columns and processed according to the manufacturer's protocol.

On-column DNase I digestion was performed to eliminate residual genomic DNA contamination. RNA concentration and purity were determined spectrophotometrically by measuring absorbance at 260 nm and 280 nm (A260/A280 > 2.0). RNA integrity was further assessed using the Agilent RNA 6000 Pico Kit (Agilent Technologies, Cat. #5067-1513) on the 2100 Bioanalyzer system (Agilent Technologies).

### 2.5.6. ELISA assay

96-well high-binding plates (Thermofisher, Cat. #442404) were coated overnight at 4 °C with 10 µg of clarified cell lysate per well, previously quantified by BCA assay, and diluted to a final volume of 40 µL in PBS. Each experimental condition was spotted in quadruplicate. Wells were subsequently blocked for 1 h at room temperature with 2% (v/v) BSA in PBS 1× + 0.01% Tween-20 (PBS-T) to minimize nonspecific binding. After washing, wells were incubated for 1 h at room temperature with anti-puromycin primary antibody (Sigma-Aldrich, Cat. # MABE343) diluted in PBS-T. Plates were then washed three times with 1× PBS and incubated under the same conditions with HRP-conjugated secondary antibody (m-IgGκ BP-HRP; Santa Cruz Biotechnology, Cat. # sc-516102). Following final washes, bound antibodies were detected using 100 µL of TMB Liquid Substrate (Sigma-Aldrich, Cat. #T0440), and the reaction was stopped by addition of an equal volume of 2 M $H_2SO_4$. Absorbance was measured at 450 nm using a microplate reader.

## 2.6. Metabolic assays

For metabolic analyses, cells were transiently transfected in 6-well plates as previously described. At 48 h post-transfection, cells were gently detached, washed once with ice-cold PBS 1X, and collected by centrifugation at 300 × g for 4 min. Cell pellets were resuspended in the appropriate assay buffer, and an aliquot of each lysate was used to determine total protein concentration using the BCA Protein Assay Kit (Thermo Fisher Scientific, Cat. #23225) to allow normalization of metabolic readouts.

### 2.6.1. ATP quantification

Equal amounts of protein from each lysate were dispensed in quadruplicate into white, flat-bottom 96-well plates. ATP levels were measured using the ATP Determination Kit (Invitrogen, Cat. #A22066) according to the manufacturer's instructions. A standard curve was prepared in parallel using known ATP concentrations to allow accurate interpolation. Following addition of the assay reagent and incubation at room temperature for 10–15 min in the dark, luminescence was recorded using a Synergy microplate reader (BioTek) with Gen5 software, employing auto-scaled luminescence settings. ATP concentrations were calculated by interpolation from the standard curve and normalized to total protein content (nmol ATP/mg protein).

### 2.6.2. Pyruvate quantification

Pyruvate levels were measured using the Pyruvate Colorimetric/Fluorometric Assay Kit (BioAssay Systems, Cat. #EPYR-100) according to the manufacturer's instructions. Cell pellets were resuspended in the supplied pyruvate assay buffer, and equal amounts of protein were dispensed in quadruplicate into MaxiSorp 96-well plates (Invitrogen). The reaction mixture was added, and plates were incubated in the dark at room temperature for 30 min. Fluorescence was measured using the Synergy microplate reader (BioTek) with excitation at 485 nm and emission at 528 nm. Sample pyruvate concentrations were interpolated from a standard curve generated with known pyruvate concentrations and normalized to total protein content (nmol pyruvate/mg protein).

## 2.7. Immunofluorescence (IF) and Confocal Microscopy

### 2.7.1. Cell preparation and staining

HeLa cells were seeded on glass coverslips, cultured, and transfected as previously described. Forty-eight hours post-transfection, cells were washed once with PBS and fixed in 4% paraformaldehyde (PFA) for 10 min at 37 °C. Following fixation, cells were washed three times for 5 min each with PBS and permeabilized in buffer containing 20 mM HEPES (pH 7.4) and 0.1% Triton X-100 for 10 min at room temperature (RT). After three additional PBS washes, non-specific binding sites were blocked for 1 h at RT in blocking buffer consisting of 3% bovine serum albumin (BSA; Sigma-Aldrich, Cat. #05470) and 2% goat serum (Sigma-Aldrich, Cat. #S26-M) in PBS.

Cells were incubated with primary antibodies diluted in 0.5× blocking buffer for 1 h at RT or overnight at 4 °C with gentle agitation. The following primary antibodies were used: eIF6 (in-house), p-eIF6 (in-house), FLAG (Sigma-Aldrich, #F1804; 1:3000), StrepII (Invitrogen, #MA5-42540; 1:4,000), and DUSP12 (Abnova, #H00011266-B01P; 1:2000).

After three washes with PBS, cells were incubated for 45 min at RT in the dark with Alexa Fluor–conjugated secondary antibodies diluted in 0.5× blocking buffer: Alexa Fluor 488 anti-mouse IgG (Invitrogen, #A-21202; 1:500), Alexa Fluor 647 anti-rabbit IgG (Invitrogen, #A-21245; 1:500), or Alexa Fluor 647 anti-chicken IgY (Invitrogen, #A-21449; 1:500). The F-actin cytoskeleton was simultaneously labeled with Phalloidin–Alexa Fluor 547 (Invitrogen, #A22283; 1:500). Following three final PBS washes, nuclei were counterstained with DAPI (Sigma-Aldrich, #D9542), and coverslips were mounted using FluorSave™ reagent (Millipore, #345789).

### 2.7.2. Confocal micrscopy and image analysis

Images were acquired using a Leica TCS SP5 laser-scanning confocal microscope equipped with a 63× oil-immersion objective (numerical aperture 1.4) and a 2× digital zoom. Excitation wavelengths were set to 405 nm for DAPI (nuclear staining), 488 nm for Alexa Fluor 488 (green fluorescence), 547 nm for Phalloidin–Alexa Fluor 547 (orange/red fluorescence), and 647 nm for Alexa Fluor 647 (far-red fluorescence).
All images were processed and analyzed using *ImageJ* (NIH). For quantitative colocalization analysis, background signal was subtracted prior to calculation of the non-thresholded Pearson's correlation coefficient (R) using the Coloc2 plugin.

## 2.8. Quantitative omics

### 2.8.1. Quantitative proteomics and phosphoproteomics

Protein extracts from HEK293T cells were obtained by lysis in 8 M urea and dilution in 100 mM triethylammonium bicarbonate (TEAB). Protein concentrations were determined by the Bradford assay (Bio-Rad, Cat. #5000006). For each experimental condition, 100 µg of total protein was processed. Proteins were reduced with 200 mM tris(2-carboxyethyl)phosphine (TCEP) for 1 h at 55 °C, alkylated with 375 mM iodoacetamide (IAA) for 30 min at room temperature in the dark, and digested overnight with sequencing-grade trypsin (enzyme-to-protein ratio 1:50; Thermo Fisher Scientific) at 37 °C under agitation (600 rpm). Peptides were labeled with the TMT10plex™ Isobaric Label Reagent Set (Thermo Scientific, Cat. #90110) following the manufacturer's protocol. Briefly, 41 µL of TMT reagent was added to each sample, incubated for 1 h, and quenched with 5% hydroxylamine for 15 min. Labeled samples were pooled, dried in a SpeedVac, resuspended in 300 µL trifluoroacetic acid (TFA), desalted with Pierce™ Peptide Desalting Spin Columns (Thermo Fisher Scientific, Cat. #89852), and dried again to completion. Phosphopeptide enrichment was performed using the High-Select™ Fe-NTA Phosphopeptide Enrichment Kit (Thermo Fisher Scientific, Cat. #A32992). Two fractions were obtained: (i) the flow-through (FT) containing the total proteome, dried and resuspended in 100 µL formic acid (FA, diluted 1:10 before MS analysis), and (ii) the phosphopeptide-enriched fraction (PP), dried and resuspended in 30 µL FA.

### 2.8.2. High-Resolution Mass Spectrometry and Data Analysis

Samples were analyzed at the UniTech OMICs Facility (University of Milan, Italy) on a Dionex Ultimate 3000 nano-LC system (Thermo Scientific) coupled to an Orbitrap Fusion™ Tribrid™ Mass Spectrometer (Thermo Fisher Scientific, Bremen, Germany) equipped with a nanospray ion source. Peptides were pre-concentrated on an Acclaim PepMap 100 C18 trap column (100 µm × 2 cm) and separated on an EASY-Spray analytical column (25 cm × 75 µm ID, Acclaim PepMap RSLC C18, 3 µm, 100 Å) at 35 °C, with a flow rate of 0.300 µL/min. Mobile phase A was 0.1% formic acid in water; mobile phase B was 0.1% formic acid in acetonitrile (20:80 v/v). Injection volumes were 2–3 µL, each sample analyzed in technical replicates, with blank runs between injections. MS data were acquired in positive ion mode over an m/z range of 375–1500 with the Orbitrap at 120,000 resolution (at m/z 200), operating in data-dependent acquisition (DDA) mode with a 3s cycle time. Fragmentation was performed by HCD with a normalized collision energy of 38 eV.
Raw data were processed with Proteome Discoverer 3.2 (Thermo Fisher Scientific). Database searches were conducted against the Homo sapiens UniProt proteome (sp_incl_isoforms, TaxID = 9606, release v2025-02-05), with trypsin set as the cleavage enzyme. For total proteome analysis, only proteins identified by ≥2 peptides were retained. For phosphoproteome datasets, all proteins with at least one phosphorylated peptide identified were included. Quantification was based on unique and razor peptides, normalized to total peptide amount. Protein abundance ratios were calculated without imputation, and statistical testing was performed using protein abundance–based one-way ANOVA.

## 2.9. Bioinformatics for integrated omics analysis

All custom data processing, statistical analyses, and visualization of multi-omics datasets were carried out in the R programming environment (version 4.3.0, R Foundation for Statistical Computing) using standard libraries and Bioconductor packages.

### 2.9.1. Phosphoproteomic data analysis

Quantitative phosphoproteomic data were analyzed at the phosphopeptide level using normalized abundance ratios comparing DUSP12-overexpressing and control samples, derived from a matched total proteome dataset. Phosphopeptide intensities were normalized to the corresponding total protein levels to correct for changes in protein abundance and to specifically assess phosphorylation-dependent regulation.

Phosphorylation sites showing a reduction in normalized phosphorylation upon DUSP12 overexpression were identified using a cutoff of phos_norm_log2fc $\leq -0.4$ combined with a q-value $\leq 0.05$. Phosphorylation sites passing these criteria were subsequently collapsed to unique protein identifiers, yielding a set of proteins exhibiting reduced phosphorylation that was used for downstream analyses.

Functional annotation was performed using Gene Ontology (GO) terms. Cellular Component (CC) and Biological Process (BP) annotations were retrieved for the selected proteins and summarized to visualize their predominant subcellular localizations and associated biological processes. GO analyses were used in a descriptive manner to characterize the functional landscape associated with proteins undergoing reduced phosphorylation upon DUSP12 overexpression.

### 2.9.2. RNA-Seq and Proteomics Integration

RNA sequencing (RNA-Seq) data were processed to generate differential expression profiles (DUSP12 vs. control). Differentially expressed transcripts were defined using an adjusted p-value (padj) $< 0.05$ and an absolute $\log_2$ fold change $> 0.5$. Volcano plots and scatterplots were generated with the ggplot2 package (v3.4.2) in R. To evaluate transcript-to-protein correlation, mRNA $\log_2$ fold changes were plotted against corresponding protein $\log_2$ fold changes for all commonly quantified targets. Overlaps between datasets from different phosphoproteomic conditions were visualized through Venn diagrams constructed using the VennDiagram R package (v1.7.3).

### 2.9.3. Functional enrichment and network analysis

Functional enrichment analysis was performed with ShinyGO (v0.8), applying a false discovery rate (FDR) threshold of <0.05. Gene Ontology (GO) terms enriched in proteomic and phosphoproteomic datasets were categorized into biological process, molecular function, and cellular component. Protein–protein interaction (PPI) networks were generated using the STRING database (v12.0) with a minimum interaction score > 0.4. Network clusterization was conducted using the Markov Cluster Algorithm (MCL), enabling the identification of densely interconnected protein modules.

### 2.9.4. Kinase Substrate Enrichment Analysis (KSEA)

Phosphorylation data were subjected to Kinase Substrate Enrichment Analysis (KSEA) in R, employing curated kinase–substrate relationships from PhosphoSitePlus. For each kinase, a z-score was calculated to represent the average shift in phosphorylation of its substrates: a positive z-score indicates predicted upregulation of kinase activity, while a negative z-score indicates downregulation.

# 3. Results

## 3.1. *In vitro* characterization of eIF6 activity and Ser235 mutation

### 3.1.1. Expression, purification and biochemical characterization of the S235A mutation

Previous work from Ceci et al. demonstrated that phosphorylation at Ser235 of eIF6 is required for its release from the 60S ribosomal subunit and for subsequent 80S ribosome assembly[119], thereby contributing to translation control. To dissect the specific contribution of Ser235 to this regulatory mechanism, we employed a non-phosphorylatable Ser235Ala (S235A) variant of the protein. As a first step, we evaluated whether the S235A substitution affects the intrinsic ability of eIF6 to interact with the large ribosomal subunit. This validation is essential to establish S235A as a reliable proxy for the non-phosphorylated state of eIF6 in later cellular assays.

WT and S235A eIF6 sequences were cloned into a plasmid containing an N-terminal His tag and expressed in *E. coli* (**Fig. 1A**). The prokaryotic system ensures that both proteins are produced in a uniformly non-phosphorylated form, allowing us to directly assess whether the alanine substitution introduces structural or functional alterations independent of phosphorylation. Recombinant His-tagged WT and S235A eIF6 were purified from *E. coli* lysates via Ni-NTA affinity chromatography followed by size-exclusion chromatography. The purification workflow yielded highly enriched preparations for both proteins. SDS-PAGE confirmed the expected molecular weight (~27 kDa; **Fig. 1B**), and silver staining showed that eIF6 was the predominant species in both samples. Minor background bands of bacterial origin were detectable, likely corresponding to abundant host factors such as chaperones, but were comparable between WT and mutant preparations (**Fig. 1C**). The similarity in yield, purity, and banding pattern indicates that the S235A mutation does not affect protein expression, solubility, or stability in this system, supporting its use in downstream biochemical assays.

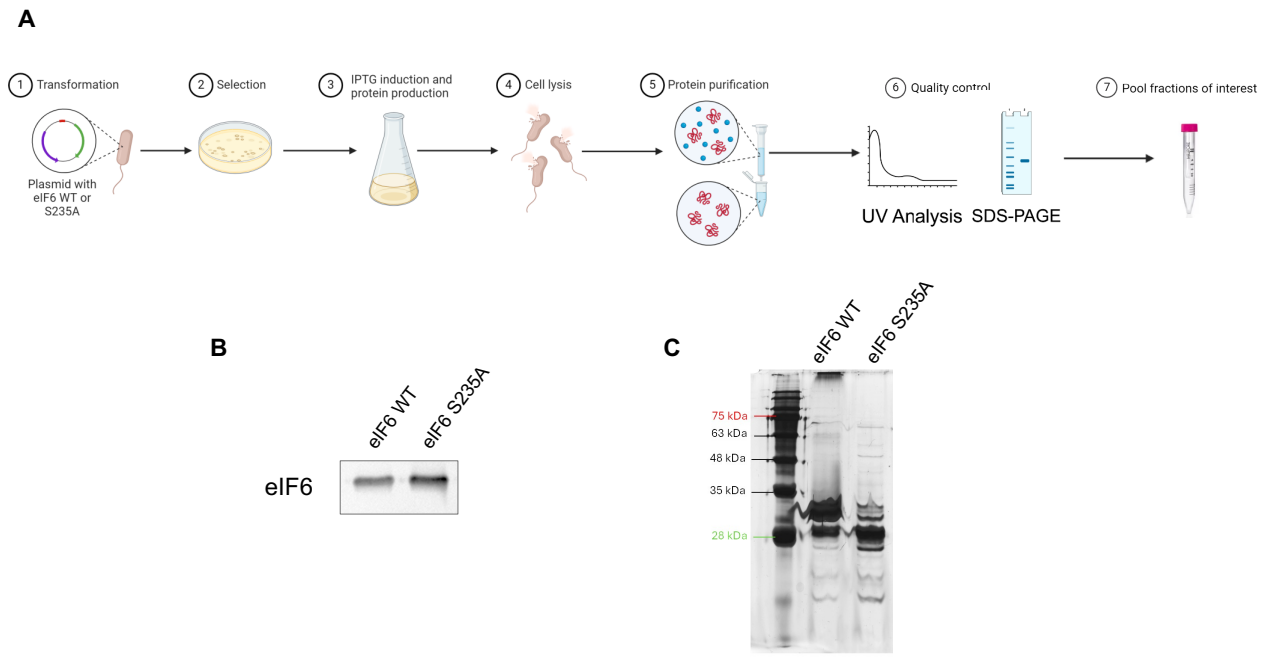

**Figure 1. Successful expression and purification of eIF6 WT and S235A proteins.** (**A**) Schematic overview of the workflow for expressing and purifying recombinant eIF6 proteins from E. coli induced with IPTG. (**B**) Western blot using an anti-eIF6 antibody, showing the successful purification of both wild-type (WT) and S235A proteins. (**C**) Silver-stained SDS-PAGE gel of the purified eIF6 protein preparations, with minor background bands corresponding to abundant *E. coli* proteins.

Given that eIF6 functions as an anti-association factor by binding the 60S subunit and preventing 80S assembly, we next assessed whether the recombinant proteins retained ribosome-binding activity. Equal amounts of WT and S235A eIF6 were incubated with purified *Artemia salina* 60S subunits, a system widely used for biochemical ribosome studies. Binding was quantified through an ELISA-based assay detecting eIF6 associated with immobilized 60S particles. As shown in **Fig. 2A**, WT and S235A displayed indistinguishable absorbance values at equal protein concentrations, indicating equivalent recruitment to the 60S subunit. Thus, the S235A substitution does not impair the 60S-interacting interface of eIF6, nor does it introduce detectable structural perturbations in this *in vitro* assay, supporting its use as a structurally competent mimic of the non-phosphorylated protein.

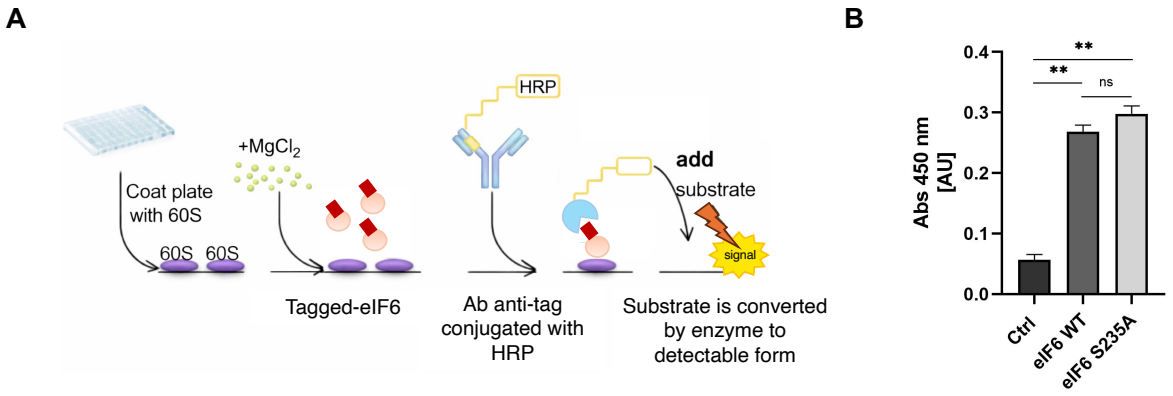


**Figure 2. Biochemical assay reveals that the S235A mutant retains 60S-binding ability comparable to WT eIF6.** (**A**) Schematic overview of the 60S binding assay (image modified from Pesce et al.[204]). (**B**) Binding of recombinant WT and S235A eIF6 to purified Artemia salina 60S ribosomal subunits was quantified using a fixed-ribosome-concentration ELISA-based assay. The control condition (Ctrl) represents the background signal obtained in the absence of recombinant eIF6. Both recombinant proteins showed a significant increase in binding compared to Ctrl (**, $p < 0.01$). No significant difference (ns) was observed between WT ($Abs_{450} \approx 0.27$ AU) and S235A ($Abs_{450} \approx 0.30$ AU), indicating that the Ser235Ala substitution does not alter the intrinsic ability of eIF6 to associate with the 60S subunit *in vitro*.

## 3.1.2. Functional validation of S235A in a cell-free translation system

We next assessed whether the S235A mutant retains the basal inhibitory activity of eIF6 in a translation reaction. To this end, we used a rabbit reticulocyte lysate (RRL) system supplemented with exogenous luciferase mRNA as a reporter (**Fig. 3A**). Addition of WT eIF6 inhibited translation by approximately 50% compared to control reactions lacking protein ($p < 0.001$). The S235A mutant produced a comparable inhibition of ~45% ($p < 0.001$ vs. control). Importantly, the difference between WT and S235A was not statistically significant (**Fig. 3B**), indicating that the alanine substitution does not impair the ability of eIF6 to suppress translation *in vitro*.

These results confirm that the S235A mutant maintains the biochemical and functional properties of WT eIF6 in a system where neither protein is phosphorylated. The absence of a detectable difference between the two forms is consistent with the lack of eukaryotic post-translational modifications in the recombinant protein preparations. Overall, S235A can be confidently used as a functional mimic of the non-phosphorylated form of eIF6 in subsequent experiments in eukaryotic systems designed to interrogate the regulatory role of Ser235 phosphorylation.

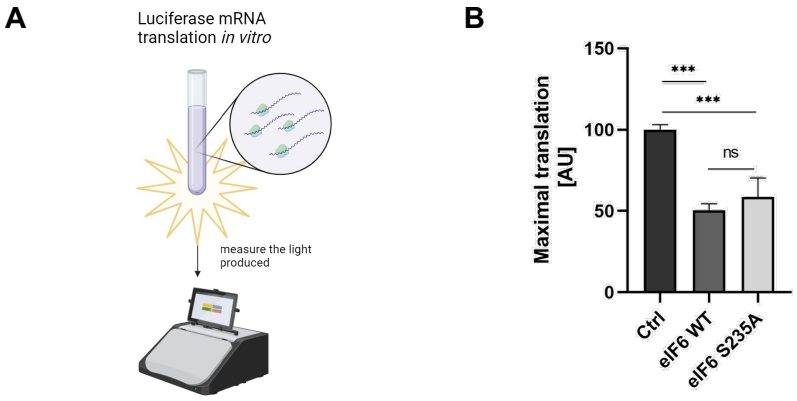


**Figure 3. S235A mutation does not impair the inhibitory effect of eIF6 on translation.** (**A**) Graphical representation of the in vitro translation assay performed in a rabbit reticulocyte lysate (RRL) system using luciferase mRNA as a reporter of active translation. (**B**) Reactions lacking exogenous eIF6 served as the control (Ctrl, defined as 100 AU). Both WT eIF6 and the S235A mutant significantly reduced luciferase production (***, $p < 0.001$ for both), consistent with the expected subunit anti-association function of eIF6. No significant difference (ns) was observed between WT (≈50 AU) and S235A (≈55 AU), indicating that the Ser235Ala substitution does not impair the ability of eIF6 to inhibit translation in this cell-free system.

# 3.2. Cellular overexpression reveals functional impact of Ser235 phosphorylation on translation dynamics

## 3.2.1. Generation and validation of tagged eIF6 constructs for cellular studies

To investigate the functional contribution of Ser235 phosphorylation in a cellular context, we generated WT and S235A versions of eIF6 for expression in mammalian cells. In contrast to recombinant proteins produced in *E. coli*, the WT protein expressed in eukaryotic cells can undergo phosphorylation at Ser235, whereas the S235A variant cannot; therefore, differences observed between the two forms reflect phosphorylation-dependent regulatory effects.

To enable affinity-based assays and to exclude artefacts associated with the use of a single tag, we generated two parallel sets of constructs bearing either an N-terminal Strep or an N-terminal Flag tag. The tags were positioned at the N-terminus to avoid interference with the C-terminal domain responsible for 60S binding. All constructs were cloned under the hPGK promoter, which ensures controlled, moderate andcomparable transcriptional output across variants while avoiding the excessively high expression levels typical of strong viral promoters, such as CMV.

Following transient transfection in HEK293T cells, both Flag- and Strep-tagged WT and S235A eIF6 were robustly expressed, as shown by western blot analysis using tag-specific antibodies (**Fig. 3A**). Densitometric quantification demonstrated that all constructs reached a consistent 3 to 4-fold increase in total protein levels relative to empty vector controls (**Fig. 3B**), with no significant differences between WT and S235A forms. These results indicate that the alanine substitution does not affect protein stability or abundance. No evidence of degradation was detected, validating the suitability of these constructs for downstream functional assays.

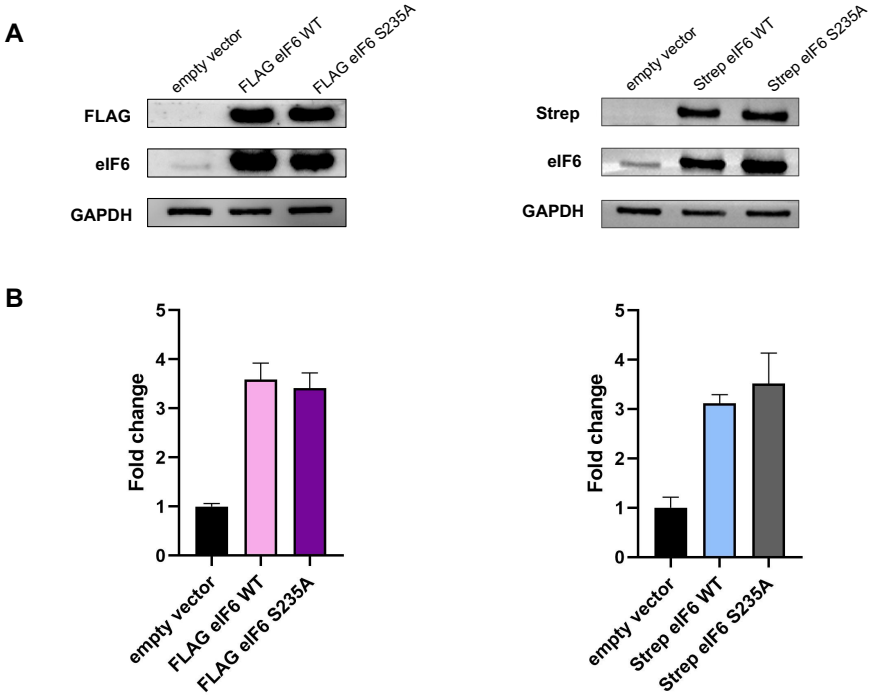


**Figure 4**. **Robust overexpression of tagged eIF6 WT and S235A constructs in HEK293T cells.** (**A**) Representative Representative Western blot from n = 3 independent experiments showing the expression of Flag- and Strep-tagged eIF6 WT and S235A constructs 48 h post-transfection. Tagged eIF6 was detected using anti-Flag or anti-Strep antibodies. No detectable degradation products were observed. GAPDH served as loading control. (**B**) Quantification of protein expression levels (derived from the WB analysis). Densitometric analysis shows a consistent ~3–4-fold increase in expression for both WT and S235A constructs relative to empty vector. Data are presented as fold change ± SEM from n = 3 biological replicates.

## 3.2.2. The S235A mutation does not alter the spatial distribution of eIF6

We next assessed whether the S235A substitution affects the subcellular distribution of eIF6. HeLa cells were used for these experiments, as they represent a well-established model for immunocytochemistry and provide clear cytoplasmic and nuclear boundaries, facilitating the evaluation of protein localization. Their flat morphology and robust intracellular architecture have long made HeLa cells a standard system for defining the localization of key cellular components and for validating antibody-based imaging approaches. Both FLAG- and Strep-tagged WT and S235A constructs were examined in parallel to exclude tag-dependent effects.

Immunofluorescence analysis revealed highly similar localization patterns for all constructs (**Fig. 5**). Endogenous eIF6 was detected using an anti-eIF6 antibody (red), whereas the overexpressed tagged proteins were visualized using anti-FLAG or anti-Strep antibodies (green, **Fig. 5A** and **5B**, respectively). Tagged eIF6 localized predominantly to the cytoplasm, with a minor but detectable nuclear fraction. This distribution was consistent across WT and S235A forms, indicating that the Ser235Ala substitution does not alter eIF6 compartmentalization under basal conditions.

Because the tagged proteins were expressed at substantially higher levels than endogenous eIF6, image acquisition parameters were adjusted accordingly. Images of non-transfected control cells were acquired at detector gain settings optimized to visualize the weaker yet specific endogenous nucleolar signal. Conversely, images of transfected cells required substantially lower gain to avoid saturation

of the strong cytoplasmic signal derived from overexpressed eIF6. As a consequence, endogenous eIF6 in the proximity of transfected cells may appear markedly reduced or near background in low-gain images. This discrepancy reflects technical imaging constraints rather than true biological variation in localization.

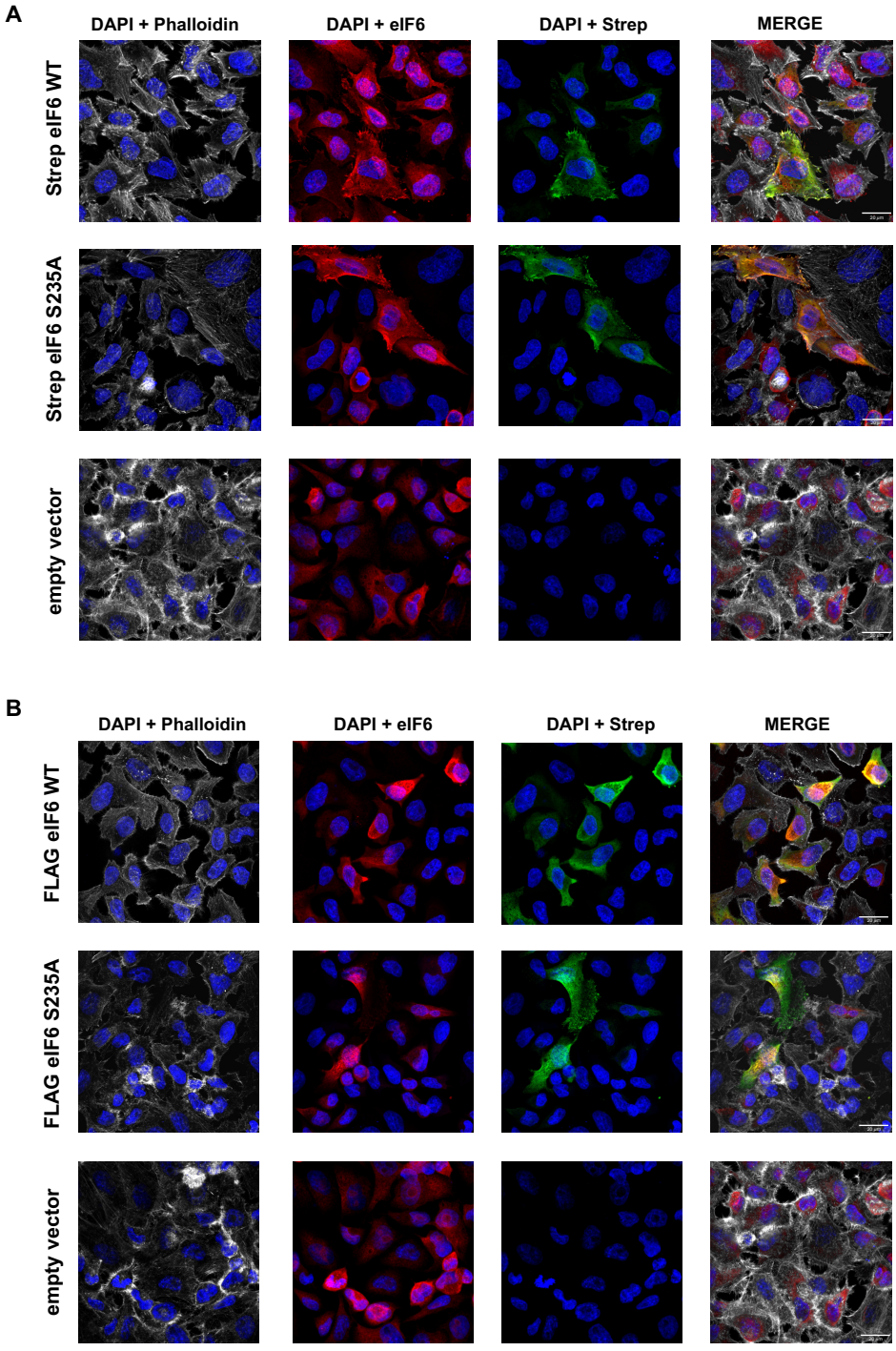


**Figure 5. Dual-tag IF analysis shows that eIF6 WT and S235A localize predominantly to the cytoplasm in HeLa cells.** Immunofluorescence (IF) analysis of HeLa cells expressing (**A**) Strep-tagged eIF6 (WT and S235A) or (**B**) FLAG-tagged eIF6 (WT and S235A). The overexpressed tagged proteins were detected using anti-Strep or anti-Flag antibodies (green), while endogenous eIF6 was visualized using an anti-eIF6 antibody (red). Nuclei were stained with DAPI (blue), and the actin cytoskeleton was labeled with Phalloidin (gray). Empty vector (EV)–transfected cells served as negative controls. Both WT and S235A constructs displayed a predominantly cytoplasmic localization with a minor nuclear fraction, consistent across both tagging strategies. The IF pattern indicates that the S235A substitution does not alter the basal subcellular distribution of eIF6.

### 3.2.3. Quantitative analysis confirms that eIF6 S235A retains WT-like nuclear–cytoplasmic distribution

To quantitatively validate the subcellular distribution suggested by immunofluorescence, confirming that the S235A substitution alters eIF6 compartmental partitioning, we performed nuclear–cytoplasmic fractionation. Fraction purity was confirmed by western blotting using Lamin B1 (nuclear marker) and β-Tubulin (cytoplasmic marker) (**Fig. 6A**).

Analysis of endogenous eIF6 established the baseline distribution, revealing a predominantly cytoplasmic localization (~65%) accompanied by a substantial nuclear pool (~35%) (**Fig. 6B**), in agreement with previous reports describing a primarily cytoplasmic but partly nuclear localization pattern.

Evaluation of the tagged constructs showed that both WT and S235A variants – regardless of whether they carried a Flag or Strep tag – displayed a nuclear–cytoplasmic distribution largely overlapping with that of the endogenous protein, with ~70–75% of the signal detected in the cytoplasmic fraction (**Fig. 6C**). The modest shift toward a higher cytoplasmic proportion is consistent with the expected effect of overexpression rather than a tag- or mutation-specific alteration. Importantly, statistical analysis revealed no significant differences (ns) in the nuclear-to-cytoplasmic ratio between WT and S235A eIF6. These quantitative data support the findings from immunofluorescence and confirm that the S235A substitution does not detectably affect the basal compartmental distribution of eIF6.

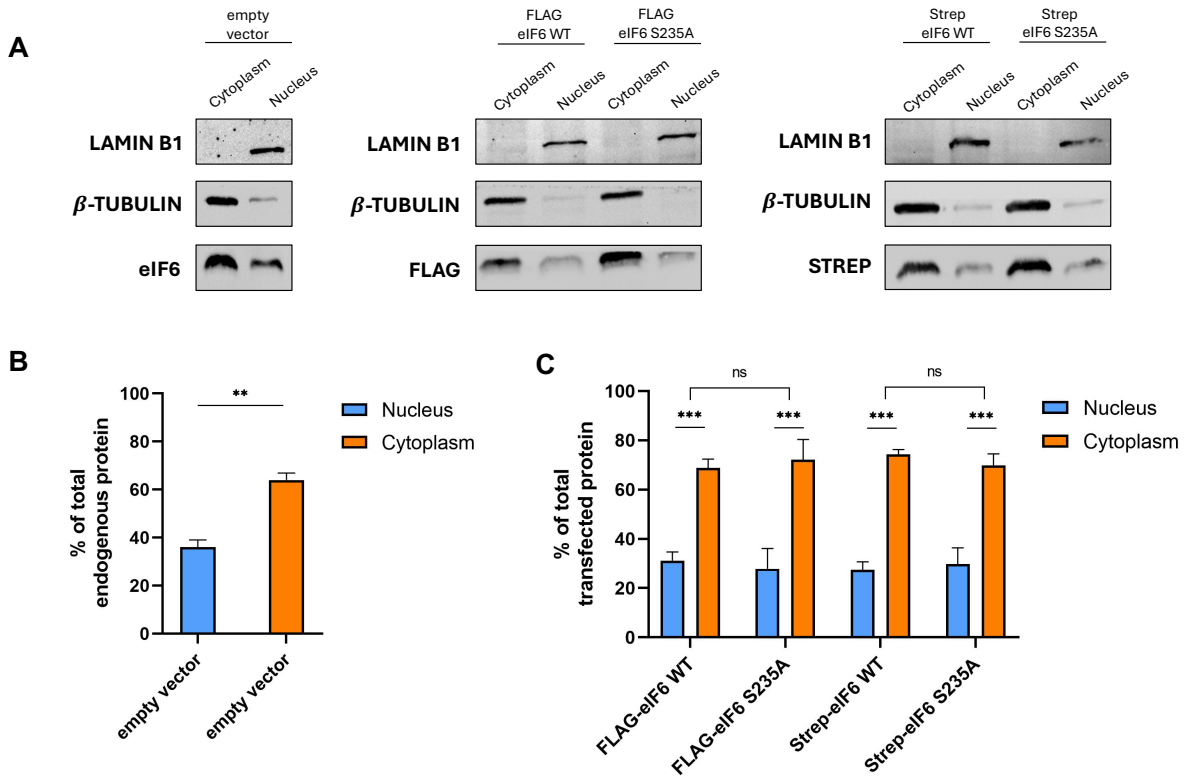


**Figure 6. Quantitative analysis of eIF6 subcellular localization.** (**A**) Western blot analysis of nuclear and cytoplasmic fractions from HEK293T cells transfected with empty vector, FLAG-tagged eIF6 constructs, and Strep-tagged eIF6 constructs. Lamin B1 and β-Tubulin were used as nuclear and cytoplasmic markers, respectively, to assess fractionation purity. eIF6, FLAG, and Strep antibodies were used to evaluate the localization of endogenous and overexpressed proteins (**B**) Quantification of endogenous eIF6 distribution between the cytoplasmic and nuclear fractions. Band intensities were measured by densitometry, normalized to the respective

compartment markers, and expressed as percentage of total eIF6. Endogenous eIF6 showed a predominantly cytoplasmic localization (63 %) (** $p < 0.01$ for cytoplasmic vs nuclear). Data represent mean ± SEM of n = 3 independent experiments. (**C**) Flag- and Strep-tagged eIF6 constructs (WT and S235A). All constructs displayed a similar cytoplasmic enrichment (~70–75%), with no significant difference (ns) between WT and S235A for either tagging strategy. Statistical significance (*** $p < 0.001$) refers to cytoplasmic vs nuclear distribution within each construct.

### 3.2.4. Ser235A mutation causes accumulation of free 60S and reduces translation initiation efficiency

Since eIF6 is considered a rate-limiting factor for translation initiation[119], we explored whether our S235A constructs, recapitulating Ser235 phosphorylation, would alter the early steps of ribosome assembly. To this aim, we performed polysome profiling in HEK293T cells overexpressing the tagged eIF6 constructs. As expected from the known anti-association activity of eIF6, overexpression of both WT and S235A variants induced a modest accumulation of free 60S subunits, consistent with transient sequestration of the large subunit by excess eIF6.

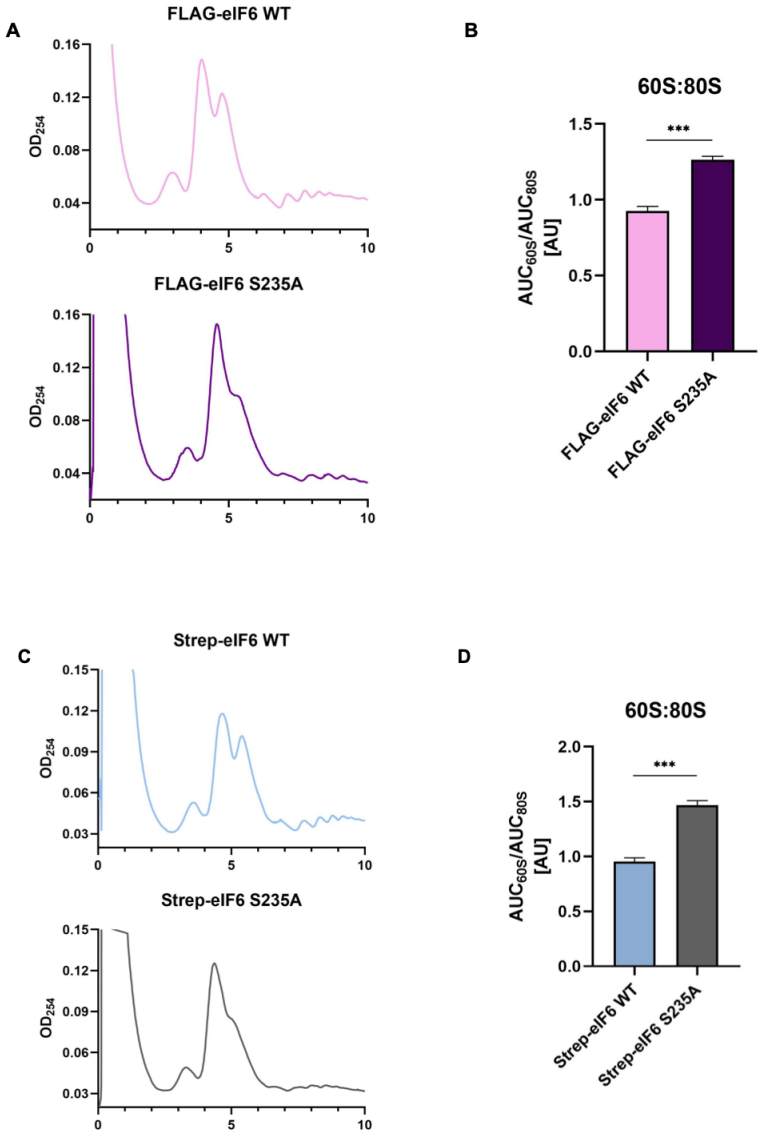


**Figure 7. The S235A mutation promotes accumulation of free 60S subunits and reduces 80S ribosome assembly.** (**A**) Rapresentative polysome profiles of HEK293T cells expressing FLAG-tagged eIF6 WT or S235A. (**B**) Quantification of the 60S/80S ratio ($AUC_{60S}/AUC_{80S}$) for the FLAG-tagged constructs. S235A exhibited a 1.32-fold increase in the ratio compared to WT (***, $p < 0.001$). (**C**) Polysome profiles of Strep-tagged eIF6 WT and S235A constructs. The S235A phenotype was fully reproduced with this

independent tagging system. (**D**) Quantification of the Strep dataset. S235A displayed a 1.61-fold increase in the 60S/80S ratio relative to WT (***, $p < 0.001$). Across both tagging strategies, S235A-expressing cells showed a qualitative reduction in polysomes, consistent with impaired 80S assembly and decreased translation initiation. Data represent mean ± SEM from $n = 3$ independent biological replicates. Statistical significance was determined using unpaired two-tailed t-test.

However, a clear functional divergence emerged between the two forms. Quantitative analysis revealed that S235A induced a substantially stronger accumulation of free 60S subunits relative to assembled 80S monosomes (**Fig. 7 B,D**). This effect was fully reproducible across both tagging strategies, with the $AUC_{60S}/AUC_{80S}$ ratio being 1.32-fold higher than WT in the FLAG dataset and 1.61-fold higher in the Strep dataset ($p < 0.001$ for both comparisons). In parallel, S235A-expressing cells exhibited a qualitative reduction in polysomes; although not quantified, this pattern is consistent with a potential impairment in translation initiation.

Importantly, the concordance between the two tagging systems excludes a tag-dependent artefact and confirms that the phenotype arises from the Ser235Ala substitution itself. Together, these results demonstrate that the S235A mutation compromises the transition from free 60S subunits to assembled 80S ribosomes, consistent with a defect in eIF6 release and a consequent reduction in translation initiation efficiency.

### 3.2.5. Phosphomimetic eIF6 S235E restores normal ribosome assembly by promoting 60S release

To test whether phosphorylation at Ser235 is not only necessary but also sufficient to regulate eIF6 release, we generated a phosphomimetic mutant (S235E), to recapitulate the negative charge induced by the the phosphorylation on Ser235. Since our earlier analyses had already demonstrated that the phenotypes observed for WT and S235A were fully independent of the tag used, we proceeded using only the Strep-tagged constructs, thereby reducing experimental redundancy while maintaining methodological robustness. The S235E variant was generated by site-directed mutagenesis starting from the Strep-eIF6 S235A construct.

Western blot analysis confirmed that S235E and S235A were expressed at comparable levels (**Fig. 8B**), as determined by densitometric quantification normalized to the loading control.

Polysome profiling revealed a marked shift in ribosome distribution between the two mutants (**Fig. 8A, C**). As observed previously, S235A caused an accumulation of free 60S subunits, with an $AUC_{60S}/AUC_{80S}$ ratio of approximately 1.25. In contrast, the S235E mutant restored a ribosomal distribution that closely approached the physiological state, exhibiting a ratio of ~0.70 and representing a 0.56-fold reduction relative to S235A.

These findings indicate that mimicking phosphorylation at Ser235 is sufficient to counteract the 60S retention defect associated with the S235A variant. Thus, the phosphorylation status of this residue emerges as a key regulatory element controlling eIF6 release from the 60S subunit and enabling efficient 80S assembly.

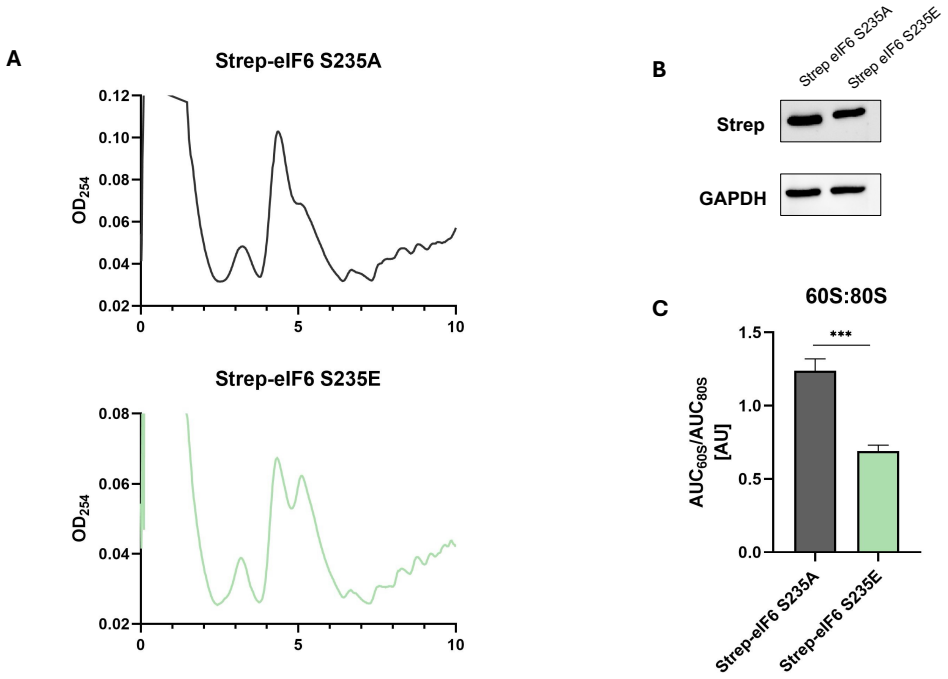


**Figure 8. The phosphomimetic eIF6 S235E mutant restores normal 60S-80S balance.** (**A**) Representative polysome profiles showing absorbance at 254 nm from HEK293T cells overexpressing the non-phosphorylatable S235A mutant and the phosphomimetic S235E mutant. (**B**) Western blot showing stable and comparable expression of both Strep-tagged mutants. GAPDH was used as loading control (**C**) Quantitative analysis of the $AUC_{60S}/AUC_{80S}$ ratio. The S235E mutant displayed a significantly lower ratio relative to S235A (***, $p < 0.001$), approaching values observed for WT eIF6. These data indicate that introduction of a negative charge at position 235 is sufficient to counteract the 60S retention phenotype associated with S235A. Data are mean ± SEM.

# 3.3. eIF6 interactome characterization: from technical challenges to *in silico* and structure-based evidence

## 3.3.1. Affinity purification approaches reveal limitated sensitivity for detecting eIF6 interactors

Having established the functional relevance of Ser235 phosphorylation, we next sought to identify candidate upstream regulators responsible for modulating this site. As an initial exploratory approach, we attempted to characterize the eIF6 interactome using affinity purification and pull-down strategies. Both FLAG- and Strep-tagged eIF6 constructs were evaluated in parallel; although both systems enabled recovery of the tagged protein, the FLAG pulldowns consistently exhibited high nonspecific background, whereas the Strep-tag system yielded markedly cleaner eluates. For this reason, subsequent analyses focused on the Strep-tagged variants.

Pull-down assays performed in HEK293T lysates confirmed efficient and comparable recovery of both Strep-eIF6 WT and Strep-eIF6 S235A (**Fig. 9A**), validating the robustness of the purification protocol based on StrepTactin resin. Nevertheless, silver staining of the eluates revealed only a small number of co-purifying proteins, and although several bands were detected above the eIF6 signal, their intensity and resolution did not allow reliable discrimination between WT and S235A (**Fig. 9B**). Thus, differences, if present, fell below the level of analytical resolution achievable with this approach.

To complement these findings, we performed *in vitro* immunoprecipitation assays using recombinant eIF6 incubated with HEK293T extracts. This approach yielded a broader and more complex spectrum of co-precipitated proteins but likewise failed to reveal clearly distinguishable candidate interactors between the WT and S235A forms (**Fig. 10**).

Together, these results suggest that eIF6 interactors involved in Ser235 regulation are likely low-affinity, transient, or present in substoichiometric amounts, features commonly associated with kinase–substrate or phosphatase–substrate interactions. These biochemical properties, combined with the limitations of affinity-based approaches in resolving weak or unstable complexes, likely account for the difficulty in isolating differential interactors in this system. Consequently, we shifted from an unbiased interactome-wide search toward a more targeted, hypothesis-driven strategy to identify the upstream regulator(s) of Ser235 phosphorylation.

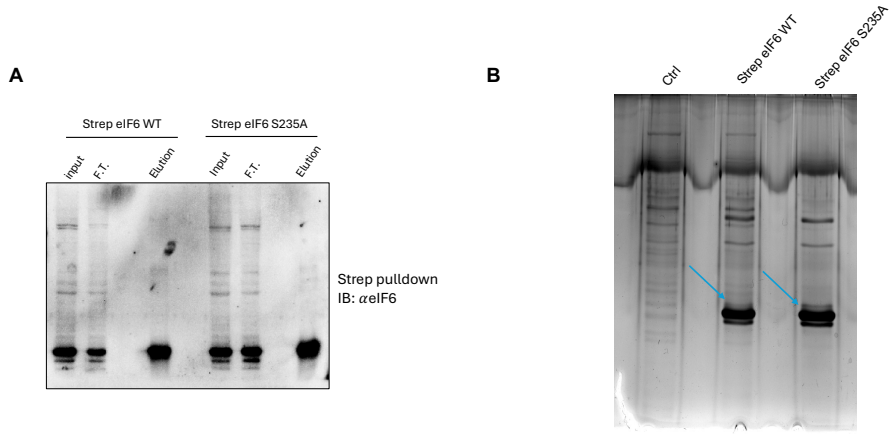


**Figure 9. Pull-down purification strategy of Strep-tagged eIF6 reveals low co-purifying interactors.** (**A**) Pull-down of Strep-tagged eIF6 WT and S235A from HEK293T lysates using StrepTactin resin. Western blot (α-eIF6) of Input, Flow-Through (F.T.), and Elution fractions confirms efficient and comparable recovery of both tagged proteins. (**B**) Silver-stained SDS-PAGE of the eluates corresponding to panel (A). Blue arrows indicate the Strep-eIF6 band. Several cellular proteins co-purify with eIF6; however, their intensity, resolution, and pattern do not reveal clearly distinguishable differences between WT and S235A, limiting the ability to identify differential interactors suitable for downstream mass spectrometry.

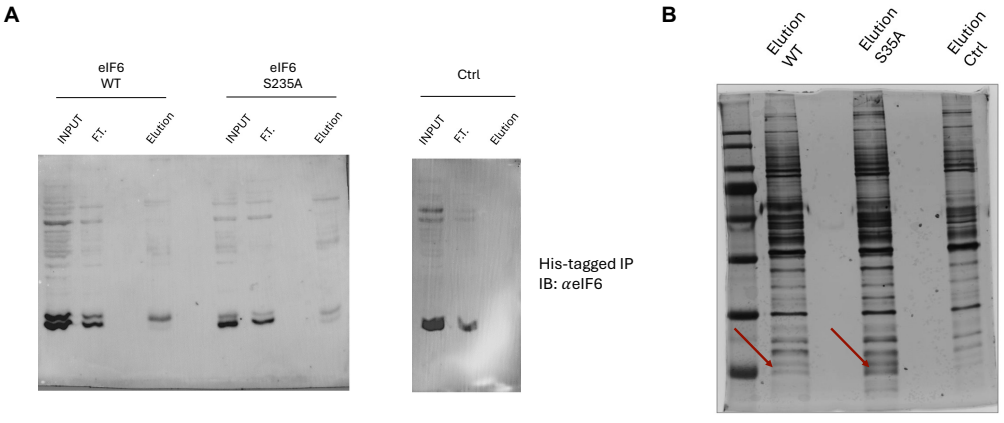


**Figure 10. In vitro immunoprecipitation with recombinant eIF6 yields nonspecific co-precipitation patterns.** (**A**) Western blot (α-eIF6) confirming the successful recovery of recombinant eIF6 WT and S235A following incubation with HEK293T lysates, alongside the control (Ctrl). (**B**) Corresponding silver-stained gel of the elution fractions. The eIF6 band is indicated by red arrows. Multiple co-precipitated proteins are visible; however, the complexity and similarity of the patterns between WT and S235A indicate that this assay lacks the specificity and resolution needed to identify differential regulators of Ser235 phosphorylation.

### 3.3.2. Identification of DUSP12 as a potential eIF6 interactor through proximity labeling and network analysis

Since affinity-purification approaches did not yield sufficiently stable or differential eIF6-associated proteins, we next turned to a computational strategy leveraging high-resolution proximity-labeling datasets to identify candidate regulatory factors. Specifically, we interrogated a published BioID screen (PMID: 34385409), which maps protein–protein proximity networks via biotinylation of proteins located within the spatial range of a BirA*–bait fusion[200]. Using the authors' online analysis platform (https://humancellmap.org), we selected eIF6 as bait and retrieved the corresponding set of high-confidence proximal proteins, acknowledging that BioID captures spatial proximity rather than strictly direct binding events.

To investigate functional relationships among these candidates, the BioID preys were analyzed using STRING (confidence ≥ 0.400, full network mode). The resulting network displayed extensive non-random connectivity, forming a module of 62 nodes and 436 edges (PPI enrichment $p < 1 \times 10^{-16}$). Application of the MCL clustering algorithm (inflation = 2.6) resolved the BioID-derived network into five major submodules. Cluster analysis was performed to uncover groups of functionally related proteins within the larger proximity dataset, which inherently contain both direct and indirect neighbors of the bait. Among the resulting clusters, the largest and most densely connected one was enriched for proteins implicated in late 60S subunit maturation and cytoplasmic export (**Fig. 11**), indicating a strong biological convergence between eIF6 and factors acting at this specific stage of ribosome biogenesis.

Within this cluster, DUSP12 emerged as a compelling candidate. Although not among the highest-ranking BioID preys by raw abundance score, its enzymatic function as a dual-specificity phosphatase makes it mechanistically compatible with the regulation of a phosphorylation-dependent switch such as Ser235 of eIF6. Importantly, DUSP12 was directly connected to eIF6 and to three factors implicated in late cytoplasmic maturation of the 60S subunit: GNL2 (a nucleolar GTPase), GTPBP4 (a ribosome-associated GTP-binding protein), and LSG1 (a cytoplasmic 60S release factor). Revisiting the original proximity-labeling dataset further revealed that DUSP12 was detected exclusively in the eIF6-BioID condition, with no peptides detected in control samples, and exhibited strong enrichment metrics (fold change ≈ 35; specificity at the upper limit of the scoring scale; FDR = 0), supporting a highly specific association.

Collectively, these observations identify DUSP12 as a high-priority candidate regulator and raise the possibility that it may participate in modulating the phosphorylation status of eIF6 at Ser235.

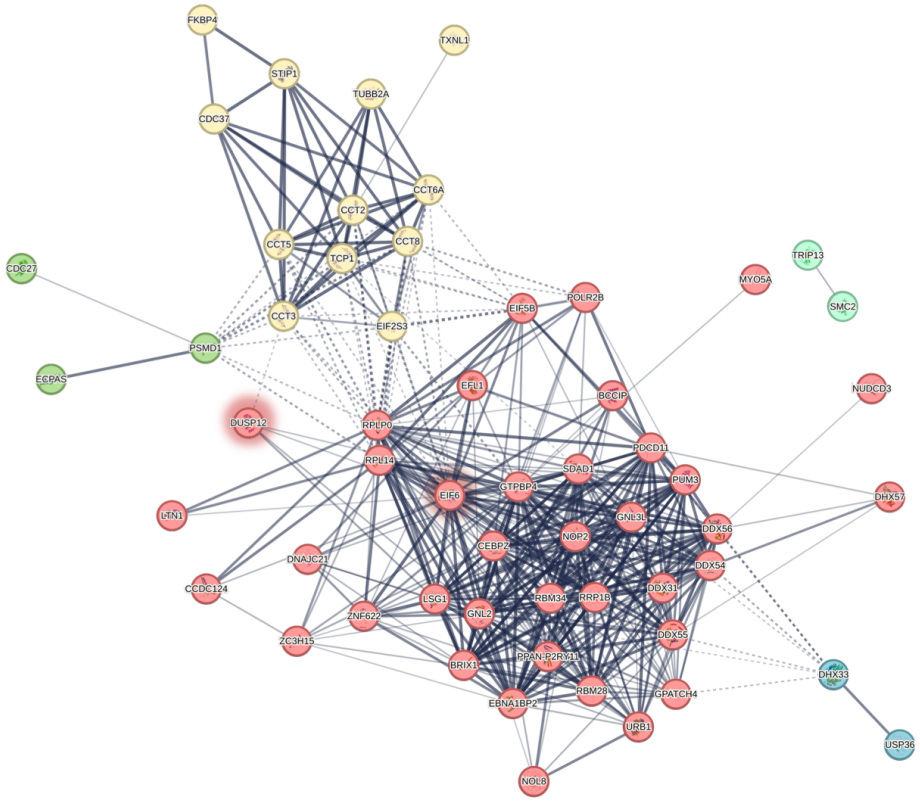


| color | cluster Id | gene count | description |
|---|---|---|---|
| | Cluster 1 | 38 | Mixed, incl. Preribosome, large subunit precursor, and Ribosomal large subunit biogenesis |
| | Cluster 2 | 12 | + Positive regulation of establishment of protein localization to telomere |
| | Cluster 3 | 3 | CDC27, ECPAS, PSMD1 |
| | Cluster 4 | 2 | SMC2, TRIP13 |
| | Cluster 5 | 2 | DHX33, USP36 |

**Figure 11. STRING network of eIF6-proximal proteins identified by BioID analysis**. **Figure 10. STRING network of eIF6-proximal proteins identified by BioID analysis.** Protein–protein interaction network derived from high-confidence proximity interactors of eIF6 obtained from the BioID dataset of Go et al. (2021). The preys retrieved through the Human Cell Map online tool were analyzed using STRING (full network mode; minimum interaction score = 0.400). Edge thickness reflects interaction confidence (range 0.4–0.9). Node colors denote cluster assignment following MCL clustering (inflation = 2.6). In red a central, densely interconnected cluster, enriched in factors involved in late 60S subunit maturation and cytoplasmic export, contains both eIF6 and DUSP12, which are highlighted with a halo. Peripheral nodes with no detectable connectivity to the main network are omitted for clarity.

### 3.3.3 Structural evidence places the yeast DUSP12 homolog Yvh1 in spatial proximity to eIF6 to eIF6 on a late pre-60S particle

To obtain orthogonal structural evidence supporting a functional connection between eIF6 and DUSP12, we examined high-resolution cryo-electron microscopy (cryo-EM) structures of yeast pre-60S maturation intermediates. This approach was guided by our network analysis (paragraph 3.3.2.), which highlighted late 60S biogenesis and export factors as a central functional module potentially linking eIF6 to DUSP12. Moreover, since eIF6 exerts its regulatory function on the large (60S) ribosomal subunit, we focused on cryo-EM structures of late pre-60S particles from *Saccharomyces cerevisiae*, a system in which ribosome maturation factors are extensively characterized.

In particular, we analyzed the structure of a cytoplasmic late pre-60S particle (PDB ID: 6N8O). Although alternative structures from the same study capture similar factor compositions or slightly

higher nominal resolutions (e.g. 6N8M), 6N8O was selected because it represents a pivotal functional checkpoint during 60S maturation. This structure captures the insertion of the P-site loop of Rpl10, a conformational rearrangement that completes the peptidyl transferase center and promotes the retraction of Nmd3 from the P-site. This transition enables Sdo1 to assess P-site integrity and activate the Efl1 GTPase, which functions as a quality control sensor licensing the large subunit for translation by triggering the release of Tif6, in yeast.

Inspection of this assembly intermediate revealed the presence of Yvh1 – the yeast ortholog of mammalian DUSP12 – bound to the solvent-exposed surface of the pre-60S subunit in the same particle that contains Tif6. Visualization using UCSF ChimeraX showed that Yvh1 and Tif6 occupy adjacent yet non-overlapping regions of the ribosome surface (**Fig. 12**), indicating spatial co-localization during this critical quality control step. Although no direct physical contacts are observed in the resolved structure, their proximity places them within the same functional neighborhood at a defined stage of ribosome maturation. This observation is notable given that Yvh1 is genetically and biochemically required for late 60S biogenesis, including the release of the ribosomal stalk placeholder Mrt4.

The conserved co-localization of Tif6 and Yvh1 on a late pre-60S maturation intermediate provides structural support for a potential regulatory relationship between their mammalian counterparts, eIF6 and DUSP12. Together with the enzymatic phosphatase activity of DUSP12, these observations prompted us to prioritize DUSP12 as a candidate modulator of eIF6 dynamics and, potentially, of its phosphorylation status at Ser235.

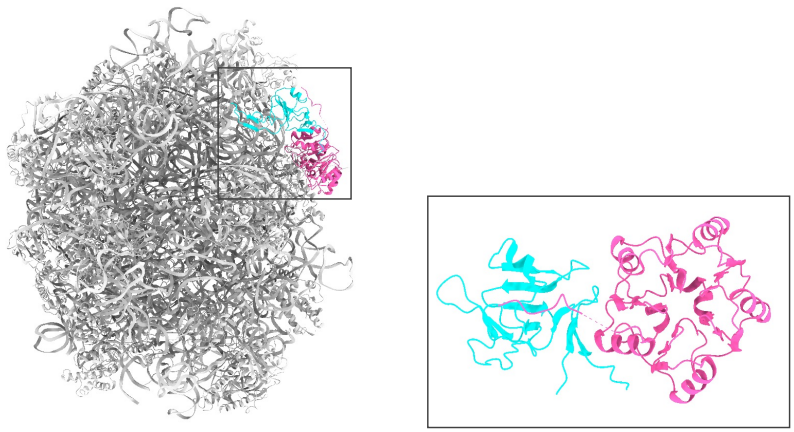

**Figure 12. Yvh1 and Tif6 are found in spatial proximity on the solvent-exposed face of the pre-60S ribosomal intermediate**. Ribbon representation of a late cytoplasmic pre-60S particle from S. *cerevisiae* (PDB ID: 6N8O), visualized using UCSF ChimeraX. The complete ribosomal particle is shown on the left (grey), while the region encompassing Yvh1 (cyan) and Tif6 eIF6 (magenta) is highlighted and magnified on the right. Although Yvh1 and Tif6 do not form direct contacts in the resolved structure, their close spatial proximity within the same maturation intermediate places them in a shared functional environment during late stages of 60S quality control. This spatial arrangement provides structural context supporting a potential regulatory relationship between their mammalian counterparts, DUSP12 and eIF6.

## 3.4. DUSP12 as a putative modulator of eIF6 activity

### 3.4.1. Overexpressed DUSP12 shows preferential cytoplasmic colocalization with phosphorylated eIF6

To investigate the potential role of DUSP12 in regulating eIF6 in a cellular context, we first examined its subcellular localization and spatial relationship with eIF6. FLAG-tagged DUSP12 (**Fig. 13A**) was transiently overexpressed in HEK293T cells, and its expression was independently confirmed by commercial anti-FLAG immunoblotting and anti-DUSP12 antibody (**Fig. 13B**). Under these conditions, endogenous DUSP12 was not readily detectable in control cells transfected with empty vector, likely reflecting its low steady-state abundance and/or limited antibody sensitivity in this cellular system.

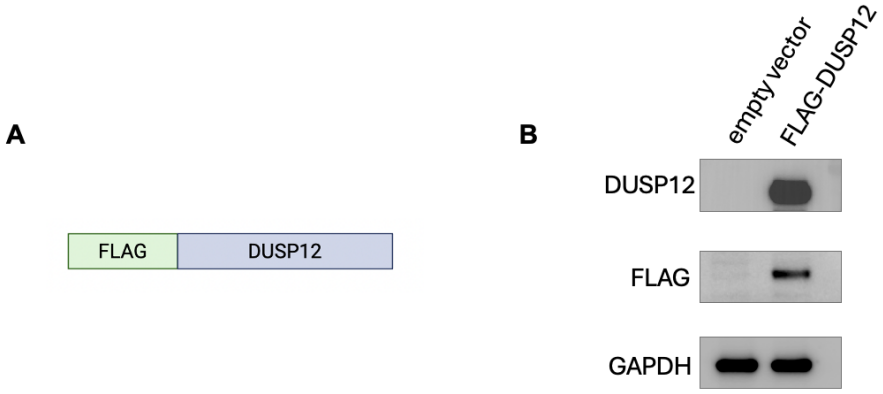


**Figure 13. Validation of FLAG-DUSP12 expression in HEK293T cells.** (**A**) Schematic representation of the FLAG-DUSP12 construct, carrying an N-terminal FLAG epitope tag. (**B**) Representative western blot analysis showing the expression of FLAG-tagged DUSP12 in HEK293T cells transiently transfected with the indicated constructs. FLAG-DUSP12 expression was detected using both an anti-FLAG antibody and a commercial anti-DUSP12 antibody. Cells transfected with empty vector (EV) served as negative controls. Endogenous DUSP12 was not detectable in this setting, likely due to its low steady-state abundance or the limited sensitivity of the antibody under these experimental conditions. GAPDH was used as a loading control. The blot shown is representative of *n*= 3 independent biological replicates.

For subcellular localization studies, immunofluorescence analyses were performed in HeLa cells, which provide optimal morphology and resolution for intracellular imaging. Overexpressed DUSP12 localized predominantly to the cytoplasm, with only a minor nuclear signal detectable. Endogenous eIF6 displayed its characteristic distribution, with strong nucleolar enrichment accompanied by a diffuse cytoplasmic pool. Upon DUSP12 overexpression, partial colocalization between DUSP12 and eIF6 was observed specifically within the cytoplasmic compartment, whereas nucleolar eIF6 remained spatially segregated (**Fig. 14A**). This pattern indicates that the detectable spatial association between the two proteins is restricted to a subset of the cytoplasmic eIF6 pool. Importantly, this observation may reflect the predominantly cytoplasmic localization of overexpressed DUSP12, rather than selective exclusion of nucleolar eIF6 from potential regulation. Therefore, while the data support a cytoplasmic site of interaction, they do not exclude additional regulatory interactions occurring in other cellular compartments under physiological conditions.

To quantitatively assess spatial association, pixel-based colocalization analysis was performed between DUSP12 and either total eIF6 or phosphorylated eIF6 (p-eIF6), the latter being largely excluded from the nucleus (**Fig. 14B**). Pearson's correlation coefficients (R) were calculated on background-corrected, non-thresholded images and validated using Costes' randomization test. The association with total eIF6 showed a moderate correlation (Pearson's R = 0.58), whereas colocalization with p-eIF6 was substantially stronger (Pearson's R = 0.84). Both correlations were statistically significant ($P < 0.005$).

Collectively, these results indicate that overexpressed DUSP12 preferentially colocalizes with the phosphorylated pool of eIF6 within the cytoplasm, consistent with a potential functional link between DUSP12 localization and phosphorylation-dependent regulation of eIF6.

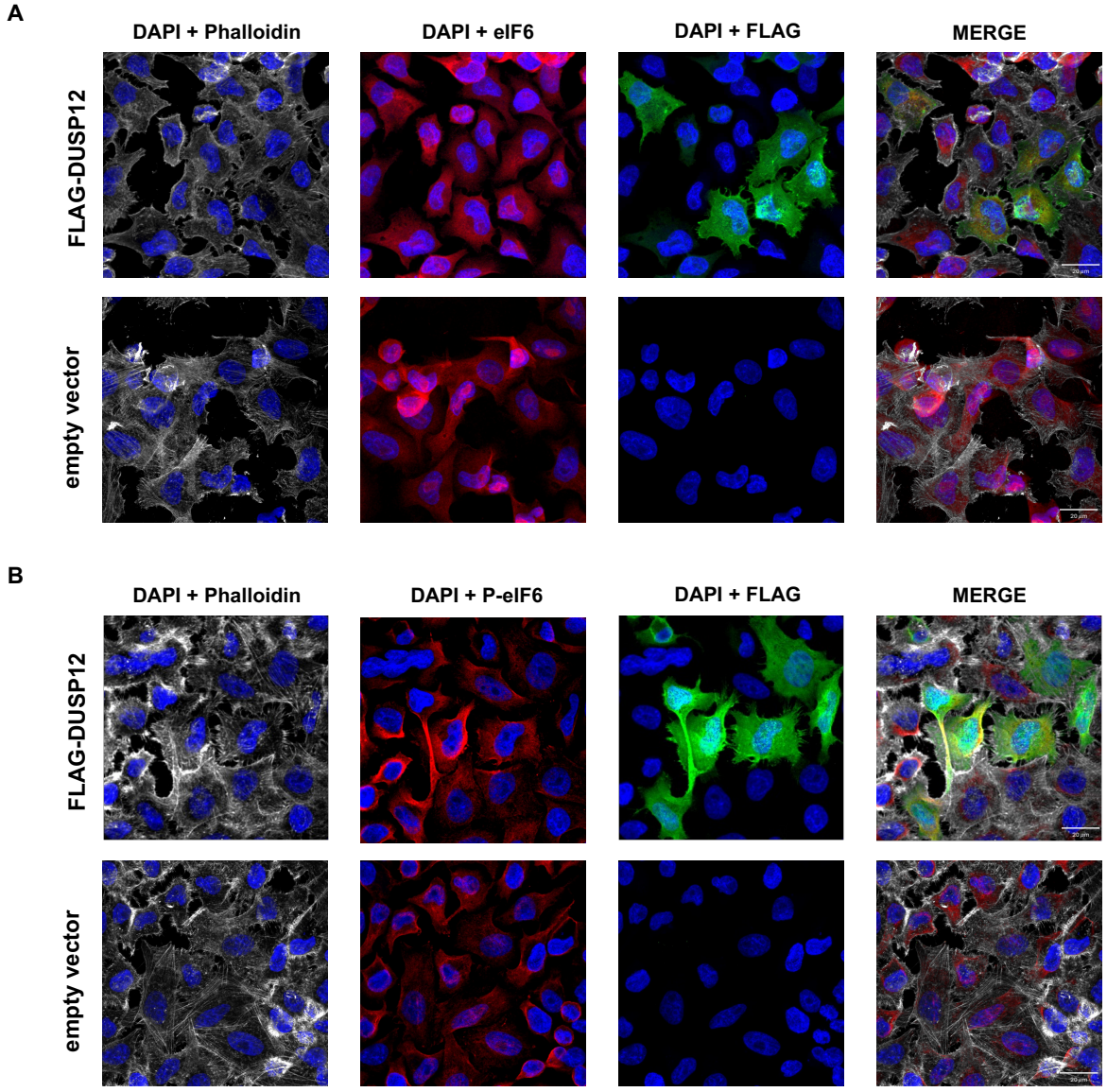


**Figure 14 DUSP12 partially colocalizes with eIF6 in the cytoplasm and preferentially associates with phosphorylated eIF6.** Representative immunofluorescence (IF) images comparing the localization of overexpressed of HeLa cells transfected with FLAG-DUSP12 or empty vector (EV). FLAG-DUSP12 is shown in green, eIF6 or phosphorylated eIF6 (p-eIF6) in red. Nuclei are stained with DAPI (blue), and phalloidin (gray) outlines cell boundaries. (**A**) FLAG-DUSP12 and total eIF6. FLAG-DUSP12 localizes predominantly to the cytoplasm and shows partial spatial overlap with the cytoplasmic pool of eIF6, while nucleolar eIF6 remains distinct. (**B**) FLAG-DUSP12 and phosphorylated eIF6 (p-eIF6). A stronger spatial overlap is observed between FLAG-DUSP12 and p-eIF6 within the cytoplasm, consistent with preferential proximity to the phosphorylated pool of eIF6.

These data indicate that transfected DUSP12 preferentially colocalizes with the phosphorylated pool of eIF6 in the cytoplasm, supporting supporting a functional link between DUSP12 localization and the phosphorylation-dependent regulation of eIF6.

### 3.4.2. DUSP12 overexpression decreases the organization of active ribosomal complexes without recapitulating eIF6 dephosphorylation

To comprehensively assess the functional impact of DUSP12 overexpression on the translational machinery, we performed polysome profiling (**Fig. 15A**). The rationale for this experiment was two-fold. First, given the reported role of DUSP12 orthologs in 60S subunit maturation in yeast[163,164], we tested whether cytoplasmic DUSP12 overexpression affects the structural integrity of ribosomal subunits in human cells. Second, building on our previous observation that a non-phosphorylatable eIF6 mutant (S235A) leads to accumulation of free 60S subunits and that DUSP12 partially colocalizes with eIF6, we aimed to evaluate potential consequences of DUSP12 overexpression on ribosomal complex organization.

We first measured the ratio of free large subunits to assembled monosomes ($AUC_{60S}/AUC_{80S}$) to determine whether DUSP12 overexpression induces accumulation of free 60S subunits. Such an effect would be indicative of altered 60S maturation or impaired subunit joining, as observed upon expression of the non-phosphorylatable eIF6 S235A mutant. Quantitative analysis revealed no statistically significant difference in the $AUC_{60S}/AUC_{80S}$ ratio between control and DUSP12-overexpressing cells (**Fig. 15B**, $p > 0.05$). In parallel, Northern blot analysis revealed comparable levels of mature 5.8S rRNA in control and DUSP12-overexpressing cells, with no detectable accumulation of pre-rRNA processing intermediates (**Fig. S1**), indicating that DUSP12 overexpression does not cause gross alterations in rRNA abundance or processing. Together, these results suggest that, under these conditions, DUSP12 overexpression does not broadly impair 60S ribosomal subunit biogenesis. Importantly, DUSP12 overexpression did not phenocopy the accumulation of free 60S subunits associated with impaired eIF6 phosphorylation observed in the S235A mutant.

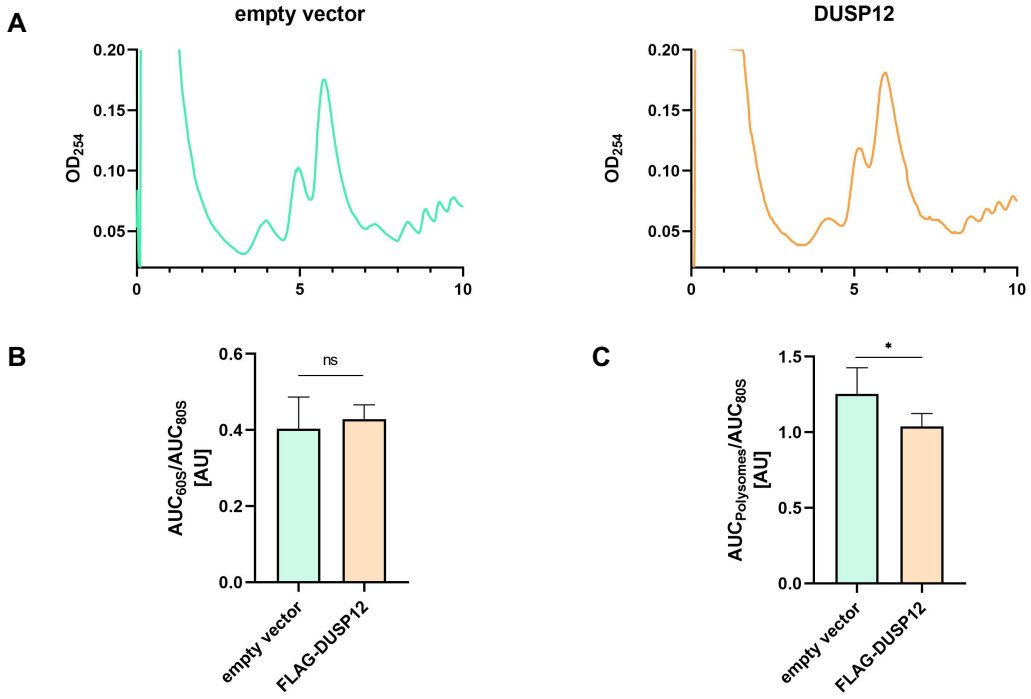


**Fiigure 14. DUSP12 overexpression alters the distibution of active ribosomal complexes without inducing free 60S subunit accumulation.** (**A**) Representive polysome profile from HEK293T cells transfected with empty vector (green line) and FLAG-DUSP12 (orange line). While the overall profile is preserved, the polysome region (to the right of the 80S peak) appears less sharply resolved in DUSP12-overexpressing cells. (**B**) Quantification of the ratio between free large subunits and monosomes ($AUC_{60S}/AUC_{80S}$ ratio), used to assess the accumulation of the free 60S subunit. No statistically significant difference was detected between control and FLAG-DUSP12 expressing cells (ns, $p > 0.05$), indicating that cytoplasmic DUSP12 overexpression does not alter the 60S/80S equilibrium

(**C**) Quantification of the polysome-to-monosome ratio ($AUC_{Polysomes}/AUC_{80S}$), used as a structural proxy for translation initiation efficiency. FLAG-DUSP12–expressing cells show a modest but statistically significant reduction compared to control (*, $p < 0.05$), consistent with a relative redistribution from polysomes toward monosomes. Data are expressed as mean ± SEM. Statistical significance was determined using the Paired t-test on n=4 indipendent biological replicates.

We next focused on ribosomal complexes engaged in active translation by quantifying the polysome-to-monosome ratio ($AUC_{Polysome}/AUC_{80S}$), commonly used as a structural indicator of translation initiation efficiency. While overall polysome profiles were preserved, DUSP12-overexpressing cells consistently displayed less sharply defined peaks in the polysome region across independent experiments. Quantitative analysis confirmed a modest but statistically significant reduction in the polysome-to-monosome ratio compared to control cells (**Fig. 14C**, $p < 0.05$). These data indicate that DUSP12 overexpression is associated with subtle alterations in the distribution of ribosomal complexes across translating mRNAs, without inducing a broad defect in ribosome assembly.

### 3.4.3. DUSP12 overexpression does not globally reduce eIF6 Ser235 phosphorylation

Given the subtle structural changes observed in the polysome profiles – where DUSP12 overexpression did not recapitulate the 60S accumulation phenotype induced by the non-phosphorylatable eIF6 S235A mutant – we next sought to directly assess whether DUSP12 overexpression affected the phosphorylation status of eIF6. To this end, total eIF6 and its phosphorylated form at Ser235 (p-eIF6) were analyzed by Western blot in whole-cell lysates. Despite the modest but significant reduction in the polysome-to-monosome ratio observed upon DUSP12 overexpression, no appreciable decrease in p-eIF6 levels was detected compared to control cells (**Fig. 15**). These results indicate that the polysome remodeling associated with DUSP12 overexpression is not accompanied by a global dephosphorylation of eIF6.

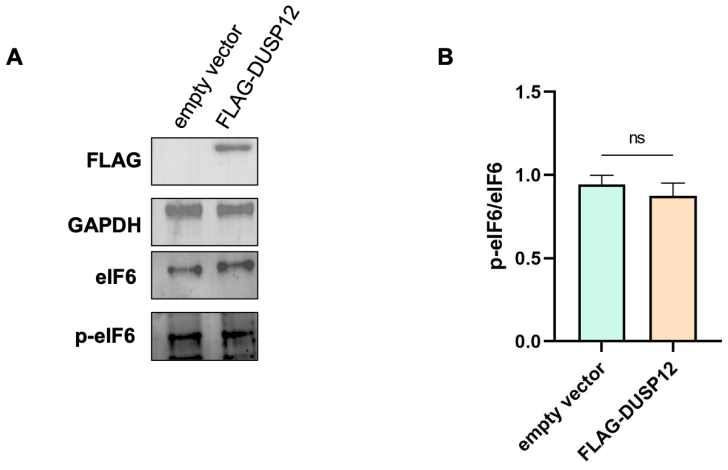


**Figure 15. eIF6 phosphorylation at Ser235 is unchanged upon DUSP12 overexpression.** (**A**) Representative Western blot analysis of whole-cell lysates from HEK293T cells transfected with empty vector or FLAG-DUSP12. The blot confirms robust overexpression of FLAG-DUSP12 (top panel). Total eIF6 and phosphorylated eIF6 (p-eIF6, Ser235) were analyzed to assess the phosphorylation status of eIF6. GAPDH was used as a loading control. (**B**) Quantitative densitometric analysis of eIF6 phosphorylation. The p-eIF6/eIF6 ratio was calculated and normalized to the empty vector condition (Fold Change = 1.0). No statistically significant difference was detected between control and FLAG-DUSP12–overexpressing cells (ns, $p > 0.05$), indicating that DUSP12 overexpression does not induce a global change in eIF6 phosphorylation under these conditions. Data are expressed as mean ± SEM. Statistical significance was assessed using a paired t-test.

This observation is consistent with at least two non-mutually exclusive scenarios. First, DUSP12 activity toward eIF6 may be spatially or temporally restricted, acting on a specific subpopulation of eIF6 that would be diluted in whole-cell lysates and therefore escape detection under our experimental conditions. Alternatively, DUSP12 may influence ribosomal complex organization through substrates other than eIF6, potentially modulating additional components of the translational machinery.

### 3.4.4. DUSP12 overexpression enhances translational output in cellular and cell-free systems

To determine whether the structural changes observed in polysome profiles were associated with functional consequences on protein synthesis, we quantified global translation using the puromycin incorporation assay. Puromycin is incorporated into elongating nascent polypeptide chains, allowing direct measurement of ongoing translation. Western blot analysis revealed a clear increase in puromycin incorporation across a broad molecular weight range in DUSP12-overexpressing cells compared to controls (**Fig. 16A**). Densitometric quantification confirmed a statistically significant 1.77-fold increase in global protein synthesis in DUSP12-transfected cells relative to controls ($p < 0.05$; **Fig. 16B**). These data indicate that, despite the sublte alterations in ribosomal complex distribution detected by polysome profiling, DUSP12 overexpression is associated with enhanced translational output *in vivo*. It is important to note that polysome profiling provides a structural snapshot of ribosome distribution and is primarily informative of translation initiation and ribosome loading, rather than elongation dynamics or overall translational output. Therefore, alterations in polysome architecture do not necessarily predict changes in global protein synthesis.

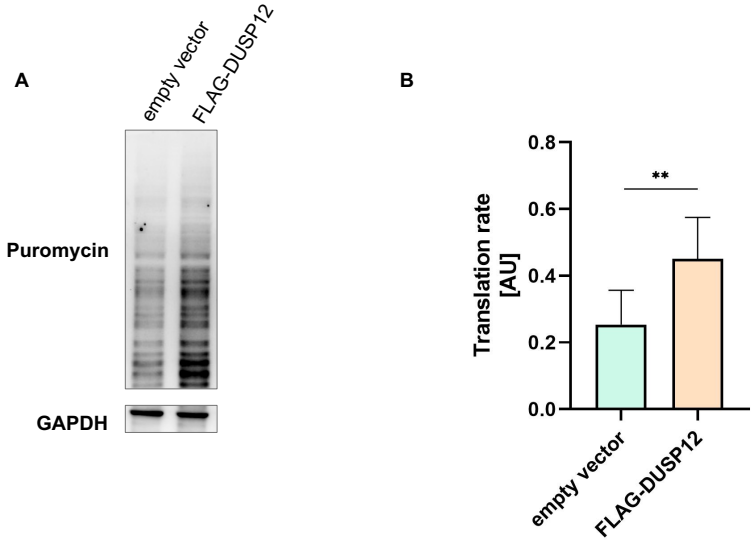


**Figure 16. DUSP12 overexpression significantly enhances the global rate of protein synthesis *in vivo*. (A)** Representative Western blot (WB) analysis of puromycin incorporation, selected from n=4 independent biological replicates. Cells were transfected with empty vector or FLAG-DUSP12, treated with puromycin, and harvested. Puromycin incorporation into nascent polypeptide chains (top) shows a visible qualitative increase in DUSP12-overexpressing cells compared to control cells. GAPDH serves as the loading control (bottom). **(B)** Quantitative analysis of the translation rate. The incorporated puromycin signal was quantified via puromycin-specific ELISA, confirming a statistically significant enhancement of the translation rate in DUSP12-overexpressing cells. Data are expressed as Translation Rate [AU], normalized to the total protein concentration. The mean translation rate is enhanced by approximately 1.77-fold in the DUSP12 sample (mean: ~0.45 AU) compared to the control (mean: ~0.25 AU). Statistical significance was determined using the paired t-test on n=4 biological replicates (**, $p < 0.01$)

To validate the pro-translational effect of overexpressed DUSP12 in a controlled, cell-free system, we established an *in vitro* translation assay using translationally active cytoplasmic lysates from HEK293T cells prepared by an optimized dual-centrifugation protocol[205] (**Fig. 17A**). Exogenous luciferase mRNA was added as a reporter, and luminescence was measured as a proxy for protein

synthesis. Lysates derived from DUSP12-overexpressing cells consistently displayed higher luminescence compared to control lysates across three independent biological replicates (n = 3). Although absolute luminescence levels varied between preparations, the stimulatory effect of DUSP12 was reproducible, with a mean increase of ~1.38-fold (**Fig. 17B**).

Taken together, data from both cellular and acellular systems indicate that DUSP12 overexpression increases translational output. The stimulation of protein synthesis observed *in vitro*, in the absence of intact upstream cellular signaling or compartmentalization, supports a direct contribution of DUSP12 to translational control. The concomitant structural alterations observed in polysome organization are therefore consistent with an effect of DUSP12 on ribosome dynamics, resulting in enhanced protein synthesis.

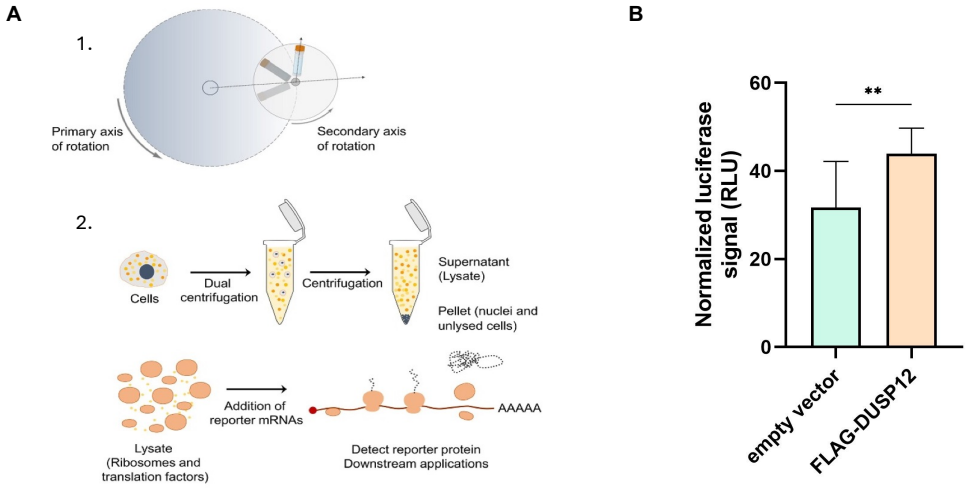


**Figure 16. DUSP12 enhances translational output in a cell-free system.** (**A**) Schematic overview of the optimized dual-centrifugation protocol used to generate translationally active cytoplasmic lysates from HEK293T cells. Panel 1 illustrates the primary and secondary axes of rotation utilized in the protocol. Panel 2 details the procedure: Sequential centrifugation steps remove intact nuclei and unlysed cells, yielding a clarified cytoplasmic extract enriched in ribosomes and translation factors, which is subsequently used for in vitro translation upon addition of a reporter mRNA (image adapted from Guerzeler et al.[205]). (**B**) Quantitative analysis of *in vitro* translational activity measured by luciferase reporter production. Data are expressed as normalized luciferase signal (RLU), corrected for total protein concentration. The mean translational activity is increased by approximately 1.38-fold in DUSP12-derived lysates. Statistical significance was assessed using a paired t-test on n = 3 independent biological replicates (**, $p < 0.01$).

# 3.5. Dissecting the molecular functions of DUSP12 through integrated omics

## 3.5.1. Quantitative phosphoproteomics show that DUSP12 targets nuclear components and RNA splicing machinery

Given the observed effects of DUSP12 overexpression on ribosomal organization and translational output, we next investigated whether these phenotypes were associated with measurable alterations in the cellular phosphoproteome. To this end, we performed a quantitative phosphoproteomic analysis comparing DUSP12-overexpressing cells with empty vector (EV) controls using a tandem mass tag (TMT)-based workflow.

Phosphopeptide-level quantification identified 5,273 phosphorylated peptides mapping to 1,783 proteins, each carrying at least one confidently assigned phosphorylation site on serine, threonine, or tyrosine residues. Relative abundance ratios between DUSP12-overexpressing and control samples

were initially obtained at the phosphopeptide level. To specifically capture phosphorylation-dependent regulation and account for potential changes in total protein abundance, phosphopeptide ratios were subsequently normalized to the corresponding protein-level abundances derived from the matched total proteome dataset.

Phosphorylation sites displaying reduced abundance upon DUSP12 overexpression were identified using combined significance and fold-change criteria (as described in Methods 2.9.1.). Collapsing these sites to unique protein identifiers enabled subsequent analyses aimed at determining whether proteins with reduced phosphorylation in response to DUSP12 overexpression shared common spatial localization and biological context.

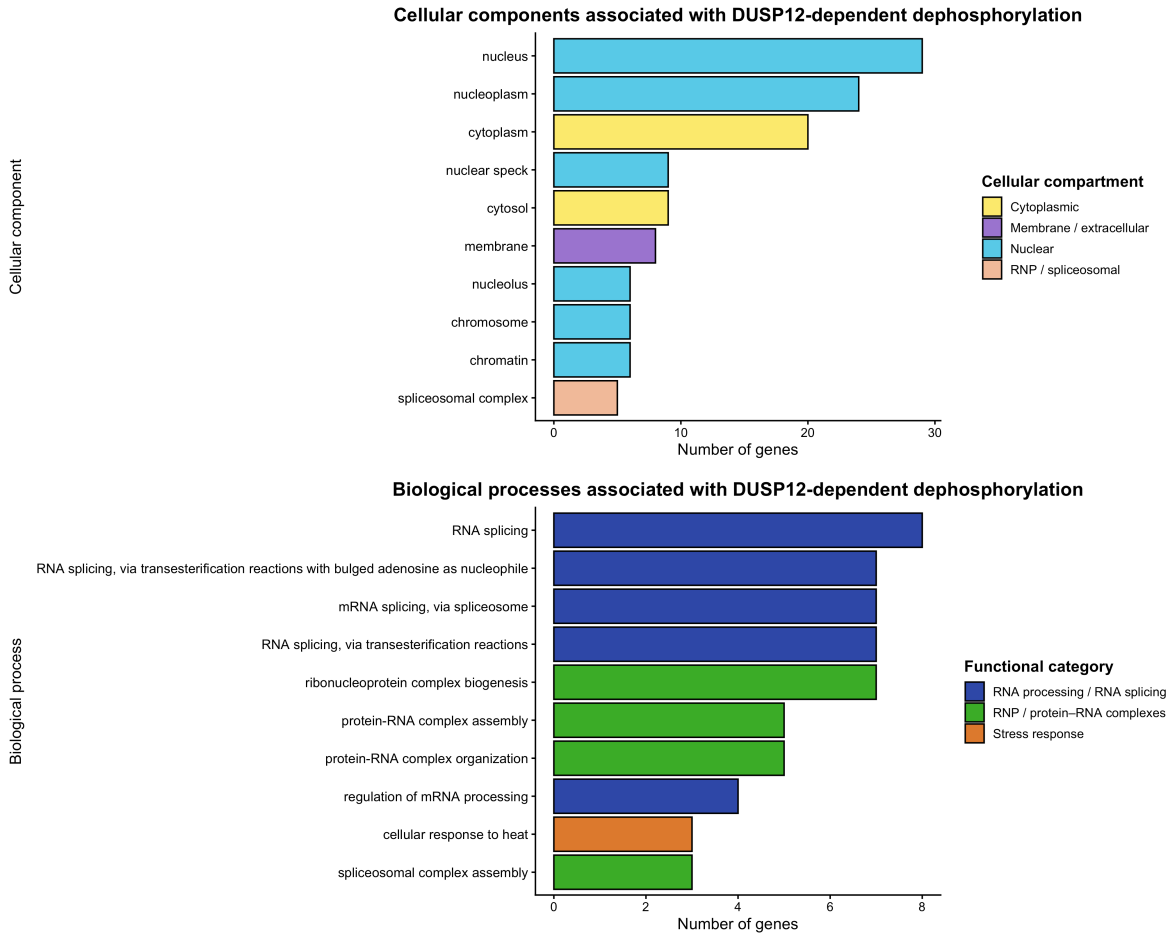


**Figure 17. Gene Ontology (GO) annotation analysis of proteins exhibiting reduced phosphorylation upon DUSP12 overexpression.** (Upper panel) Distribution of Cellular Component (CC) annotations, highlighting a predominant association with nuclear and nucleoplasmic compartments, together with cytoplasmic and ribonucleoprotein-related categories. (Lower panel) Distribution of Biological Process (BP) annotations, indicating a strong representation of RNA metabolism–related processes, including RNA processing, RNA splicing, and ribonucleoprotein complex assembly Bars represent the number of proteins annotated to each GO category. GO terms were grouped for clarity and visualization purposes

To gain an overview of the cellular and functional context of proteins exhibiting reduced phosphorylation upon DUSP12 overexpression, we performed a descriptive annotation-based analysis of Gene Ontology (GO) terms associated with this protein set. GO Cellular Component annotations revealed a predominant association with nuclear compartments, with the largest fraction of proteins annotated to the nucleus and nucleoplasm (**Fig. 17**, upper panel). Additional nuclear

substructures, including nuclear speckles, chromatin- and chromosome-associated regions, and the nucleolus, were also represented. Notably, a substantial subset of proteins was annotated to cytoplasmic and cytosolic compartments, and a smaller fraction was associated with membrane-related categories, indicating that DUSP12-dependent dephosphorylation is not exclusively restricted to the nuclear compartment. Proteins associated with ribonucleoprotein and spliceosomal complexes were also identified.

To further contextualize these observations, we examined Gene Ontology Biological Process annotations associated with the same protein set (**Fig. 17**, lower panel). This analysis highlighted a strong representation of RNA metabolism–related processes, particularly RNA splicing and spliceosome-mediated reactions. Processes related to ribonucleoprotein and protein–RNA complex assembly and organization were also prominent. In addition, a smaller subset of proteins was associated with stress response–related processes, including cellular responses to heat.

Overall, this descriptive functional categorization indicates that proteins exhibiting reduced phosphorylation upon DUSP12 overexpression are preferentially linked to nuclear compartments and RNA processing–related biological processes. This functional and spatial convergence provides a coherent contextual framework that is compatible with the observed effects of DUSP12 on ribosomal organization and translational output, while supporting a model in which DUSP12-dependent phosphoregulation may act upstream of cytoplasmic translation through modulation of nuclear RNA-related pathways.

### 3.5.2. DUSP12 activity associates with suppression of CK/CDK-driven phosphorylation events

Closer inspection of the most significantly downregulated phosphorylation sites upon DUSP12 overexpression (**Fig. 18**) revealed recurrent involvement of proteins previously annotated as substrates of defined kinase pathways. Among these, several sites have been reported to be phosphorylated by Casein Kinases (CKs) and Cyclin-Dependent Kinases (CDKs). For instance, phosphorylation of Calnexin at Ser554 and Ser583 – both previously described as CK-dependent sites – was markedly reduced. Similarly, dephosphorylation of Topoisomerase IIα (TOP2A) at Ser1106 affects a CK1-dependent priming site required for subsequent CDK1-mediated phosphorylation, suggesting potential convergence of DUSP12-dependent dephosphorylation on CK/CDK-regulated signaling axes.

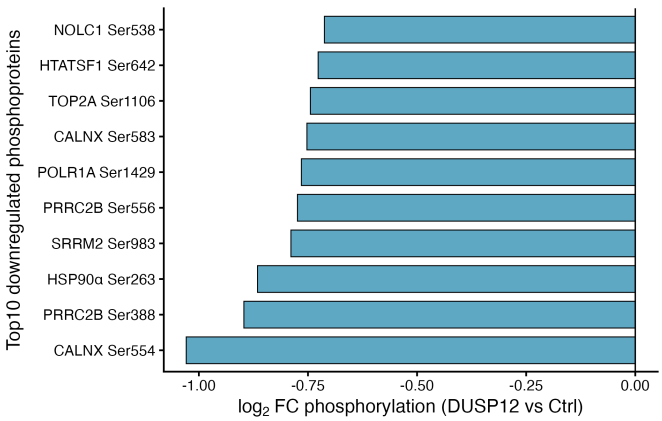

**Figure 18. Representative phosphosites exhibiting the strongest reduction in phosphorylation upon DUSP12 overexpression**.Bar plot showing the $\log_2$ fold change of the ten most significantly downregulated phosphopeptides in DUSP12-overexpressing cells compared to empty vector controls (Ctrl). Values represent normalized phosphopeptide abundance ratios.

To systematically assess whether this observation reflected a broader, pathway-level trend rather than isolated site-specific effects, we applied Kinase Substrate Enrichment Analysis (KSEA) to the full set of significantly regulated phosphopeptides (q-value ≤ 0.05). This analysis revealed a significant negative enrichment score for Casein Kinase 2 (CSNK2A1) and Cyclin-Dependent Kinase 1 (CDK1), both displaying z-scores below −2.0 (**Fig. 19**), indicative of a coordinated reduction in phosphorylation across their annotated substrates. Additional kinases displayed weaker or heterogeneous signatures, suggesting that the observed effect was not global but preferentially associated with specific kinase networks.

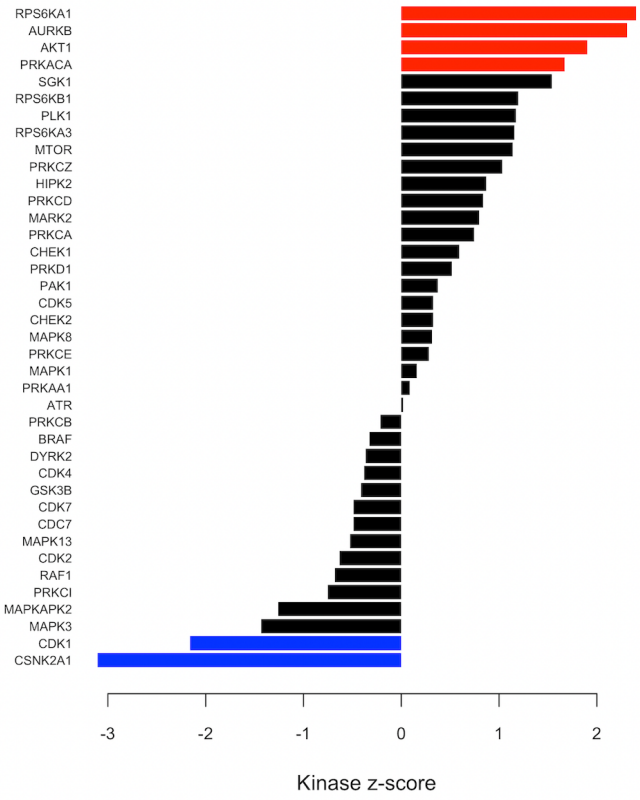


**Figure 19. Kinase Substrate Enrichment Analysis (KSEA) reveals reduced CK and CDK signaling signatures upon DUSP12 overexpression.** Bar plot showing kinase z-scores derived from KSEA, calculated based on coordinated changes in phosphorylation levels of annotated kinase substrates in DUSP12-overexpressing cells relative to empty vector controls. Negative z-scores indicate reduced phosphorylation across known substrates of the corresponding kinase, whereas positive z-scores indicate increased substrate phosphorylation. CSNK2A1 and CDK1 display strongly negative z-scores, suggesting attenuation of CK- and CDK-associated phosphorylation signatures. KSEA infers kinase-associated trends based on substrate behavior and does not directly measure kinase activity.

While KSEA does not provide a direct measurement of kinase enzymatic activity, the coordinated reduction of multiple annotated substrates supports the notion that DUSP12 overexpression is associated with attenuation of CK- and CDK-linked phosphorylation output. These data suggest that DUSP12 may functionally intersect with CK/CDK-driven signaling networks, either by directly counteracting phosphorylation events or by modulating upstream regulatory mechanisms that converge on these kinases.

### 3.5.3. The C-terminal Zinc-Binding Domain of DUSP12 contributes to selective phosphoregulation

To investigate the structural determinants underlying DUSP12 substrate selectivity, we compared the phosphoproteomes of cells expressing wild-type DUSP12 (WT) and a truncated mutant lacking the conserved C-terminal Zinc-Binding Domain (ΔZBD; residues 179–340), a region previously reported as potentially involced in protein–protein interactions. This comparative approach was designed to identify phosphorylation events that depend on the presence of the DUSP12 C-terminus. Phosphopeptides were analyzed across three conditions (empty vector, DUSP12 WT, and DUSP12 ΔZBD), and differential phosphorylation patterns were compared to identify a subset of sites that were dephosphorylated upon WT DUSP12 expression but remained unchanged in the ΔZBD mutant. This filtering strategy allowed the identification of phosphorylation events whose regulation is selectively dependent on the C-terminal domain of DUSP12 (**Fig. 20A**).

Among the phosphorylation events whose regulation was sensitive to the presence of the DUSP12 C-terminal Zinc-Binding Domain (ZBD), the nucleolar protein NOLC1 (Nucleolar and Coiled-Body Phosphoprotein 1) emerged as a particularly informative case. NOLC1 is a key regulator of nucleolar function and ribosome biogenesis, where it coordinates RNA polymerase I activity with ribosomal RNA processing and modification. Quantitative analysis of the Ser538 phosphorylation site showed a pronounced reduction upon overexpression of wild-type DUSP12, with phosphorylation levels decreasing to approximately 40% relative to control cells. In contrast, this decrease was largely attenuated in cells expressing the ΔZBD mutant, in which Ser538 phosphorylation remained close to control levels (approximately 85%) (**Fig. 20B**). These data indicate that efficient reduction of NOLC1 Ser538 phosphorylation requires the presence of the C-terminal domain of DUSP12.

Together, these findings suggest that the C-terminal Zinc-Binding Domain contributes to the selective modulation of specific phosphorylation events associated with nucleolar and ribonucleoprotein-related pathways, including nucleolar factors such as NOLC1. While the underlying mechanism remains to be determined, the dependence on the ZBD points to a role for this domain in shaping the context in which DUSP12-dependent phosphoregulation occurs, without implying direct catalytic action on NOLC1 itself.

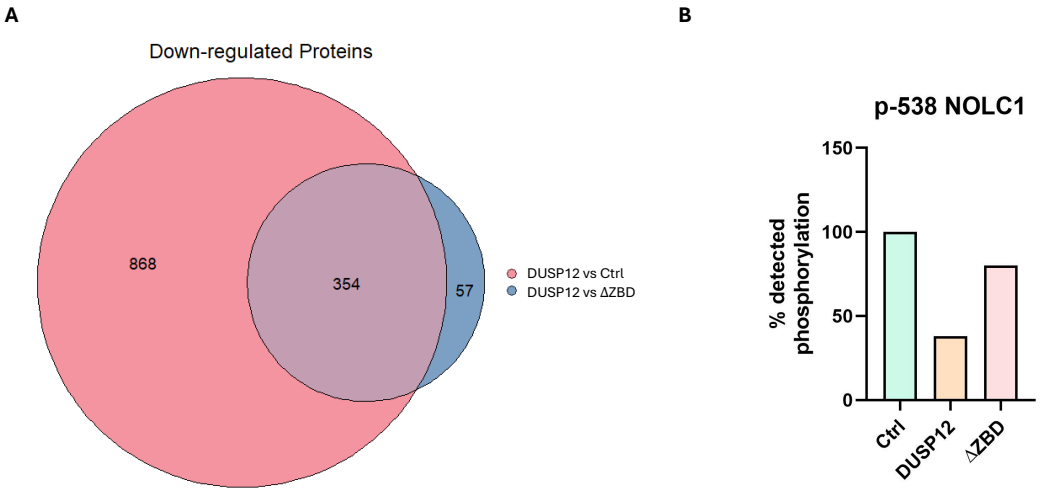

**Figure 20. The DUSP12 C-terminal Zinc-Binding Domain contributes to selective regulation of NOLC1 phosphorylation.** (**A**) Venn diagram comparing proteins associated with significantly reduced phosphorylation in DUSP12-overexpressing cells relative to control (red) and proteins differentially phosphorylated in the comparison between full-length DUSP12 and the ΔZBD mutant (blue). The overlap (n = 354) represents a shared subset of phosphoproteins whose regulation is detected in both comparative analyses. (**B**) Quantitative analysis of NOLC1 phosphorylation at Ser538. Phosphorylation levels are expressed as percentage relative to control cells (Ctrl, set to 100%). Overexpression of full-length DUSP12 is associated with a marked reduction in Ser538 phosphorylation, with levels decreasing to approximately 40%. In contrast, cells expressing the ΔZBD mutant display phosphorylation levels close to control values (approximately 85%), indicating that efficient reduction of NOLC1 Ser538 phosphorylation depends on the presence of the C-terminal Zinc-Binding Domain.

### 3.5.4. DUSP12 overexpression is associated with a mitochondrial-enriched proteomic profile that is lost upon ZBD deletion

We next asked whether DUSP12 overexpression could be associated with broader changes in cellular proteome composition, beyond the phosphorylation-dependent effects described above. To capture these downstream consequences at the protein level, we performed a TMT-based quantitative proteomic analysis comparing cells overexpressing full-length DUSP12, the ΔZBD mutant, or an empty vector control.

In cells overexpressing full-length DUSP12, a subset of proteins was significantly upregulated relative to control cells. GO enrichment analysis focused on the Biological Process and Cellular Component categories, which provided the most informative functional annotations. Gene Ontology (GO) enrichment analysis of proteins upregulated upon full-length DUSP12 overexpression revealed a modest enrichment for mitochondrial-related terms. In the Cellular Component category (**Fig. 21**, upper panel), the most significantly enriched terms included mitochondrion, mitochondrial matrix, and mitochondrial membranes, indicating preferential association with mitochondrial compartments. Consistently, enrichment analysis of the Biological Process category (**Fig. 21**, lower panel) highlighted pathways related to cellular respiration, aerobic respiration, energy derivation by oxidation of organic compounds, and the tricarboxylic acid cycle.

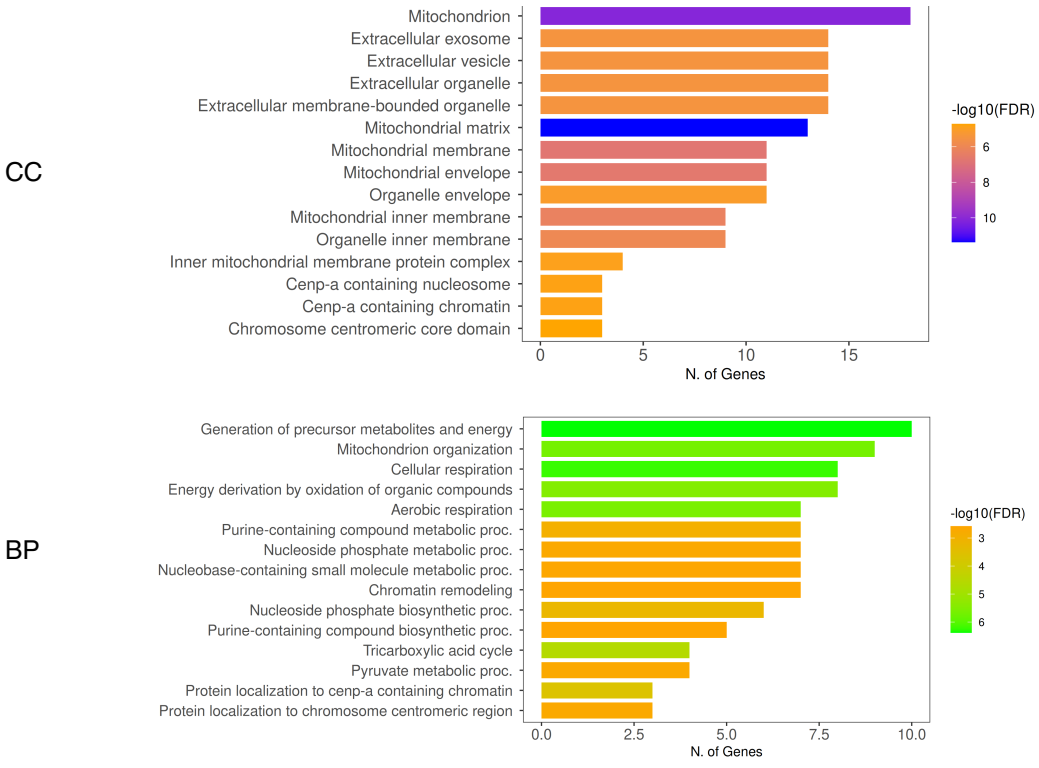

**Figure 21. Gene Ontology enrichment analysis of proteins upregulated upon full-length DUSP12 overexpression.** Gene Ontology (GO) enrichment analysis was performed on proteins significantly upregulated in cells overexpressing full-length DUSP12 compared to empty vector control ($p < 0.05$). The top enriched terms for the Cellular Component (CC, upper panel) and Biological Process (BP, lower panel) categories are shown. Enriched CC terms highlight a strong association with mitochondrial compartments, including the mitochondrion, mitochondrial matrix, and mitochondrial membranes. Consistently, BP enrichment reveals over-representation of pathways related to cellular respiration, aerobic metabolism, and the tricarboxylic acid cycle. Bar length indicates the number of proteins associated with each term, while color intensity represents the significance of enrichment expressed as -log10(FDR).

The enriched GO terms were supported by the presence of multiple established mitochondrial proteins among the upregulated subset, including components of the pyruvate dehydrogenase complex (PDHA1, PDHB), oxidative phosphorylation machinery (SDHA, ATP5F1B), and mitochondrial chaperones (HSPD1, HSPD10), consistent with a mitochondrial-enriched proteomic profile.

In contrast, cells expressing the ΔZBD mutant displayed a markedly reduced set of upregulated proteins under the same statistical thresholds (**Supplementary Table S2**). GO enrichment analysis of this subset did not identify any significantly enriched biological process terms. Instead, enrichment was limited to a small number of low-significance cellular component categories, primarily related to extracellular vesicular structures (**Supplementary Fig. S3**).

Together, these results indicate that overexpression of full-length DUSP12 is associated with the emergence of a coordinated mitochondrial-enriched proteomic profile, whereas deletion of the C-terminal Zinc-Binding Domain abolishes this functional coherence. While these findings do not establish a direct mechanistic role for DUSP12 in mitochondrial regulation, they suggest that the ZBD is required for establishing the cellular context in which mitochondrial-associated proteins are selectively upregulated.

### 3.5.5. Metabolic remodeling induced by DUSP12 overexpression occurs without detectable changes in mitochondrial abundance

To determine whether the enrichment of mitochondrial-associated proteins upon DUSP12 overexpression reflected an increase in mitochondrial abundance or rather changes in the composition of existing mitochondria, we assessed the levels of TOMM20, a widely used marker of the outer mitochondrial membrane.

Immunofluorescence analysis showed comparable mitochondrial staining patterns in cells expressing full-length DUSP12, the ΔZBD mutant, or empty vector controls (**Fig. 22A**). Consistently, immunoblot analysis confirmed robust expression of both DUSP12 variants but did not reveal statistically significant differences in TOMM20 protein levels relative to control cells (**Fig. 22 B,C**). These results indicate that DUSP12 overexpression does not induce detectable changes in mitochondrial abundance, suggesting that the mitochondrial enrichment observed by quantitative proteomics is unlikely to be driven by increased organelle mass.

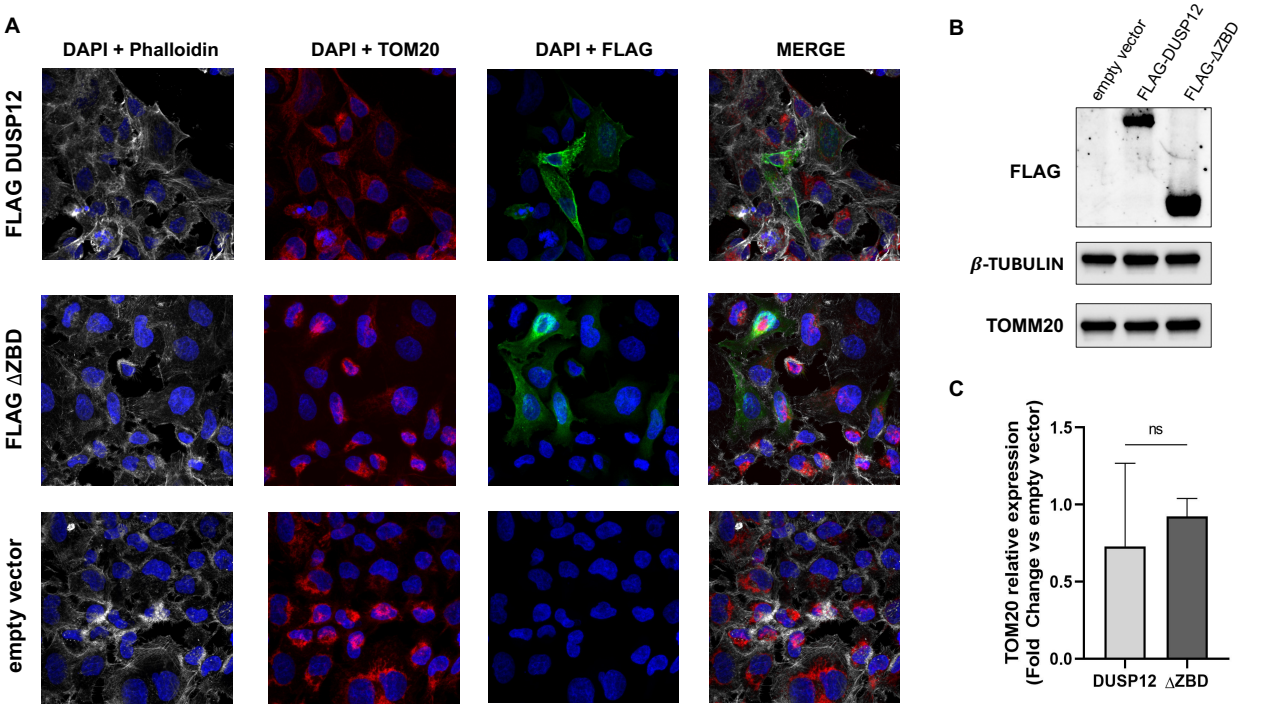


**Figure 22. DUSP12 overexpression does not induce detectable changes in mitochondrial abundance.** (**A**) Representative immunofluorescence images showing the subcellular localization of FLAG-DUSP12 and the ΔZBD mutant. Nuclei are stained with DAPI (blue), the actin cytoskeleton is labeled with phalloidin (gray), and mitochondria are visualized using TOMM20 (red), a marker of the outer mitochondrial membrane. (**B**) Representative immunoblot confirming expression of FLAG-DUSP12 and the ΔZBD mutant, with β-tubulin used as a loading control. (**C**) Quantification of TOMM20 protein levels reveals no statistically significant differences (ns) between cells overexpressing full-length DUSP12 or the ΔZBD mutant compared to empty vector controls. Together, these data indicate that DUSP12 overexpression does not result in detectable changes in mitochondrial abundance.

We next asked whether the proteomic changes associated with full-length DUSP12 overexpression were accompanied by alterations in cellular metabolic outputs. Intracellular lactate and ATP levels were therefore measured as readouts of glycolytic flux and overall cellular energy status, respectively.

Cells overexpressing full-length DUSP12 exhibited a significant reduction in lactate levels compared to control cells, consistent with decreased reliance on glycolytic metabolism (**Fig. 23**, left panel). This effect was not observed in cells expressing the ΔZBD mutant. In parallel, full-length DUSP12 overexpression was associated with increased intracellular ATP levels relative to control cells, whereas no significant changes were detected in the ΔZBD condition (**Fig. 23**, right panel).

Collectively, these data show that DUSP12 overexpression promotes functional enhancement of mitochondrial energy metabolism without increasing mitochondrial mass, and that this effect critically depends on the integrity of the C-terminal Zinc-Binding Domain. These findings support a model in which DUSP12 influences mitochondrial bioenergetics through selective proteome remodeling rather than organelle biogenesis.

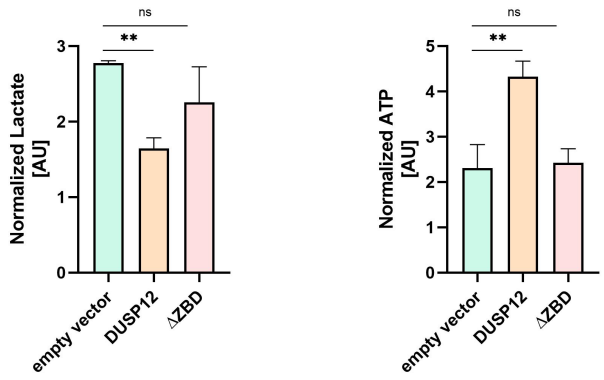


**Figure 23. DUSP12 overexpression is associated with ZBD-dependent changes in cellular metabolic readouts.** Bar graphs showing intracellular metabolic parameters in cells expressing full-length DUSP12, the ΔZBD mutant, or empty vector controls. (A) Intracellular lactate levels are significantly reduced in cells overexpressing full-length DUSP12 compared to control cells, consistent with decreased glycolytic output. This effect is not observed in cells expressing the ΔZBD mutant, which display lactate levels comparable to controls. (B) Intracellular ATP levels are increased in cells overexpressing full-length DUSP12 relative to controls, whereas no significant changes are detected in the ΔZBD condition. Data are expressed as normalized arbitrary units (AU) and corrected for total protein content. Statistical significance was assessed using a two-tailed paired t-test. **p < 0.01; ns, not significant.

## 3.5.6. Transcriptomic profiling reveals modest and selective transcriptional changes and limited RNA–protein correspondence following DUSP12 overexpression

To investigate whether the proteomic and metabolic changes associated with DUSP12 overexpression were accompanied by alterations at the transcriptional level, we performed RNA sequencing analysis comparing cells overexpressing DUSP12 with empty vector controls.

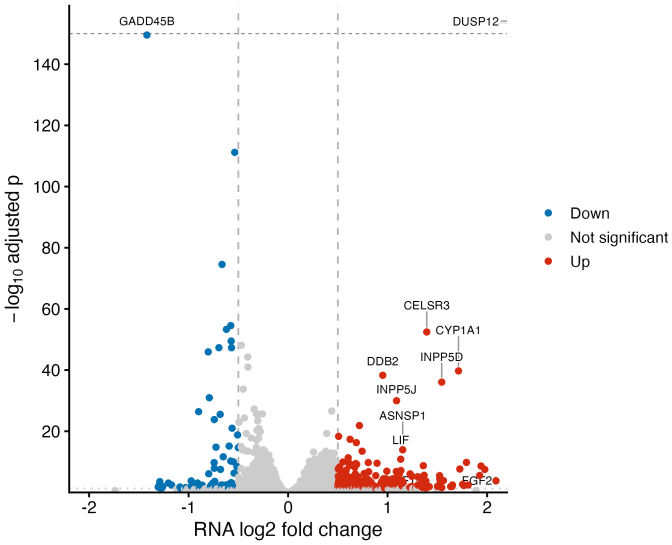


**Figure 24. Transcriptional response to DUSP12 overexpression reveals a limited and selective gene expression program.** Volcano plot showing RNA sequencing results comparing DUSP12-overexpressing cells with empty vector control cells (CTRL). The x-axis represents the RNA $\log_2$ fold change, while the y-axis indicates the $-\log_{10}$ adjusted p-value. Transcripts with an adjusted p-value < 0.05 are highlighted in red (upregulated) and blue (downregulated), whereas non-significant transcripts are shown in grey. Overall, only a limited number of genes display significant differential expression, with the majority of transcripts clustering around a $\log_2$ fold change close to zero, indicating that DUSP12 overexpression does not induce widespread transcriptional reprogramming. For visualization purposes, the y-axis was capped at $-\log_{10}$(adjusted p-value) = 150; the DUSP12 transcript, which displays a higher significance, is therefore shown at the upper boundary of the plot and is out of scale.

Differential expression analysis revealed a relatively limited number of significantly regulated transcripts, indicating that the extensive remodeling observed at the proteomic level is not mirrored by widespread transcriptional changes (**Fig. 24**). Consistent with this observation, most transcripts clustered around a $\log_2$ fold change close to zero, suggesting that DUSP12 overexpression does not globally reprogram gene expression.

To directly compare transcriptional and proteomic responses, RNA-Seq and quantitative proteomic datasets were integrated by plotting mRNA $\log_2$ fold changes against corresponding protein $\log_2$ fold changes (**Fig. 25**). Across the overlapping dataset, no significant correlation was observed between transcript and protein abundance changes. Notably, several mitochondrial proteins that were robustly upregulated at the proteomic level, including TUFM**,** SDHA, and MDH2, displayed minimal or no changes at the mRNA level. This systematic dissociation indicates that the mitochondrial protein enrichment observed upon DUSP12 overexpression is largely uncoupled from transcriptional regulation, suggesting a substantial contribution of post-transcriptional mechanisms, potentially involving translational control or protein stability.

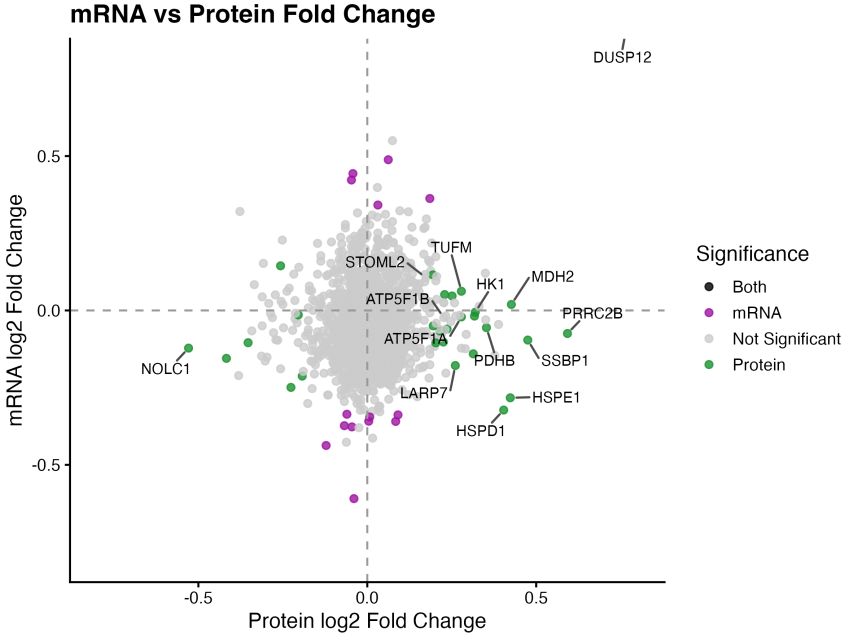


**Figure 25. Proteome reprogramming is driven by post-transcriptional control.** Scatter plot comparing the log2 Fold Change of mRNA levels (Y-axis) with the corresponding $\log_2$ Fold Change of protein levels (X-axis) in DUSP12-overexpressing cells versus control cells. The analysis included only proteins quantified in both RNA-Seq and proteomics datasets. Green dots represent proteins significantly regulated at the protein level. The plot shows a lack of positive correlation, with key upregulated mitochondrial proteins (e.g., TUFM, SDHA, MDH2) being not significant for mRNA regulation line.

Despite the modest number of differentially expressed genes, Gene Ontology enrichment analysis identified transcriptional signatures consistent with selective modulation of stress- and signaling-associated molecular functions (**Fig. 26**). Among the enriched categories, receptor regulator activity and receptor ligand activity were driven by the upregulation of secreted or extracellular signaling molecules, including LIF, INHBE, FGF21, GDF15, SCG2, CHGB, and CGB7, genes commonly associated with intercellular communication and adaptive responses to metabolic or cellular stress.

In parallel, other overrapresented terms converged on oxidoreductase- and monooxygenase-related molecular functions was observed, driven by cytochrome P450 family members (CYP1A1, CYP4F2, CYP4F3) and associated heme and tetrapyrrole binding activities. These findings point to potential alterations in redox-related enzymatic processes and lipid-derived signaling molecule metabolism following DUSP12 overexpression.

Beyond metabolism-associated genes, RNA-Seq analysis also revealed modulation of transcripts involved in cellular stress signaling and fate regulation. These included INPP5D and INPP5J, enzymes known to regulate phosphoinositide-dependent signaling pathways downstream of activated receptors, as well as downregulation of stress- and survival-associated genes, most notably GADD45B.

Although these enriched categories are supported by a limited number of genes, they point to a coherent and selective transcriptional response involving stress signaling and signal transduction pathways, rather than a broad reprogramming of gene expression, while the extensive mitochondrial proteome remodeling described above occurs largely independently of corresponding transcriptional changes.

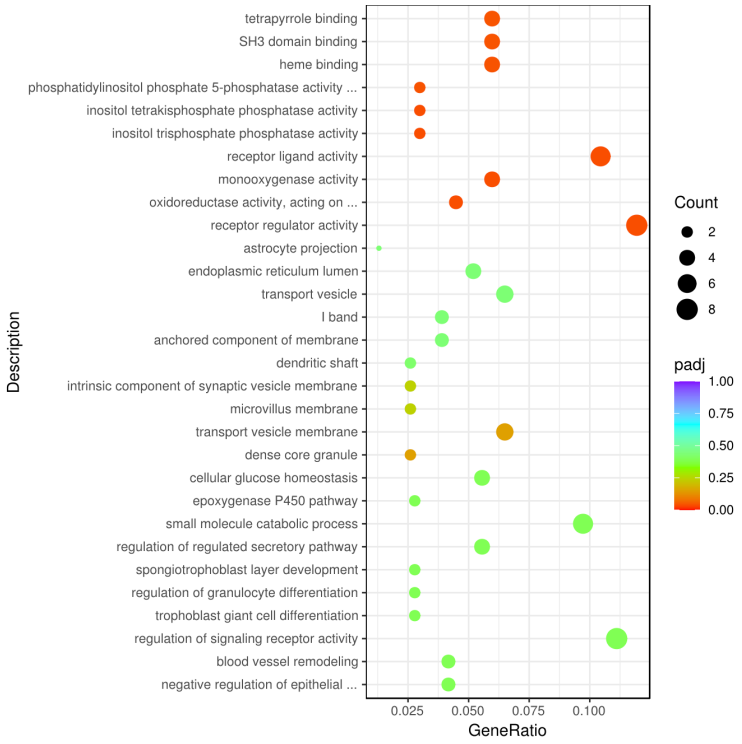


**Figure 26. Gene Ontology (GO) enrichment analysis following DUSP12 overexpression in HEK293T cells.** Dot plot showing functional enrichment categories (GO) for transcripts regulated by DUSP12 overexpression (RNA-Seq data). The x-axis represents the GeneRatio, while the y-axis indicates GO term descriptions. Dot size corresponds to the number of genes associated with each term, and dot color reflects the adjusted p-value (padj). Enriched categories include receptor regulatory and ligand activities, phosphoinositide phosphatase functions, and oxidoreductase-related enzymatic activities.

# 4. Discussion

Our initial investigations aimed to identify functional regulators of the eukaryotic initiation factor 6 (eIF6), with particular attention to the phosphorylation dynamics of its C-terminal residue Ser235. eIF6 is a well-established anti-association factor that binds the 60S ribosomal subunit and prevents the formation of 80S ribosomes, thereby blocking translation initiation[119]. The C-terminal tail of eIF6 is flexible and largely unstructured, which makes it highly accessible and susceptible to multiple post-translational modifications (PTMs) that may fine-tune its activity[111]. Among these, Ser235 has emerged as a key regulatory residue, whose phosphorylation is predicted to be critical for eIF6 release.

One of the most studied mechanisms for eIF6 release and subsequent 60S activation is mediated by the cooperative action of the GTPase EFL1 (Elongation Factor Like 1) and the scaffolding protein SBDS (Shwachman-Bodian-Diamond syndrome protein). SBDS monitors the integrity of the ribosomal peptidyl (P) site and promotes a conformational switch in EFL1 upon GTP hydrolysis. This conformational change allows the EFL1-SBDS complex to compete for the eIF6 binding site on the 60S subunit, ultimately displacing eIF6 and enabling 80S ribosome formation[123].

Importantly, this canonical pathway does not preclude the existence of additional, context-dependent regulatory layers. Phosphorylation-dependent mechanisms are particularly plausible, as they could provide both constitutive regulation under physiological conditions and adaptive responses to stress or signaling stimuli. Prior studies have implicated Protein Kinase C (PKC)[119] as potential regulators of eIF6, although it was never demonstrated direct interaction. Intriguingly, Glycogen Synthase Kinase 3β (GSK3β) has been shown to phosphorylate eIF6 in a hierarchical manner, initiating at Ser243, proceeding to Ser239, and finally targeting the critical Ser235[129]. Such sequential phosphorylation is a hallmark of GSK3β function, which typically integrates signals from upstream pathways. This observation suggests that Ser235 phosphorylation may serve as a convergence point for specific environmental or metabolic inputs.

Given the central role of eIF6 in ribosome biogenesis and its association with disease, defining the molecular switch that governs Ser235 phosphorylation is of particular interest. eIF6 is increasingly recognized as an oncoprotein and is aberrantly overexpressed in several human carcinomas. Its tumor-promoting effects are mechanistically linked to its translational activity: elevated eIF6 can drive the upregulation of factors such as Cdc42 in ovarian cancer and melanoma, thereby promoting cell migration and invasion[42]. These observations highlight the potential of targeting eIF6 regulation as a therapeutic strategy to disrupt a critical translational node in cancer.

In our experimental system, the functional equivalence observed between recombinant wild-type eIF6 and the non-phosphorylatable S235A mutant – both produced in bacteria and thus lacking eukaryotic PTMs – indicated that post-translational modifications, rather than intrinsic binding affinity, are the key determinants of the differences observed *in vivo*. This finding validated the use of the S235A mutant in cellular assays, where its overexpression caused a significant accumulation of free 60S subunits relative to 80S monosomes, consistent with defective eIF6 release and reduced translation initiation. By contrast, the phosphomimetic S235E mutant restored the normal ribosomal balance,

demonstrating that mimicking phosphorylation at Ser235 is sufficient to promote eIF6 release and 80S assembly.

Despite the robust cellular phenotype observed with the S235A mutant, unbiased affinity purification approaches failed to identify stable, differential interactors capable of explaining the phosphorylation status of eIF6. This indicates that the relevant regulatory interactions are likely transient or of low affinity, or spatially restricted. To overcome this limitation, we adopted a hypothesis-driven approach, drawing on high-throughput proximity labeling datasets that had identified DUSP12 (Dual-Specificity Phosphatase 12) as a high-confidence, specific proximity interactor of eIF6. DUSP12 is classified as an atypical dual-specificity phosphatase, and its yeast ortholog Yvh1 is known to participate in 60S ribosome biogenesis, cell cycle progression, and cell survival. A distinctive feature of DUSP12 is its C-terminal Zinc-Binding Domain (ZBD). This domain, first characterized by Muda et al., is highly conserved across evolution and, in yeast, was shown to be both necessary and sufficient to modulate cell cycle progression independently of the catalytic phosphatase domain[167].

Our data showed that DUSP12 preferentially colocalized with the phosphorylated cytoplasmic pool of eIF6 (p-eIF6), supporting the hypothesis that p-eIF6 represents a biologically relevant substrate. However, DUSP12 overexpression did not trigger global eIF6 dephosphorylation, nor did it reproduce the pronounced 60S accumulation phenotype observed with the S235A mutant. This suggests that DUSP12's activity toward eIF6 is highly compartmentalized, transient, or restricted to a specific subpopulation of the protein, thereby exerting minimal impact on the total phophorylation levels detected in whole-cell lysates.

The most prominent functional consequence of DUSP12 overexpression was its pro-translational activity, reflected by a 1.77-fold increase in global protein synthesis as measured by puromycin incorporation. This effect, which was also recapitulated in an acellular lysate system, indicates that DUSP12 possesses an intrinsic capacity to influence the translational machinery. A plausible explanation for the apparent discrepancy between largely unchanged polysome profiles with subtle structural alterations and the marked increase in protein synthesis is that DUSP12 acts on components of the elongation machinery. For example, eukaryotic elongation factor 2 (eEF2) is tightly controlled by inhibitory phosphorylation through eEF2 kinase (eEF2K) at Thr56 in mammals, and dephosphorylation by PP2A is required for productive ribosome binding[208]. By analogy, DUSP12 could potentially modulate translation through similar mechanisms targeting elongation factors.

Alternatively, the observed increase in puromycin incorporation may partially reflect altered protein quality control. If DUSP12 impacts proteasomal activity or other degradation pathways, reduced protein turnover could manifest as higher apparent protein accumulation in puromycin-based assays. While further experiments are needed to disentangle these mechanisms, these findings establish a functional link between DUSP12 and translational output, providing a foundation for future mechanistic dissection.

Consistent with this notion, phosphoproteomic analyses revealed broad DUSP12-dependent dephosphorylation events, particularly affecting nuclear proteins, splicing factors, and components of the translation machinery. Among the most striking changes was the dephosphorylation of the endoplasmic reticulum (ER) chaperone Calnexin at multiple sites. Calnexin is a central component

of the ER quality control system, ensuring proper folding of nascent glycoproteins as they emerge from the translocon[209]. Phosphorylation of Calnexin – particularly at Ser563, a site regulated by ERK1/CK2 – has been described as a signal that promotes its recruitment to ER-membrane–bound ribosomes during conditions of protein misfolding[209]. Thus, the observed dephosphorylation of these sites by DUSP12 may hinder Calnexin's recruitment to the ribosome–translocon complex and attenuate ER-associated quality control (ERQC)[210]. Such an impairment could in turn reduce the degradation of newly synthesized proteins, offering a plausible mechanistic link to the robust increase in global puromycin incorporation observed in our translational assays. Given that ERQC is tightly coupled to the unfolded protein response (UPR) and proteostasis, DUSP12-mediated modulation of Calnexin phosphorylation may have broader implications for cellular adaptation to ER stress and translational fidelity. Although these findings provide a mechanistic framework linking DUSP12 activity to protein quality control, direct validation of Calnexin as a physiological substrate or indiract target will be required to corroborate this putative model.

Kinase Substrate Enrichment Analysis (KSEA) further suggested altered activity of Casein Kinase 2 (CK2) and Cyclin-Dependent Kinase 1 (CDK1). CK2 is a pleiotropic kinase with roles in ribosome biogenesis, splicing, and translation initiation[211]. By contrast, CDK1 serves as the master regulator of the $G_2$/M transition. At first glance, the predicted downregulation of CDK1 activity may appear inconsistent with prior studies showing that DUSP12 promotes cell cycle progression and increases the $G_2$/M population. One possible explanation is that KSEA captures indirect signatures of CDK1 modulation rather than a complete inhibition, reflecting a role for DUSP12 in fine-tuning rather than abolishing CDK1 activity. This interpretation aligns with evidence that DUSP12 interacts with the mitotic regulator ZPR9 to prevent mitotic defects and stress-induced apoptosis, consistent with a buffering role that ensures orderly cell cycle progression[193]. Taken together, the convergence of CK2- and CDK1-associated pathways supports the view that DUSP12 might acts as a regulatory hub, integrating signals from translation and cell cycle machinery to coordinate cellular growth with proliferative decisions. Future work should therefore address whether DUSP12 modulates CDK1 activity in a context-dependent manner, or whether the KSEA prediction reflects indirect effects on upstream regulatory networks.

The importance of the Zinc-Binding Domain (ZBD) in conferring functional specificity to DUSP12 became particularly evident from comparative phosphoproteomic analyses. Deletion of the ZBD abolished dephosphorylation of the nucleolar protein NOLC1, a key regulator of rRNA transcription and ribosome biogenesis. Functionally, its overexpression has been associated with activation of the DNA damage response, induction of apoptosis, and nuclear-to-nucleolar translocation of the telomeric repeat-binding factor 2 (TRF2)[212]. Notably, DUSP12-mediated dephosphorylation of NOLC1 at Ser538 correlated with a pronounced reduction in total NOLC1 protein levels, suggesting that phosphorylation at this site stabilizes the protein. Given that NOLC1 accumulation has been linked to nucleolar stress and apoptotic signaling[213], its clearance upon DUSP12 overexpression is consistent with attenuation of nucleolar stress responses and supports a cytoprotective role for DUSP12.

While these data suggest a role for DUSP12 in coordinating nucleolar stress responses, proteomic analyses also indicated its involvement in cellular metabolism. Quantitative proteomics revealed an enrichment of proteins involved in aerobic respiration and central carbon metabolism, which

translated into functional metabolic changes, including increased ATP levels and reduced lactate production, consistent with a shift towards enhanced aerobic respiration. What is particularly striking is that this signature is completely lost upon deletion of the C-terminal Zinc-Binding Domain, despite the presence of detectable proteomic changes in the ΔZBD condition, indicating that this domain is required for the establishment of a functionally coherent proteomic response linked to mitochondrial pathways. Importantly, the loss of mitochondrial biological process enrichment in the ΔZBD condition does not simply reflect a reduction in the number of differentially expressed proteins, but rather a failure of these changes to converge on defined functional pathways. This observation suggests that the ZBD contibutes to define the cellular context in which specific functional programs – such as those associated with mitochondrial metabolism – can emerge.

A key question arising from this observation is whether the mitochondrial enrichment detected at the proteomic level reflects an increase in mitochondrial abundance or instead a remodeling of the existing organelle pool. The analysis of TOMM20 levels by both immunofluorescence and immunoblotting did not reveal detectable differences among cells expressing full-length DUSP12, the ΔZBD mutant, or control cells, arguing against gross changes in mitochondrial mass. Although more subtle alterations in mitochondrial morphology or ultrastructure cannot be excluded, these results suggest that the proteomic signature observed upon DUSP12 overexpression is unlikely to be driven by organelle biogenesis, and instead reflects selective changes in mitochondrial protein composition.

While the present data do not establish a direct mechanistic role for DUSP12 in mitochondrial regulation, they indicate that integrity of the ZBD is necessary for the proteomic coherence underlying the mitochondrial-enriched signature observed upon full-length DUSP12 overexpression. One possibility is that the ZBD enables specific protein–protein interactions, subcellular localization, or regulatory scaffolding events that are required to support this coordinated response, although these hypotheses remain to be experimentally addressed.

Integration of transcriptomic data further clarified the hierarchical nature of these responses. RNA sequencing revealed only limited transcriptional changes upon DUSP12 overexpression, and direct comparison of mRNA and protein abundance demonstrated a systematic uncoupling between transcript and protein levels for many mitochondrial components. This is consistent with the hypotesis that the extensive mitochondrial proteome remodeling occurs largely through post-transcriptional mechanisms. While the present data do not resolve whether these mechanisms involve altered translation efficiency, protein stability, or both, the overall dissociation between mRNA and protein levels argues against transcription as the dominant driver of the observed mitochondrial remodeling.

Despite the absence of broad transcriptional rewiring, RNA-Seq analysis reveals a selective transcriptional response centered on genes involved in cellular stress adaptation and signaling. The upregulation of secreted factors such as GDF15, LIF, and FGF21 – often associated with metabolic stress and intercellular communication – suggests that DUSP12 overexpression may elicit a stress-adaptive signaling state rather than a canonical metabolic transcriptional program. In parallel, the modulation of genes linked to redox regulation, including NR1D1 and CYP1A1, is consistent with transcriptional fine-tuning of pathways that interface with metabolic flux and cellular redox balance.

Within this adaptive framework, DUSP12 overexpression is also associated with the downregulation of key regulators of cellular stress responses and fate decisions, such as GADD45B. GADD45B (Growth Arrest and DNA Damage-inducible protein β) is a stress-inducible growth inhibitor that activates the p38/JNK pathways, leading to cell cycle arrest and apoptosis. Notably, GADD45B has been associated with chromatin regulators, suggesting a broader role in modulating transcriptional and post-transcriptional programs. In pathological contexts such as ischemia–reperfusion injury, where DUSP12 has been described to exert protective effects[214,215], GADD45B expression correlates strongly with cellular stress and apoptotic signaling[216]. The reduced expression of GADD45B observed here may therefore reflect an attenuation of stress-induced growth arrest pathways in cells overexpressing DUSP12.

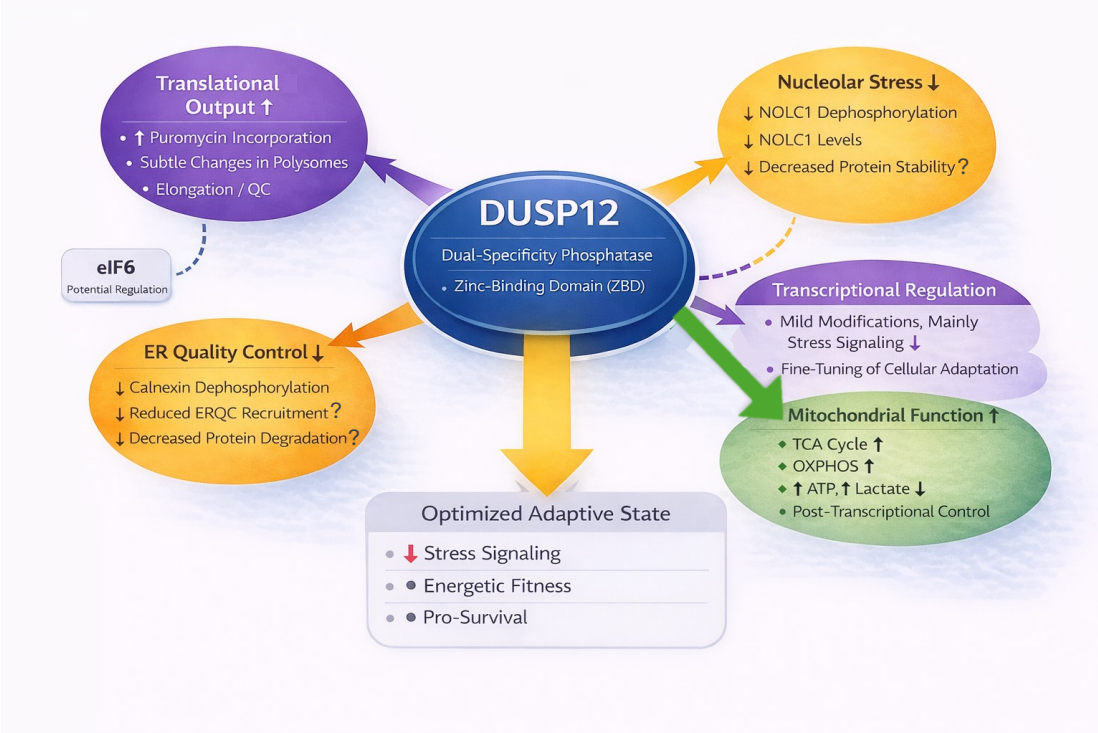


**Figure 27. Functional model of DUSP12-dependent cellular remodeling.** Schematic representation summarizing the multilayered cellular effects associated with DUSP12 overexpression. DUSP12 (center) is depicted as an atypical dual-specificity phosphatase containing a C-terminal Zinc-Binding Domain (ZBD), which confers functional specificity and compartmentalized activity. Purple nodes represent processes that are experimentally observed but mechanistically unresolved. DUSP12 enhances translational output, as evidenced by increased puromycin incorporation, subtle changes in polysome profiles, and a putative impact on elongation and translational quality control. A mild transcriptional regulatory response, primarily involving modulation of stress-signaling genes, is also observed and is interpreted as fine-tuning of cellular adaptation rather than a primary driver of the phenotype.Yellow nodes indicate pathways supported by phosphoproteomic evidence but involving mechanistic speculation. DUSP12-dependent dephosphorylation of the ER chaperone Calnexin suggests attenuation of ER quality control, with reduced ERQC recruitment and decreased protein degradation remaining putative outcomes (question marks). In the nucleolus, dephosphorylation of NOLC1 correlates with reduced NOLC1 protein levels, consistent with decreased protein stability and attenuation of nucleolar stress. Green node highlights experimentally supported and functionally validated effects on mitochondrial metabolism. DUSP12 overexpression induces a ZBD-dependent enrichment of mitochondrial proteins involved in the TCA cycle and oxidative phosphorylation, accompanied by increased ATP levels, reduced lactate production. These converging pathways predict an optimized adaptive state characterized by reduced stress signaling, enhanced energetic fitness, and a pro-survival cellular configuration.

In this integrated view, DUSP12 overexpression primarily reshapes cellular physiology through post-transcriptional and proteomic mechanisms, with transcriptional modulation acting to fine-tune stress signaling, redox balance, and fate-regulatory pathways. Together, these multilayered responses converge on a cellular configuration characterized by optimized mitochondrial function, restrained stress signaling, and a metabolically efficient adaptive state.

# Conclusions and Future Perspective

Our studies on eIF6, including the use of the S235E mutant, highlight the critical role of Ser235 in regulating eIF6 in the context of translation initiation, suggesting that multiple layers of eIF6 regulation exist beyond the canonical SBDS-EFL1 axis. While subsequent analyses shifted focus toward DUSP12, no direct mechanistic connection with eIF6 was observed. Nevertheless, a functional link cannot be excluded: co-localization exists, regulation may occur via other residues, and specific spatio-temporal windows may be relevant. Limitations in the proteomic and phosphoproteomic datasets – particularly the absence of eIF6 and related translation factors among over 2000 identified proteins – pose significant technical challenges and constrain definitive conclusions regarding transient or low-abundance interactions.

Focusing on DUSP12, our findings support a model in which this phosphatase integrates cytoplasmic and nuclear/nucleolar functions. In the cytoplasm, it enhances global translational output, likely by counteracting inhibitory phosphorylation on quality control factors (e.g., Calnexin) or translational elongation factors (e.g., eEF2K targets). Concurrently, the ZBD directs DUSP12 to nuclear and nucleolar substrates such as NOLC1, suppressing nucleolar stress and apoptosis. Most notably, the ZBD mediates post-transcriptional enhancement of mitochondrial protein expression, promoting a highly energetic, stress-adaptive metabolic state.

Nevertheless, several important questions remain. First, the molecular mechanisms underlying DUSP12-mediated mitochondrial regulation are unclear: does DUSP12 act downstream of upstream sensors, or function as a primary sensor coordinating metabolic remodeling? High-resolution studies are needed to define how the ZBD mediates post-transcriptional enhancement of mitochondrial protein expression. Second, further validation of substrate specificity, including additional residues on eIF6 and other nucleolar or cytoplasmic targets, is necessary to clarify the full spectrum of DUSP12 action. Targeted phosphoproteomic approaches – potentially including proximity labeling or in situ assays – will be critical to determine whether DUSP12 directly regulates eIF6 or other translation factors. Third, extending these studies to relevant disease models, particularly liver (given DUSP12's involvement in NAFLD) and heart (due to its role in cardiovascular function), will be crucial to link molecular mechanisms to physiological and pathological contexts. Finally, comprehensive proteomic, phosphoproteomic, and functional analyses under stress and pathological conditions are required to fully understand how DUSP12 orchestrates metabolic adaptation, stress resilience, and pro-survival signaling.

In summary, this work positions DUSP12 as a central integrator of nucleolar stress, translation control, and mitochondrial function, providing a mechanistic framework for future studies. Unraveling the precise mechanisms of DUSP12 action will not only advance our understanding of fundamental cellular adaptation processes but may also reveal novel therapeutic opportunities in diseases where metabolic and stress-response pathways are dysregulated, highlighting DUSP12 as a potential master regulator of cellular resilience.

# Supplementary information

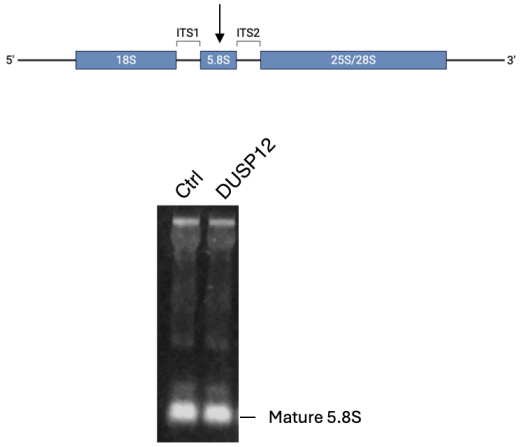


**Supplementary Figure S1. Analysis of 5.8S rRNA abundance.** (Upper panel) Schematic representation of the rRNA organization within the large ribosomal subunit, highlighting the position of the 5.8S rRNA. (Lower panel) Northern blot analysis of total RNA from Ctrl and DUSP12 samples probed for mature 5.8S rRNA. Equal amounts of RNA were loaded. No obvious differences in 5.8S rRNA abundance were observed between conditions.

| Accession | SYMBOL | Description | ratio | log2FC | pvalue | Regulation |
|---|---|---|---|---|---|---|
| Q14978 | NOLC1 | Nucleolar and coiled-body phosphoprotein 1 [OS=Homo sapiens] | 0,693 | -0,52907 | 6,46E-08 | Down |
| P53985 | SLC16A1 | Monocarboxylate transporter 1 [OS=Homo sapiens] | 0,749 | -0,41696 | 0,046479 | Down |
| P35659 | DEK | Protein DEK [OS=Homo sapiens] | 0,783 | -0,35292 | 0,006958 | Down |
| Q9H0U4 | RAB1B | Ras-related protein Rab-1B [OS=Homo sapiens] | 0,837 | -0,2567 | 0,004582 | Down |
| P25685 | DNAJB1 | DnaJ homolog subfamily B member 1 [OS=Homo sapiens] | 0,855 | -0,226 | 0,005962 | Down |
| P51149 | RAB7A | Ras-related protein Rab-7a [OS=Homo sapiens] | 0,868 | -0,20423 | 0,000491 | Down |
| Q5VZF2 | MBNL2 | Muscleblind-like protein 2 [OS=Homo sapiens] | 1,124 | 0,168642 | 0,038361 | Up |
| Q9UJZ1 | STOML2 | Stomatin-like protein 2, mitochondrial [OS=Homo sapiens] | 1,128 | 0,173767 | 0,029676 | Up |
| P28799 | GRN | Progranulin [OS=Homo sapiens] | 1,144 | 0,194087 | 0,003876 | Up |
| Q15291 | RBBP5 | Retinoblastoma-binding protein 5 [OS=Homo sapiens] | 1,145 | 0,195348 | 0,001633 | Up |
| Q9NZR1 | TMOD2 | Tropomodulin-2 [OS=Homo sapiens] | 1,151 | 0,202888 | 0,025092 | Up |
| P30048 | PRDX3 | Thioredoxin-dependent peroxide reductase, mitochondrial [OS=Homo sapiens] | 1,161 | 0,215368 | 0,005457 | Up |
| P61978 | HNRNPK | Heterogeneous nuclear ribonucleoprotein K [OS=Homo sapiens] | 1,169 | 0,225275 | 0,025774 | Up |
| P31040 | SDHA | Succinate dehydrogenase [ubiquinone] flavoprotein subunit, mitochondrial [OS=Homo sapiens] | 1,172 | 0,228973 | 0,005185 | Up |
| P04908 | H2AC8 | Histone H2A type 1-B/E [OS=Homo sapiens] | 1,176 | 0,233888 | 0,026795 | Up |
| P04908 | H2AC4 | Histone H2A type 1-B/E [OS=Homo sapiens] | 1,176 | 0,233888 | 0,026795 | Up |
| P35232 | PHB1 | Prohibitin 1 [OS=Homo sapiens] | 1,177 | 0,235114 | 0,013791 | Up |
| P08559 | PDHA1 | Pyruvate dehydrogenase E1 component subunit alpha, somatic form, mitochondrial [OS=Homo sapiens] | 1,178 | 0,23634 | 0,01348 | Up |
| Q9NX63 | CHCHD3 | MICOS complex subunit MIC19 [OS=Homo sapiens] | 1,188 | 0,248535 | 0,0084 | Up |
| P30405 | PPIF | Peptidyl-prolyl cis-trans isomerase F, mitochondrial [OS=Homo sapiens] | 1,19 | 0,250962 | 0,002136 | Up |
| Q99623 | PHB2 | Prohibitin-2 [OS=Homo sapiens] | 1,191 | 0,252173 | 0,008363 | Up |
| Q4G0J3 | LARP7 | La-related protein 7 [OS=Homo sapiens] | 1,198 | 0,260628 | 0,028733 | Up |
| P25705 | ATP5F1A | ATP synthase subunit alpha, mitochondrial [OS=Homo sapiens] | 1,213 | 0,27858 | 2,12E-07 | Up |
| P49411 | TUFM | Elongation factor Tu, mitochondrial [OS=Homo sapiens] | 1,213 | 0,27858 | 0,000274 | Up |
| P38646 | HSPA9 | Stress-70 protein, mitochondrial [OS=Homo sapiens] | 1,243 | 0,313826 | 0,044311 | Up |
| P38117 | ETFB | Electron transfer flavoprotein subunit beta [OS=Homo sapiens] | 1,246 | 0,317304 | 0,006614 | Up |
| P19367 | HK1 | Hexokinase-1 [OS=Homo sapiens] | 1,248 | 0,319618 | 0,000931 | Up |
| P11177 | PDHB | Pyruvate dehydrogenase E1 component subunit beta, mitochondrial [OS=Homo sapiens] | 1,277 | 0,352759 | 0,026189 | Up |
| P16403 | H1-2 | Histone H1.2 [OS=Homo sapiens] | 1,292 | 0,369606 | 0,014757 | Up |
| P10809 | HSPD1 | 60 kDa heat shock protein, mitochondrial [OS=Homo sapiens] | 1,323 | 0,403813 | 2,72E-08 | Up |
| P61604 | HSPE1 | 10 kDa heat shock protein, mitochondrial [OS=Homo sapiens] | 1,341 | 0,423309 | 1,8E-08 | Up |
| P62805 | H4C9 | Histone H4 [OS=Homo sapiens] | 1,341 | 0,423309 | 1,12E-06 | Up |
| P62805 | H4C1 | Histone H4 [OS=Homo sapiens] | 1,341 | 0,423309 | 1,12E-06 | Up |
| P62805 | H4C4 | Histone H4 [OS=Homo sapiens] | 1,341 | 0,423309 | 1,12E-06 | Up |
| P62805 | H4C6 | Histone H4 [OS=Homo sapiens] | 1,341 | 0,423309 | 1,12E-06 | Up |
| P62805 | H4C12 | Histone H4 [OS=Homo sapiens] | 1,341 | 0,423309 | 1,12E-06 | Up |
| P62805 | H4C11 | Histone H4 [OS=Homo sapiens] | 1,341 | 0,423309 | 1,12E-06 | Up |
| P62805 | H4C3 | Histone H4 [OS=Homo sapiens] | 1,341 | 0,423309 | 1,12E-06 | Up |
| P62805 | H4C8 | Histone H4 [OS=Homo sapiens] | 1,341 | 0,423309 | 1,12E-06 | Up |
| P62805 | H4C2 | Histone H4 [OS=Homo sapiens] | 1,341 | 0,423309 | 1,12E-06 | Up |
| P62805 | H4C5 | Histone H4 [OS=Homo sapiens] | 1,341 | 0,423309 | 1,12E-06 | Up |
| P62805 | H4C13 | Histone H4 [OS=Homo sapiens] | 1,341 | 0,423309 | 1,12E-06 | Up |
| P62805 | H4C14 | Histone H4 [OS=Homo sapiens] | 1,341 | 0,423309 | 1,12E-06 | Up |
| P62805 | H4C16 | Histone H4 [OS=Homo sapiens] | 1,341 | 0,423309 | 1,12E-06 | Up |
| P62805 | H4C15 | Histone H4 [OS=Homo sapiens] | 1,341 | 0,423309 | 1,12E-06 | Up |
| P40926 | MDH2 | Malate dehydrogenase, mitochondrial [OS=Homo sapiens] | 1,344 | 0,426533 | 1,01E-08 | Up |
| Q04837 | SSBP1 | Single-stranded DNA-binding protein, mitochondrial [OS=Homo sapiens] | 1,39 | 0,475085 | 0,000144 | Up |
| Q5JSZ5 | PRRC2B | Protein PRRC2B [OS=Homo sapiens] | 1,508 | 0,592636 | 8,42E-06 | Up |
| Q9UNI6 | DUSP12 | Dual specificity protein phosphatase 12 [OS=Homo sapiens] | 4,863 | 2,281847 | 4,22E-15 | Up |

**Supplementary Table S1**. **Proteomic identification of proteins upregulated upon DUSP12 overexpression.** List of proteins significantly upregulated in DUSP12-overexpressing cells compared to empty vector control cells, as identified by quantitative

proteomic analysis. For each protein, UniProt accession number, gene symbol, protein description, abundance ratio, $log_2$ fold change, p-value, and direction of regulation are reported.

| Accession | SYMBOL | Description | ratio | log2FC | pvalue | Regulation |
|---|---|---|---|---|---|---|
| Q7L4I2 | RSRC2 | Arginine/serine-rich coiled-coil protein 2 [OS=Homo sapiens] | 1,118 | 0,16092 | 0,016412 | Up |
| Q9UJU6 | DBNL | Drebrin-like protein [OS=Homo sapiens] | 1,12 | 0,163499 | 0,045515 | Up |
| Q92688 | ANP32B | Acidic leucine-rich nuclear phosphoprotein 32 family member B [OS=Homo sapiens] | 1,121 | 0,164786 | 0,034919 | Up |
| P14550 | AKR1A1 | Aldo-keto reductase family 1 member A1 [OS=Homo sapiens] | 1,145 | 0,195348 | 0,000204 | Up |
| P06454 | PTMA | Prothymosin alpha [OS=Homo sapiens] | 1,151 | 0,202888 | 4,72E-05 | Up |
| Q06203 | PPAT | Amidophosphoribosyltransferase [OS=Homo sapiens] | 1,152 | 0,204141 | 0,033107 | Up |
| P35659 | DEK | Protein DEK [OS=Homo sapiens] | 1,156 | 0,209141 | 0,033384 | Up |
| Q9BRJ6 | CHLSN | Protein cholesin [OS=Homo sapiens] | 1,172 | 0,228973 | 0,012251 | Up |
| Q9BXS5 | AP1M1 | AP-1 complex subunit mu-1 [OS=Homo sapiens] | 1,243 | 0,313826 | 0,015632 | Up |
| P62805 | H4C9 | Histone H4 [OS=Homo sapiens] | 1,282 | 0,358396 | 0,000105 | Up |
| P62805 | H4C1 | Histone H4 [OS=Homo sapiens] | 1,282 | 0,358396 | 0,000105 | Up |
| P62805 | H4C4 | Histone H4 [OS=Homo sapiens] | 1,282 | 0,358396 | 0,000105 | Up |
| P62805 | H4C6 | Histone H4 [OS=Homo sapiens] | 1,282 | 0,358396 | 0,000105 | Up |
| P62805 | H4C12 | Histone H4 [OS=Homo sapiens] | 1,282 | 0,358396 | 0,000105 | Up |
| P62805 | H4C11 | Histone H4 [OS=Homo sapiens] | 1,282 | 0,358396 | 0,000105 | Up |
| P62805 | H4C3 | Histone H4 [OS=Homo sapiens] | 1,282 | 0,358396 | 0,000105 | Up |
| P62805 | H4C8 | Histone H4 [OS=Homo sapiens] | 1,282 | 0,358396 | 0,000105 | Up |
| P62805 | H4C2 | Histone H4 [OS=Homo sapiens] | 1,282 | 0,358396 | 0,000105 | Up |
| P62805 | H4C5 | Histone H4 [OS=Homo sapiens] | 1,282 | 0,358396 | 0,000105 | Up |
| P62805 | H4C13 | Histone H4 [OS=Homo sapiens] | 1,282 | 0,358396 | 0,000105 | Up |
| P62805 | H4C14 | Histone H4 [OS=Homo sapiens] | 1,282 | 0,358396 | 0,000105 | Up |
| P62805 | H4C16 | Histone H4 [OS=Homo sapiens] | 1,282 | 0,358396 | 0,000105 | Up |
| P62805 | H4C15 | Histone H4 [OS=Homo sapiens] | 1,282 | 0,358396 | 0,000105 | Up |
| Q8NFW8 | CMAS | N-acylneuraminate cytidylyltransferase [OS=Homo sapiens] | 1,315 | 0,395063 | 0,028307 | Up |
| Q14690 | PDCD11 | Protein RRP5 homolog [OS=Homo sapiens] | 1,529 | 0,612588 | 0,035155 | Up |
| P15531 | NME1 | Nucleoside diphosphate kinase A [OS=Homo sapiens] | 1,831 | 0,872632 | 0,004757 | Up |
| Q5JSZ5 | PRRC2B | Protein PRRC2B [OS=Homo sapiens] | 1,883 | 0,913033 | 8,01E-08 | Up |
| P53999 | SUB1 | Activated RNA polymerase II transcriptional coactivator p15 [OS=Homo sapiens] | 1,952 | 0,964953 | 0,000265 | Up |
| Q9UNI6 | DUSP12 | Dual specificity protein phosphatase 12 [OS=Homo sapiens] | 4,745 | 2,246408 | 4,22E-15 | Up |

**Supplementary Table S2**. **Proteomic identification of proteins upregulated upon ΔZBD overexpression.** List of proteins significantly upregulated in ΔZBD-overexpressing cells compared to empty vector control cells, as identified by quantitative proteomic analysis. For each protein, UniProt accession number, gene symbol, protein description, abundance ratio, $log_2$ fold change, p-value, and direction of regulation are reported.

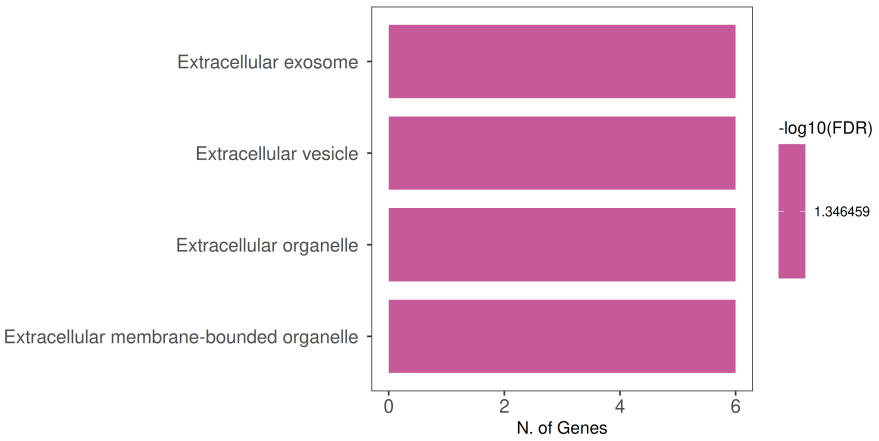


**Supplementary Figure S3. Limited Gene Ontology enrichment in cells expressing mutant DUSP12.** Bar plot showing the only Gene Ontology (GO) terms significantly enriched following expression of mutant DUSP12 compared to control cells. Enriched categories are restricted to extracellular compartment–related terms, including extracellular exosome, extracellular vesicle, extracellular organelle, and extracellular membrane-bounded organelle. The x-axis indicates the number of genes associated with each term, and bar color represents the $-\log_{10}$(FDR). No additional GO categories reached statistical significance under the thresholds applied in this analysis.

# References


1. Schwanhäusser, B. *et al.* Global quantification of mammalian gene expression control. *Nature* **473**, 337–342 (2011).
2. Sonenberg, N. & Hinnebusch, A. G. Regulation of Translation Initiation in Eukaryotes: Mechanisms and Biological Targets. *Cell* **136**, 731–745 (2009).
3. Proud, C. G. Phosphorylation and Signal Transduction Pathways in Translational Control. *Cold Spring Harb. Perspect. Biol.* **11**, a033050 (2019).
4. Iadevaia, V., Liu, R. & Proud, C. G. mTORC1 signaling controls multiple steps in ribosome biogenesis. *Semin. Cell Dev. Biol.* **36**, 113–120 (2014).
5. Piazzi, M., Bavelloni, A., Gallo, A., Faenza, I. & Blalock, W. L. Signal Transduction in Ribosome Biogenesis: A Recipe to Avoid Disaster. *Int. J. Mol. Sci.* **20**, 2718 (2019).
6. Ponti, D. The Nucleolus: A Central Hub for Ribosome Biogenesis and Cellular Regulatory Signals. *Int. J. Mol. Sci.* **26**, 4174 (2025).
7. Blanchet, S. & Ranjan, N. Translation Phases in Eukaryotes. in *Ribosome Biogenesis* (ed. Entian, K.-D.) vol. 2533 217–228 (Springer US, New York, NY, 2022).
8. Shine, J. & Dalgarno, L. The 3′-Terminal Sequence of *Escherichia coli* 16S Ribosomal RNA: Complementarity to Nonsense Triplets and Ribosome Binding Sites. *Proc. Natl. Acad. Sci.* **71**, 1342–1346 (1974).
9. Myasnikov, A. G., Simonetti, A., Marzi, S. & Klaholz, B. P. Structure–function insights into prokaryotic and eukaryotic translation initiation. *Curr. Opin. Struct. Biol.* **19**, 300–309 (2009).
10. Gualerzi, C. O. & Pon, C. L. Initiation of mRNA translation in bacteria: structural and dynamic aspects. *Cell. Mol. Life Sci.* **72**, 4341–4367 (2015).
11. Brito Querido, J., Díaz-López, I. & Ramakrishnan, V. The molecular basis of translation initiation and its regulation in eukaryotes. *Nat. Rev. Mol. Cell Biol.* **25**, 168–186 (2024).
12. Jackson, R. J., Hellen, C. U. T. & Pestova, T. V. The mechanism of eukaryotic translation initiation and principles of its regulation. *Nat. Rev. Mol. Cell Biol.* **11**, 113–127 (2010).

13. Kohler, R., Mooney, R. A., Mills, D. J., Landick, R. & Cramer, P. Architecture of a transcribing-translating expressome. *Science* **356**, 194–197 (2017).

14. *Molecular Biology of the Cell*. (Garland Science, New York, 2002).

15. Hinnebusch, A. G. The Scanning Mechanism of Eukaryotic Translation Initiation. *Annu. Rev. Biochem.* **83**, 779–812 (2014).

16. Kahvejian, A., Svitkin, Y. V., Sukarieh, R., M'Boutchou, M.-N. & Sonenberg, N. Mammalian poly(A)-binding protein is a eukaryotic translation initiation factor, which acts via multiple mechanisms. *Genes Dev.* **19**, 104–113 (2005).

17. Amrani, N., Ghosh, S., Mangus, D. A. & Jacobson, A. Translation factors promote the formation of two states of the closed-loop mRNP. *Nature* **453**, 1276–1280 (2008).

18. Price, N. T. & Proud, C. G. Phosphorylation of protein synthesis initiation factor-2. Identification of the site in the α-subunit phosphorylated in reticulocyte lysates. *Biochim. Biophys. Acta BBA - Mol. Cell Res.* **1054**, 83–88 (1990).

19. Wek, R. C. Role of eIF2α Kinases in Translational Control and Adaptation to Cellular Stress. *Cold Spring Harb. Perspect. Biol.* **10**, a032870 (2018).

20. Lu, H., Koju, N. & Sheng, R. Mammalian integrated stress responses in stressed organelles and their functions. *Acta Pharmacol. Sin.* **45**, 1095–1114 (2024).

21. Dey, M. *et al.* Requirement for kinase-induced conformational change in eukaryotic initiation factor 2α (eIF2α) restricts phosphorylation of Ser51. *Proc. Natl. Acad. Sci.* **108**, 4316–4321 (2011).

22. Donnelly, N., Gorman, A. M., Gupta, S. & Samali, A. The eIF2α kinases: their structures and functions. *Cell. Mol. Life Sci.* **70**, 3493–3511 (2013).

23. Deng, J. *et al.* Translational repression mediates activation of nuclear factor kappa B by phosphorylated translation initiation factor 2. *Mol. Cell. Biol.* **24**, 10161–10168 (2004).

24. Sidrauski, C., McGeachy, A. M., Ingolia, N. T. & Walter, P. The small molecule ISRIB reverses the effects of eIF2α phosphorylation on translation and stress granule assembly. *eLife* **4**, e05033 (2015).

25. Hu, S.-I. *et al.* MNK2 Inhibits eIF4G Activation Through a Pathway Involving Serine-Arginine–Rich Protein Kinase in Skeletal Muscle. *Sci. Signal.* **5**, (2012).

26. Qin, X., Jiang, B. & Zhang, Y. 4E-BP1, a multifactor regulated multifunctional protein. *Cell Cycle* **15**, 781–786 (2016).

27. Waskiewicz, A. J. Mitogen-activated protein kinases activate the serine/threonine kinases Mnk1 and Mnk2. *EMBO J.* **16**, 1909–1920 (1997).

28. Vary, T. C. & Lynch, C. J. Meal feeding enhances formation of eIF4F in skeletal muscle: role of increased eIF4E availability and eIF4G phosphorylation. *Am. J. Physiol.-Endocrinol. Metab.* **290**, E631–E642 (2006).

29. Dobrikov, M., Dobrikova, E., Shveygert, M. & Gromeier, M. Phosphorylation of Eukaryotic Translation Initiation Factor 4G1 (eIF4G1) by Protein Kinase Cα Regulates eIF4G1 Binding to Mnk1. *Mol. Cell. Biol.* **31**, 2947–2959 (2011).

30. Dobrikov, M. I., Shveygert, M., Brown, M. C. & Gromeier, M. Mitotic Phosphorylation of Eukaryotic Initiation Factor 4G1 (eIF4G1) at Ser1232 by Cdk1:Cyclin B Inhibits eIF4A Helicase Complex Binding with RNA. *Mol. Cell. Biol.* **34**, 439–451 (2014).

31. Dobrikov, M. I., Dobrikova, E. Y. & Gromeier, M. Dynamic Regulation of the Translation Initiation Helicase Complex by Mitogenic Signal Transduction to Eukaryotic Translation Initiation Factor 4G. *Mol. Cell. Biol.* **33**, 937–946 (2013).

32. Ling, J., Morley, S. J. & Traugh, J. A. Inhibition of cap-dependent translation via phosphorylation of eIF4G by protein kinase Pak2: Phosphorylation of eIF4G inhibits translation. *EMBO J.* **24**, 4094–4105 (2005).

33. Bettegazzi, B. *et al.* eIF4B phosphorylation at Ser504 links synaptic activity with protein translation in physiology and pathology. *Sci. Rep.* **7**, 10563 (2017).

34. Shahbazian, D., Parsyan, A., Petroulakis, E., Hershey, J. W. B. & Sonenberg, N. eIF4B controls survival and proliferation and is regulated by proto-oncogenic signaling pathways. *Cell Cycle* **9**, 4106–4109 (2010).

35. Damoc, E. *et al.* Structural Characterization of the Human Eukaryotic Initiation Factor 3 Protein Complex by Mass Spectrometry. *Mol. Cell. Proteomics* **6**, 1135–1146 (2007).

36. Borgo, C. *et al.* Protein kinase CK2 potentiates translation efficiency by phosphorylating eIF3j at Ser127. *Biochim. Biophys. Acta BBA - Mol. Cell Res.* **1853**, 1693–1701 (2015).

37. Marchione, R., Leibovitch, S. A. & Lenormand, J.-L. The translational factor eIF3f: the ambivalent eIF3 subunit. *Cell. Mol. Life Sci.* **70**, 3603–3616 (2013).

38. Mukhopadhyay, S., Amodeo, M. E. & Lee, A. S. Y. eIF3d controls the persistent integrated stress response. *Mol. Cell* **83**, 3303-3313.e6 (2023).

39. Gamble, N., Paul, E. E., Anand, B. & Marintchev, A. Regulation of the interactions between human eIF5 and eIF1A by the CK2 kinase. *Curr. Res. Struct. Biol.* **4**, 308–319 (2022).

40. Biffo, S. *et al.* Isolation of a Novel β4 Integrin-binding Protein (p27BBP) Highly Expressed in Epithelial Cells. *J. Biol. Chem.* **272**, 30314–30321 (1997).

41. Sanvito, F. *et al.* The β4 Integrin Interactor p27BBP/eIF6 Is an Essential Nuclear Matrix Protein Involved in 60S Ribosomal Subunit Assembly. *J. Cell Biol.* **144**, 823–838 (1999).

42. Zhu, W., Li, G. X., Chen, H. L. & Liu, X. Y. The role of eukaryotic translation initiation factor 6 in tumors. *Oncol. Lett.* **14**, 3–9 (2017).

43. Pelletier, J., Thomas, G. & Volarević, S. Ribosome biogenesis in cancer: new players and therapeutic avenues. *Nat. Rev. Cancer* **18**, 51–63 (2018).

44. Dörner, K., Ruggeri, C., Zemp, I. & Kutay, U. Ribosome biogenesis factors—from names to functions. *EMBO J.* **42**, e112699 (2023).

45. De La Cruz, J., Karbstein, K. & Woolford, J. L. Functions of Ribosomal Proteins in Assembly of Eukaryotic Ribosomes In Vivo. *Annu. Rev. Biochem.* **84**, 93–129 (2015).

46. Granneman, S., Petfalski, E. & Tollervey, D. A cluster of ribosome synthesis factors regulate pre-rRNA folding and 5.8S rRNA maturation by the Rat1 exonuclease: Pre-60S ribosome synthesis. *EMBO J.* **30**, 4006–4019 (2011).

47. LaCava, J. *et al.* RNA Degradation by the Exosome Is Promoted by a Nuclear Polyadenylation Complex. *Cell* **121**, 713–724 (2005).

48. Ingolia, N. T., Lareau, L. F. & Weissman, J. S. Ribosome Profiling of Mouse Embryonic Stem Cells Reveals the Complexity and Dynamics of Mammalian Proteomes. *Cell* **147**, 789–802 (2011).

49. Guzikowski, A. R. *et al.* Differential translation elongation directs protein synthesis in response to acute glucose deprivation in yeast. *RNA Biol.* **19**, 636–649 (2022).

50. Xie, J. *et al.* Regulation of the Elongation Phase of Protein Synthesis Enhances Translation Accuracy and Modulates Lifespan. *Curr. Biol.* **29**, 737-749.e5 (2019).

51. Zhou, Z., Dang, Y., Zhou, M., Yuan, H. & Liu, Y. Codon usage biases co-evolve with transcription termination machinery to suppress premature cleavage and polyadenylation. *eLife* **7**, e33569 (2018).

52. Lyu, X., Yang, Q., Zhao, F. & Liu, Y. Codon usage and protein length-dependent feedback from translation elongation regulates translation initiation and elongation speed. *Nucleic Acids Res.* **49**, 9404–9423 (2021).

53. Zhao, F. *et al.* Genome-wide role of codon usage on transcription and identification of potential regulators. *Proc. Natl. Acad. Sci.* **118**, e2022590118 (2021).

54. Mishra, R., Bansal, A. & Mishra, A. LISTERIN E3 Ubiquitin Ligase and Ribosome-Associated Quality Control (RQC) Mechanism. *Mol. Neurobiol.* **58**, 6593–6609 (2021).

55. D'Orazio, K. N. & Green, R. Ribosome states signal RNA quality control. *Mol. Cell* **81**, 1372–1383 (2021).

56. Szaflarski, W. *et al.* Early rRNA processing is a stress-dependent regulatory event whose inhibition maintains nucleolar integrity. *Nucleic Acids Res.* **50**, 1033–1051 (2022).

57. Mayer, C., Zhao, J., Yuan, X. & Grummt, I. mTOR-dependent activation of the transcription factor TIF-IA links rRNA synthesis to nutrient availability. *Genes Dev.* **18**, 423–434 (2004).

58. Voit, R., Seiler, J. & Grummt, I. Cooperative Action of Cdk1/cyclin B and SIRT1 Is Required for Mitotic Repression of rRNA Synthesis. *PLoS Genet.* **11**, e1005246 (2015).

59. Voit, R. & Grummt, I. Phosphorylation of UBF at serine 388 is required for interaction with RNA polymerase I and activation of rDNA transcription. *Proc. Natl. Acad. Sci.* **98**, 13631–13636 (2001).

60. Panov, K. I., Friedrich, J. K., Russell, J. & Zomerdijk, J. C. B. M. UBF activates RNA polymerase I transcription by stimulating promoter escape. *EMBO J.* **25**, 3310–3322 (2006).

61. Panwar, V. *et al.* Multifaceted role of mTOR (mammalian target of rapamycin) signaling pathway in human health and disease. *Signal Transduct. Target. Ther.* **8**, 375 (2023).

62. Szwed, A., Kim, E. & Jacinto, E. Regulation and metabolic functions of mTORC1 and mTORC2. *Physiol. Rev.* **101**, 1371–1426 (2021).

63. Ragupathi, A., Kim, C. & Jacinto, E. The mTORC2 signaling network: targets and cross-talks. *Biochem. J.* **481**, 45–91 (2024).

64. Ruvinsky, I. & Meyuhas, O. Ribosomal protein S6 phosphorylation: from protein synthesis to cell size. *Trends Biochem. Sci.* **31**, 342–348 (2006).

65. Laplante, M. & Sabatini, D. M. mTOR signaling at a glance. *J. Cell Sci.* **122**, 3589–3594 (2009).

66. Bielinski, V. & Mumby, M. Functional analysis of the PP2A subfamily of protein phosphatases in regulating Drosophila S6 kinase. *Exp. Cell Res.* **313**, 3117–3126 (2007).

67. Yang, M., Lu, Y., Piao, W. & Jin, H. The Translational Regulation in mTOR Pathway. *Biomolecules* **12**, 802 (2022).

68. Jia, J.-J. *et al.* mTORC1 promotes TOP mRNA translation through site-specific phosphorylation of LARP1. *Nucleic Acids Res.* **49**, 3461–3489 (2021).

69. Truitt, M. L. & Ruggero, D. New frontiers in translational control of the cancer genome. *Nat. Rev. Cancer* **16**, 288–304 (2016).

70. Nguyen, L. X. T. & Mitchell, B. S. Akt activation enhances ribosomal RNA synthesis through casein kinase II and TIF-IA. *Proc. Natl. Acad. Sci.* **110**, 20681–20686 (2013).

71. Lee, S. B. *et al.* Nuclear Akt interacts with B23/NPM and protects it from proteolytic cleavage, enhancing cell survival. *Proc. Natl. Acad. Sci.* **105**, 16584–16589 (2008).

72. Ahn, J.-Y. *et al.* Nucleophosmin/B23, a Nuclear PI(3,4,5)P3 Receptor, Mediates the Antiapoptotic Actions of NGF by Inhibiting CAD. *Mol. Cell* **18**, 435–445 (2005).

73. Davis, W. J., Lehmann, P. Z. & Li, W. Nuclear PI3K signaling in cell growth and tumorigenesis. *Front. Cell Dev. Biol.* **3**, (2015).

74. Cerezo, E. L. *et al.* RIOK2 phosphorylation by RSK promotes synthesis of the human small ribosomal subunit. *PLOS Genet.* **17**, e1009583 (2021).

75. Harding, H. P. *et al.* An Integrated Stress Response Regulates Amino Acid Metabolism and Resistance to Oxidative Stress. *Mol. Cell* **11**, 619–633 (2003).

76. Pakos-Zebrucka, K. *et al.* The integrated stress response. *EMBO Rep.* **17**, 1374–1395 (2016).

77. Dever, T. E. *et al.* Phosphorylation of initiation factor 2α by protein kinase GCN2 mediates gene-specific translational control of GCN4 in yeast. *Cell* **68**, 585–596 (1992).

78. Harding, H. P. *et al.* Regulated Translation Initiation Controls Stress-Induced Gene Expression in Mammalian Cells. *Mol. Cell* **6**, 1099–1108 (2000).

79. Vattem, K. M. & Wek, R. C. Reinitiation involving upstream ORFs regulates *ATF4* mRNA translation in mammalian cells. *Proc. Natl. Acad. Sci.* **101**, 11269–11274 (2004).

80. Nguyen, L. K., Matallanas, D., Croucher, D. R., Von Kriegsheim, A. & Kholodenko, B. N. Signalling by protein phosphatases and drug development: a systems-centred view. *FEBS J.* **280**, 751–765 (2013).

81. Hahn, K. *et al.* PP2A Regulatory Subunit PP2A-B′ Counteracts S6K Phosphorylation. *Cell Metab.* **11**, 438–444 (2010).

82. Fowle, H., Zhao, Z. & Graña, X. PP2A holoenzymes, substrate specificity driving cellular functions and deregulation in cancer. in *Advances in Cancer Research* vol. 144 55–93 (Elsevier, 2019).

83. Truitt, M. L. & Ruggero, D. New frontiers in translational control of the cancer genome. *Nat. Rev. Cancer* **16**, 288–304 (2016).

84. Aguilo, F. & Dassi, E. Editorial: Translational control in cancer. *NAR Cancer* **6**, zcae031 (2024).

85. Levene, P. A. & Alsberg, C. L. The Cleavage Products of Vitellin. *J. Biol. Chem.* **2**, 127–133 (1906).

86. Voet, D., Voet, J. G., Pratt, C. W. & Melloni, E. *Principi di biochimica*. (Zanichelli, Bologna, 2018).

87. Krebs, E. G. & Fischer, E. H. The phosphorylase b to a converting enzyme of rabbit skeletal muscle. *Biochim. Biophys. Acta* **20**, 150–157 (1956).

88. Ochoa, D. *et al.* The functional landscape of the human phosphoproteome. *Nat. Biotechnol.* **38**, 365–373 (2020).

89. Muneer, G., Chen, C. & Chen, Y. Advancements in Global Phosphoproteomics Profiling: Overcoming Challenges in Sensitivity and Quantification. *PROTEOMICS* **25**, e202400087 (2025).

90. Needham, E. J., Parker, B. L., Burykin, T., James, D. E. & Humphrey, S. J. Illuminating the dark phosphoproteome. *Sci. Signal.* **12**, eaau8645 (2019).

91. Olsen, J. V. & Mann, M. Status of Large-scale Analysis of Post-translational Modifications by Mass Spectrometry. *Mol. Cell. Proteomics* **12**, 3444–3452 (2013).

92. Brandi, J., Noberini, R., Bonaldi, T. & Cecconi, D. Advances in enrichment methods for mass spectrometry-based proteomics analysis of post-translational modifications. *J. Chromatogr. A* **1678**, 463352 (2022).

93. Humphrey, S. J., Azimifar, S. B. & Mann, M. High-throughput phosphoproteomics reveals in vivo insulin signaling dynamics. *Nat. Biotechnol.* **33**, 990–995 (2015).

94. Leutert, M., Rodríguez-Mias, R. A., Fukuda, N. K. & Villén, J. R2-P2 rapid-robotic phosphoproteomics enables multidimensional cell signaling studies. *Mol. Syst. Biol.* **15**, e9021 (2019).

95. Dass, C. *Fundamentals of Contemporary Mass Spectrometry*. (Wiley-Interscience, Hoboken (N.J.), 2007).

96. Li, J., Smith, L. S. & Zhu, H.-J. Data-independent acquisition (DIA): An emerging proteomics technology for analysis of drug-metabolizing enzymes and transporters. *Drug Discov. Today Technol.* **39**, 49–56 (2021).

97. Collins, B. C. *et al.* Quantifying protein interaction dynamics by SWATH mass spectrometry: application to the 14-3-3 system. *Nat. Methods* **10**, 1246–1253 (2013).

98. Nissa, M. U. *et al.* Organ-Based Proteome and Post-Translational Modification Profiling of a Widely Cultivated Tropical Water Fish, *Labeo rohita*. *J. Proteome Res.* **21**, 420–437 (2022).

99. Chen, X., Wei, S., Ji, Y., Guo, X. & Yang, F. Quantitative proteomics using SILAC: Principles, applications, and developments. *PROTEOMICS* **15**, 3175–3192 (2015).

100. Boersema, P. J., Raijmakers, R., Lemeer, S., Mohammed, S. & Heck, A. J. R. Multiplex peptide stable isotope dimethyl labeling for quantitative proteomics. *Nat. Protoc.* **4**, 484–494 (2009).

101. Sivanich, M. K., Gu, T., Tabang, D. N. & Li, L. Recent advances in isobaric labeling and applications in quantitative proteomics. *PROTEOMICS* **22**, 2100256 (2022).

102. Li, J. *et al.* TMTpro-18plex: The Expanded and Complete Set of TMTpro Reagents for Sample Multiplexing. *J. Proteome Res.* **20**, 2964–2972 (2021).

103. Asara, J. M., Christofk, H. R., Freimark, L. M. & Cantley, L. C. A label-free quantification method by MS/MS TIC compared to SILAC and spectral counting in a proteomics screen. *PROTEOMICS* **8**, 994–999 (2008).

104. Knight, Z. A. & Shokat, K. M. Features of Selective Kinase Inhibitors. *Chem. Biol.* **12**, 621–637 (2005).

105. Russell, D. W. & Spremulli, L. L. Purification and characterization of a ribosome dissociation factor (eukaryotic initiation factor 6) from wheat germ. *J. Biol. Chem.* **254**, 8796–8800 (1979).

106. Valenzuela, D. M., Chaudhuri, A. & Maitra, U. Eukaryotic ribosomal subunit anti-association activity of calf liver is contained in a single polypeptide chain protein of Mr = 25,500 (eukaryotic initiation factor 6). *J. Biol. Chem.* **257**, 7712–7719 (1982).

107. Miluzio, A., Beugnet, A., Volta, V. & Biffo, S. Eukaryotic initiation factor 6 mediates a continuum between 60S ribosome biogenesis and translation. *EMBO Rep.* **10**, 459–465 (2009).

108. Brina, D., Miluzio, A., Ricciardi, S. & Biffo, S. eIF6 anti-association activity is required for ribosome biogenesis, translational control and tumor progression. *Biochim. Biophys. Acta BBA - Gene Regul. Mech.* **1849**, 830–835 (2015).

109. Si, K., Chaudhuri, J., Chevesich, J. & Maitra, U. Molecular cloning and functional expression of a human cDNA encoding translation initiation factor 6. *Proc. Natl. Acad. Sci.* **94**, 14285–14290 (1997).

110. Ceci, M., Offenhäuser, N., Carlo Marchisio, P. & Biffo, S. Formation of nuclear matrix filaments by p27BBP/eIF6. *Biochem. Biophys. Res. Commun.* **295**, 295–299 (2002).

111. Groft, C. M., Beckmann, R., Sali, A. & Burley, S. K. Crystal structures of ribosome anti-association factor IF6. *Nat. Struct. Biol.* **7**, 1156–1164 (2000).

112. Wood, L. C., Ashby, M. N., Grunfeld, C. & Feingold, K. R. Cloning of Murine Translation Initiation Factor 6 and Functional Analysis of the Homologous Sequence YPR016c in Saccharomyces cerevisiae. *J. Biol. Chem.* **274**, 11653–11659 (1999).

113. Si, K. & Maitra, U. The *Saccharomyces cerevisiae* Homologue of Mammalian Translation Initiation Factor 6 Does Not Function as a Translation Initiation Factor. *Mol. Cell. Biol.* **19**, 1416–1426 (1999).

114. Fatica, A. & Tollervey, D. Making ribosomes. *Curr. Opin. Cell Biol.* **14**, 313–318 (2002).

115. Volta, V. *et al.* Sen34p depletion blocks tRNA splicing in vivo and delays rRNA processing. *Biochem. Biophys. Res. Commun.* **337**, 89–94 (2005).

116. Basu, U., Si, K., Warner, J. R. & Maitra, U. The *Saccharomyces cerevisiae TIF6* Gene Encoding Translation Initiation Factor 6 Is Required for 60S Ribosomal Subunit Biogenesis. *Mol. Cell. Biol.* **21**, 1453–1462 (2001).

117. Gandin, V. *et al.* Eukaryotic initiation factor 6 is rate-limiting in translation, growth and transformation. *Nature* **455**, 684–688 (2008).

118. Biswas, A. *et al.* Opposing Action of Casein Kinase 1 and Calcineurin in Nucleo-cytoplasmic Shuttling of Mammalian Translation Initiation Factor eIF6. *J. Biol. Chem.* **286**, 3129–3138 (2011).

119. Ceci, M. *et al.* Release of eIF6 (p27BBP) from the 60S subunit allows 80S ribosome assembly. *Nature* **426**, 579–584 (2003).

120. Benelli, D. *et al.* Function and ribosomal localization of aIF6, a translational regulator shared by archaea and eukarya. *Nucleic Acids Res.* **37**, 256–267 (2009).

121. Gartmann, M. *et al.* Mechanism of eIF6-mediated Inhibition of Ribosomal Subunit Joining. *J. Biol. Chem.* **285**, 14848–14851 (2010).

122. Klinge, S., Voigts-Hoffmann, F., Leibundgut, M., Arpagaus, S. & Ban, N. Crystal Structure of the Eukaryotic 60 *S* Ribosomal Subunit in Complex with Initiation Factor 6. *Science* **334**, 941–948 (2011).

123. Weis, F. *et al.* Mechanism of eIF6 release from the nascent 60S ribosomal subunit. *Nat. Struct. Mol. Biol.* **22**, 914–919 (2015).

124. Jaako, P. *et al.* eIF6 rebinding dynamically couples ribosome maturation and translation. *Nat. Commun.* **13**, 1562 (2022).

125. Pisarev, A. V. *et al.* The Role of ABCE1 in Eukaryotic Posttermination Ribosomal Recycling. *Mol. Cell* **37**, 196–210 (2010).

126. Sengupta, J. *et al.* Identification of the versatile scaffold protein RACK1 on the eukaryotic ribosome by cryo-EM. *Nat. Struct. Mol. Biol.* **11**, 957–962 (2004).

127. Volta, V. *et al.* RACK1 depletion in a mouse model causes lethality, pigmentation deficits and reduction in protein synthesis efficiency. *Cell. Mol. Life Sci.* **70**, 1439–1450 (2013).

128. Brina, D., Grosso, S., Miluzio, A. & Biffo, S. Translational control by 80S formation and 60S availability: The central role of eIF6, a rate limiting factor in cell cycle progression and tumorigenesis. *Cell Cycle* **10**, 3441–3446 (2011).

129. Jungers, C. F., Elliff, J. M., Masson-Meyers, D. S., Phiel, C. J. & Origanti, S. Regulation of eukaryotic translation initiation factor 6 dynamics through multisite phosphorylation by GSK3. *J. Biol. Chem.* **295**, 12796–12813 (2020).

130. Brina, D. *et al.* eIF6 coordinates insulin sensitivity and lipid metabolism by coupling translation to transcription. *Nat. Commun.* **6**, 8261 (2015).

131. Scagliola, A. *et al.* Targeting of eIF6-driven translation induces a metabolic rewiring that reduces NAFLD and the consequent evolution to hepatocellular carcinoma. *Nat. Commun.* **12**, 4878 (2021).

132. Tan, S. *et al.* EFL1 mutations impair eIF6 release to cause Shwachman-Diamond syndrome. *Blood* **134**, 277–290 (2019).

133. Hou, S., Tang, H., Dong, Z. & Zhou, W. eIF6: a promising therapeutic target for gastric carcinoma via PI3K/AKT pathway modulation. *World J. Surg. Oncol.* **23**, 113 (2025).

134. Zhao, Z. *et al.* Cytoplasmic eIF6 promotes OSCC malignant behavior through AKT pathway. *Cell Commun. Signal.* **19**, 121 (2021).

135. Pinzaglia, M. *et al.* eIF6 over-expression increases the motility and invasiveness of cancer cells by modulating the expression of a critical subset of membrane-bound proteins. *BMC Cancer* **15**, 131 (2015).

136. Roshan, P. *et al.* Sequestration of ribosomal subunits as inactive 80S by targeting eIF6 limits mitotic exit and cancer progression. *Nucleic Acids Res.* **53**, gkae1272 (2025).

137. Scagliola, A. *et al.* Inhibition of eIF6 Activity Reduces Hepatocellular Carcinoma Growth: An In Vivo and In Vitro Study. *Int. J. Mol. Sci.* **23**, 7720 (2022).

138. Mestareehi, A. & Abu-Farsakh, N. Impact of Protein Phosphatase Expressions on the Prognosis of Hepatocellular Carcinoma Patients. *ACS Omega* **9**, 10299–10331 (2024).

139. Manning, G., Whyte, D. B., Martinez, R., Hunter, T. & Sudarsanam, S. The Protein Kinase Complement of the Human Genome. *Science* **298**, 1912–1934 (2002).

140. Tonks, N. K. Protein tyrosine phosphatases – from housekeeping enzymes to master regulators of signal transduction. *FEBS J.* **280**, 346–378 (2013).

141. Tonks, N. K. Protein tyrosine phosphatases: from genes, to function, to disease. *Nat. Rev. Mol. Cell Biol.* **7**, 833–846 (2006).

142. Alonso, A. *et al.* Protein Tyrosine Phosphatases in the Human Genome. *Cell* **117**, 699–711 (2004).

143. Tautz, L., Critton, D. A. & Grotegut, S. Protein Tyrosine Phosphatases: Structure, Function, and Implication in Human Disease. in *Phosphatase Modulators* (ed. Millán, J. L.) vol. 1053 179–221 (Humana Press, Totowa, NJ, 2013).

144. Shillingford, S. R. & Bennett, A. M. Mitogen-Activated Protein Kinase Phosphatases: No Longer Undruggable? *Annu. Rev. Pharmacol. Toxicol.* **63**, 617–636 (2023).

145. He, R., Yu, Z., Zhang, R. & Zhang, Z. Protein tyrosine phosphatases as potential therapeutic targets. *Acta Pharmacol. Sin.* **35**, 1227–1246 (2014).

146. Netto, L. E. S. & Machado, L. E. S. F. Preferential redox regulation of cysteine-based protein tyrosine phosphatases: structural and biochemical diversity. *FEBS J.* **289**, 5480–5504 (2022).

147. Barford, D., Das, A. K. & Egloff, M.-P. THE STRUCTURE AND MECHANISM OF PROTEIN PHOSPHATASES: Insights into Catalysis and Regulation. *Annu. Rev. Biophys. Biomol. Struct.* **27**, 133–164 (1998).

148. Wakula, P. *et al.* The translation initiation factor eIF2β is an interactor of protein phosphatase-1. *Biochem. J.* **400**, 377–383 (2006).

149. Quevedo, C., Salinas, M. & Alcázar, A. Initiation Factor 2B Activity Is Regulated by Protein Phosphatase 1, Which Is Activated by the Mitogen-activated Protein Kinase-dependent Pathway in Insulin-like Growth Factor 1-stimulated Neuronal Cells. *J. Biol. Chem.* **278**, 16579–16586 (2003).

150. Woo, C. W., Kutzler, L., Kimball, S. R. & Tabas, I. Toll-like receptor activation suppresses ER stress factor CHOP and translation inhibition through activation of eIF2B. *Nat. Cell Biol.* **14**, 192–200 (2012).

151. Ueda, T., Watanabe-Fukunaga, R., Fukuyama, H., Nagata, S. & Fukunaga, R. Mnk2 and Mnk1 Are Essential for Constitutive and Inducible Phosphorylation of Eukaryotic Initiation Factor 4E but Not for Cell Growth or Development. *Mol. Cell. Biol.* **24**, 6539–6549 (2004).

152. Topisirovic, I., Ruiz-Gutierrez, M. & Borden, K. L. B. Phosphorylation of the Eukaryotic Translation Initiation Factor eIF4E Contributes to Its Transformation and mRNA Transport Activities. *Cancer Res.* **64**, 8639–8642 (2004).

153. Bu, X. & Hagedorn, C. H. Phosphoprotein phosphatase 2A dephosphorylates eIF-4E and does not alter binding to the mRNA cap. *FEBS Lett.* **301**, 15–18 (1992).

154. Eom, T. *et al.* Neuronal BC RNAs cooperate with eIF4B to mediate activity-dependent translational control. *J. Cell Biol.* **207**, 237–252 (2014).

155. Gingras, A.-C. *et al.* Hierarchical phosphorylation of the translation inhibitor 4E-BP1. *Genes Dev.* **15**, 2852–2864 (2001).

156. Gardner, T. W., Abcouwer, S. F., Losiewicz, M. K. & Fort, P. E. Phosphatase control of 4E-BP1 phosphorylation state is central for glycolytic regulation of retinal protein synthesis. *Am. J. Physiol.-Endocrinol. Metab.* **309**, E546–E556 (2015).

157. Liu, J., Stevens, P. D., Eshleman, N. E. & Gao, T. Protein Phosphatase PPM1G Regulates Protein Translation and Cell Growth by Dephosphorylating 4E Binding Protein 1 (4E-BP1). *J. Biol. Chem.* **288**, 23225–23233 (2013).

158. Hong-Brown, L. Q., Brown, C. R., Huber, D. S. & Lang, C. H. Alcohol Regulates Eukaryotic Elongation Factor 2 Phosphorylation via an AMP-activated Protein Kinase-dependent Mechanism in C2C12 Skeletal Myocytes. *J. Biol. Chem.* **282**, 3702–3712 (2007).

159. Kaitsuka, T., Tomizawa, K. & Matsushita, M. Heat Shock-Induced Dephosphorylation of Eukaryotic Elongation Factor 1BδL by Protein Phosphatase 1. *Front. Mol. Biosci.* **7**, 598578 (2021).

160. Song, H. *et al.* The Crystal Structure of Human Eukaryotic Release Factor eRF1—Mechanism of Stop Codon Recognition and Peptidyl-tRNA Hydrolysis. *Cell* **100**, 311–321 (2000).

161. Chamousset, D. *et al.* RRP1B Targets PP1 to Mammalian Cell Nucleoli and Is Associated with Pre-60S Ribosomal Subunits. *Mol. Biol. Cell* **21**, 4212–4226 (2010).

162. Qin, W. *et al.* Nom1 Mediates Pancreas Development by Regulating Ribosome Biogenesis in Zebrafish. *PLoS ONE* **9**, e100796 (2014).

163. Kemmler, S., Occhipinti, L., Veisu, M. & Panse, V. G. Yvh1 is required for a late maturation step in the 60S biogenesis pathway. *J. Cell Biol.* **186**, 863–880 (2009).

164. Lo, K.-Y., Li, Z., Wang, F., Marcotte, E. M. & Johnson, A. W. Ribosome stalk assembly requires the dual-specificity phosphatase Yvh1 for the exchange of Mrt4 with P0. *J. Cell Biol.* **186**, 849–862 (2009).

165. DaDalt, A. A., Bonham, C. A., Lotze, G. P., Luiso, A. A. & Vacratsis, P. O. Src-mediated phosphorylation of the ribosome biogenesis factor hYVH1 affects its localization, promoting partitioning to the 60S ribosomal subunit. *J. Biol. Chem.* **298**, 102679 (2022).

166. Guan, K. *et al.* A yeast protein phosphatase related to the vaccinia virus VH1 phosphatase is induced by nitrogen starvation. *Proc. Natl. Acad. Sci.* **89**, 12175–12179 (1992).

167. Muda, M., Manning, E. R., Orth, K. & Dixon, J. E. Identification of the Human YVH1 Protein-tyrosine Phosphatase Orthologue Reveals a Novel Zinc Binding Domain Essential for in Vivo Function. *J. Biol. Chem.* **274**, 23991–23995 (1999).

168. Ensembl Project. Ensembl Gene: DUSP12 ENSG00000081721. (115 AD).

169. Gratias, S. *et al.* Genomic gains on chromosome 1q in retinoblastoma: Consequences on gene expression and association with clinical manifestation. *Int. J. Cancer* **116**, 555–563 (2005).

170. Kresse, S. H. *et al.* Mapping and characterization of the amplicon near APOA2 in 1q23 in human sarcomas by FISH and array CGH. *Mol. Cancer* **4**, 39 (2005).

171. Hepworth, E. M. W. & Hinton, S. D. Pseudophosphatases as Regulators of MAPK Signaling. *Int. J. Mol. Sci.* **22**, 12595 (2021).

172. Lee, H., Yi, J.-S., Lawan, A., Min, K. & Bennett, A. M. Mining the function of protein tyrosine phosphatases in health and disease. *Semin. Cell Dev. Biol.* **37**, 66–72 (2015).

173. Guan, K. L. & Dixon, J. E. Evidence for protein-tyrosine-phosphatase catalysis proceeding via a cysteine-phosphate intermediate. *J. Biol. Chem.* **266**, 17026–17030 (1991).

174. Jeong, D. G. *et al.* The family-wide structure and function of human dual-specificity protein phosphatases. *Acta Crystallogr. D Biol. Crystallogr.* **70**, 421–435 (2014).

175. Bonham, C. A. & Vacratsis, P. O. Redox Regulation of the Human Dual Specificity Phosphatase YVH1 through Disulfide Bond Formation. *J. Biol. Chem.* **284**, 22853–22864 (2009).

176. Muñoz-Alonso, M. J. *et al.* A Novel Cytosolic Dual Specificity Phosphatase, Interacting with Glucokinase, Increases Glucose Phosphorylation Rate. *J. Biol. Chem.* **275**, 32406–32412 (2000).

177. Park, H.-D., Beeser, A. E., Clancy, M. J. & Cooper, T. G. TheS. cerevisiae nitrogen starvation-induced Yvh1p and Ptp2p phosphatases play a role in control of sporulation. *Yeast* **12**, 1135–1151 (1996).

178. Beeser, A. E. & Cooper, T. G. The Dual-Specificity Protein Phosphatase Yvh1p Regulates Sporulation, Growth, and Glycogen Accumulation Independently of Catalytic Activity in *Saccharomyces cerevisiae* via the Cyclic AMP-Dependent Protein Kinase Cascade. *J. Bacteriol.* **182**, 3517–3528 (2000).

179. Lo, K.-Y., Li, Z., Wang, F., Marcotte, E. M. & Johnson, A. W. Ribosome stalk assembly requires the dual-specificity phosphatase Yvh1 for the exchange of Mrt4 with P0. *J. Cell Biol.* **186**, 849–862 (2009).

180. Grela, P. *et al.* Human ribosomal P1-P2 heterodimer represents an optimal docking site for ricin A chain with a prominent role for P1 C-terminus. *Sci. Rep.* **7**, 5608 (2017).

181. Sugiyama, M. *et al.* Genetic interactions of ribosome maturation factors Yvh1 and Mrt4 influence mRNA decay, glycogen accumulation, and the expression of early meiotic genes in Saccharomyces cerevisiae. *J. Biochem. (Tokyo)* **150**, 103–111 (2011).

182. Zhou, Y., Musalgaonkar, S., Johnson, A. W. & Taylor, D. W. Tightly-orchestrated rearrangements govern catalytic center assembly of the ribosome. *Nat. Commun.* **10**, 958 (2019).

183. Sakumoto, N., Yamashita, H., Mukai, Y., Kaneko, Y. & Harashima, S. Dual-Specificity Protein Phosphatase Yvh1p, Which Is Required for Vegetative Growth and Sporulation, Interacts with Yeast Pescadillo Homolog in Saccharomyces cerevisiae. *Biochem. Biophys. Res. Commun.* **289**, 608–615 (2001).

184. Zang, H., Shackelford, R., Bewley, A. & Beeser, A. E. Mutational Analyses of the Cysteine-Rich Domain of Yvh1, a Protein Required for Translational Competency in Yeast. *Biology* **11**, 1246 (2022).

185. Genuth, N. R. & Barna, M. The Discovery of Ribosome Heterogeneity and Its Implications for Gene Regulation and Organismal Life. *Mol. Cell* **71**, 364–374 (2018).

186. Li, D. & Wang, J. Ribosome heterogeneity in stem cells and development. *J. Cell Biol.* **219**, e202001108 (2020).

187. Nakhoul, H. *et al.* Ribosomopathies: Mechanisms of Disease. *Clin. Med. Insights Blood Disord.* **7**, CMBD.S16952 (2014).

188. Geng, Q., Xhabija, B., Knuckle, C., Bonham, C. A. & Vacratsis, P. O. The Atypical Dual Specificity Phosphatase hYVH1 Associates with Multiple Ribonucleoprotein Particles. *J. Biol. Chem.* **292**, 539–550 (2017).

189. DaDalt, A. A., Bonham, C. A., Lotze, G. P., Luiso, A. A. & Vacratsis, P. O. Src-mediated phosphorylation of the ribosome biogenesis factor hYVH1 affects its localization, promoting partitioning to the 60S ribosomal subunit. *J. Biol. Chem.* **298**, 102679 (2022).

190. Sharda, P. R., Bonham, C. A., Mucaki, E. J., Butt, Z. & Vacratsis, P. O. The dual-specificity phosphatase hYVH1 interacts with Hsp70 and prevents heat-shock-induced cell death. *Biochem. J.* **418**, 391–401 (2009).

191. Sharda, P. R., Bonham, C. A., Mucaki, E. J., Butt, Z. & Vacratsis, P. O. The dual-specificity phosphatase hYVH1 interacts with Hsp70 and prevents heat-shock-induced cell death. *Biochem. J.* **418**, 391–401 (2009).

192. Kozarova, A., Hudson, J. W. & Vacratsis, P. O. The dual-specificity phosphatase hYVH1 (DUSP12) is a novel modulator of cellular DNA content. *Cell Cycle* **10**, 1669–1678 (2011).

193. Abdusamad, M. *et al.* DUSP12 promotes cell cycle progression and protects cells from cell death by regulating ZPR9. Preprint at https://doi.org/10.1101/2025.01.13.632830 (2025).

194. Mouse Phenotyping Consortium (IMPC). (2025). Dusp12 phenotypes.

195. Gao, J. *et al.* RAB3B Dictates mTORC1/S6 Signaling in Chordoma and Predicts Response to mTORC1-Targeted Therapy. *Adv. Sci.* **12**, 2415384 (2025).

196. Ju, G. *et al.* DUSP12 regulates the tumorigenesis and prognosis of hepatocellular carcinoma. *PeerJ* **9**, e11929 (2021).

197. Huang, Z. *et al.* Dual Specificity Phosphatase 12 Regulates Hepatic Lipid Metabolism Through Inhibition of the Lipogenesis and Apoptosis Signal–Regulating Kinase 1 Pathways. *Hepatology* **70**, 1099–1118 (2019).

198. Li, H. *et al.* Dual-specificity phosphatase 12 attenuates oxidative stress injury and apoptosis in diabetic cardiomyopathy via the ASK1-JNK/p38 signaling pathway. *Free Radic. Biol. Med.* **192**, 13–24 (2022).

199. Boldorini, R., Clemente, N., Alchera, E. & Carini, R. DUSP12 acts as a novel endogenous protective signal against hepatic ischemia–reperfusion damage by inhibiting ASK1 pathway. *Clin. Sci.* **135**, 161–166 (2021).

200. Go, C. D. *et al.* A proximity-dependent biotinylation map of a human cell. *Nature* **595**, 120–124 (2021).

201. Dull, T. *et al.* A Third-Generation Lentivirus Vector with a Conditional Packaging System. *J. Virol.* **72**, 8463–8471 (1998).

202. Jeong, H., Kim, H. J. & Lee, S. J. Complete Genome Sequence of Escherichia coli Strain BL21. *Genome Announc.* **3**, e00134-15 (2015).

203. De Marco, A., Vigh, L., Diamant, S. & Goloubinoff, P. Native folding of aggregation-prone recombinant proteins in Escherichia coli by osmolytes, plasmid- or benzyl alcohol–overexpressed molecular chaperones. *Cell Stress Chaperones* **10**, 329 (2005).

204. Pesce, E. *et al.* Direct and high throughput (HT) interactions on the ribosomal surface by iRIA. *Sci. Rep.* **5**, 15401 (2015).

205. Gurzeler, L.-A., Ziegelmüller, J., Mühlemann, O. & Karousis, E. D. Production of human translation-competent lysates using dual centrifugation. *RNA Biol.* **19**, 78–88 (2022).

206. Miluzio, A. *et al.* Impairment of Cytoplasmic eIF6 Activity Restricts Lymphomagenesis and Tumor Progression without Affecting Normal Growth. *Cancer Cell* **19**, 765–775 (2011).

207. Johnson, L. F., Levis, R., Abelson, H. T., Green, H. & Penman, S. Changes in RNA in relation to growth of the fibroblast. IV. Alterations in theproduction and processing of mRNA and rRNA in resting and growing cells. *J. Cell Biol.* **71**, 933–938 (1976).

208. Wang, X. Regulation of elongation factor 2 kinase by p90RSK1 and p70 S6 kinase. *EMBO J.* **20**, 4370–4379 (2001).

209. Chevet, E., Smirle, J., Cameron, P. H., Thomas, D. Y. & Bergeron, J. J. M. Calnexin phosphorylation: Linking cytoplasmic signalling to endoplasmic reticulum lumenal functions. *Semin. Cell Dev. Biol.* **21**, 486–490 (2010).

210. Paskevicius, T., Farraj, R. A., Michalak, M. & Agellon, L. B. Calnexin, More Than Just a Molecular Chaperone. *Cells* **12**, 403 (2023).

211. Canton, D. A. & Litchfield, D. W. The shape of things to come: An emerging role for protein kinase CK2 in the regulation of cell morphology and the cytoskeleton. *Cell. Signal.* **18**, 267–275 (2006).

212. Yuan, F., Li, G. & Tong, T. Nucleolar and coiled-body phosphoprotein 1 (NOLC1) regulates the nucleolar retention of TRF2. *Cell Death Discov.* **3**, 17043 (2017).

213. Lu, L. *et al.* Nucleolar stress: is there a reverse version? *J. Cancer* **9**, 3723–3727 (2018).

214. Qiu, T. *et al.* DUSP12 protects against hepatic ischemia–reperfusion injury dependent on ASK1-JNK/p38 pathway *in vitro* and *in vivo*. *Clin. Sci.* **134**, 2279–2294 (2020).

215. Cheng, J., Ji, M., Jing, H. & Lin, H. DUSP12 ameliorates myocardial ischemia–reperfusion injury through HSPB8-induced mitophagy. *J. Biochem. Mol. Toxicol.* **37**, e23310 (2023).

216. Xie, M., Xie, R., Huang, P., Yap, D. Y. H. & Wu, P. GADD45A and GADD45B as Novel Biomarkers Associated with Chromatin Regulators in Renal Ischemia-Reperfusion Injury. *Int. J. Mol. Sci.* **24**, 11304 (2023).